Tire Force Estimation in Off-Road Vehicles Using Suspension Strain and Deflection Measurements

by

Ryan Sessions Hill

A thesis submitted to the Graduate Faculty of
Auburn University
in partial fulfillment of the
requirements for the Degree of
Master of Science

Auburn, Alabama
May 7, 2012

Keywords: Vehicle Dynamics, Suspension, Vehicle Modeling, Tire Forces, Estimation

Approved by:

David M. Bevly, Chair, Albert J. Smith Associate Professor of Mechanical Engineering
David Beale, Professor of Mechanical Engineering
Song-Yul Choe, Associate Professor of Mechanical Engineering

Abstract

This thesis develops and analyzes the improvement of tire force estimation and analysis using strain gauge sensors and displacement sensors mounted on the suspension of an all-terrain vehicle. Vehicle dynamic models are developed and validated against simulation data acquired from commercially available CarSIM vehicle simulation software. Improved measurements of the vehicle provide more accurate model parameters used in simulation of the test platform. These improved models are then compared against real data collected from the Prowler All Terrain Vehicle, a fully instrumented ATV. Suspension force measurement techniques, including strain gauges mounted to the a-arm linkages and deflection potentiometers mounted to the coil-spring assembly were developed and installed onto the testbed. A method for analyzing these force measurements and a methodology to decouple the forces at the tire contact patch into vertical, lateral, and longitudinal components is developed. Results show that this measurement technique is a viable and relatively low-cost method to augment dynamic tire force knowledge in unmanned vehicle systems. Finally, a discussion on the benefits and drawbacks of using this type of sensing method is presented, as well as potential applications of this work.

Acknowledgments

I would like to first and foremost thank God for the blessings and opportunities presented to me throughout my experience as a graduate student and during the completion of this thesis. As is the case so often in life, without Him none of this is realizable.

My sincere gratitude goes to Dr. David Bevly for the providing me the opportunity to further my education under him. I'm not sure what prompted him to offer a graduate position to an "idiot" who was miserably failing his class, but whatever it was, I am very grateful for that. Throughout graduate school, Dr. Bevly's willingness to allow me to develop on my own while providing a challenging and dynamic environment for learning and research has been a true blessing in my life.

Thanks to all the GAVLAB members, past and present, for all their support, help, and endless knowledge. The countless distractions, debates, political discussions, sports arguments, frisbee sessions, coffee trips, and lunches made grad school a memory I will cherish.

Thanks to my parents for staying on me throughout. Their consistent support helped me to continue onwards and upwards.

Lastly and most importanly, thanks to my wonderful and loving wife Jill. Myself included, no other person has had to sacrifice more and put up with more than she has throughout these last 3 years. She has been my motivation and my inspiration, and without her unfailing love and support, I would not be where I am today. This thesis is dedicated solely to her.

Table of Contents

Abstract ii
Acknowledgments iii
List of Figures vii
List of Tables xi
1 Introduction 1
1.1 Motivation and Prior Work 1
1.2 Contributions 5
1.3 Thesis Outline 6
2 Modeling 7
2.1 Vehicle Modeling 7
2.1.1 Bicycle Model 8
2.1.2 Nonlinear Four Wheel Vehicle Model 13
2.2 Suspension Modeling 18
2.2.1 Quarter Car Model 18
2.2.2 Half Car Model 20
2.2.3 Full Car Model 22
2.2.4 Kinematic Suspension Effects 22
2.3 Tire Modeling 25
2.4 Vehicle Parameter Identification 30
2.4.1 Vehicle Inertia 30
2.4.2 Roll Center Height 32
2.4.3 Measured Parameters 34
2.4.4 Roll and Pitch Parameters 34

2.4.5 Cornering Stiffness . . . 36
2.5 Model Validation . . . 38
3 Vehicle Force Measurements Using Suspension Deflection and Strain . . . 46
3.1 Deflection . . . 46
3.2 Strain Theory and Strain Gauges . . . 47
3.3 Strain Suspension Forces . . . 49
3.4 Strain Gauge Selection and Circuit Design . . . 52
3.5 Suspension Strain Gauge Mounting . . . 59
4 Experimental Results and Analysis . . . 66
4.1 Experimental Setup . . . 66
4.2 Force Measurements Results . . . 72
4.2.1 Constant Radius Turn . . . 72
4.2.2 Sinusoidal Steering Input . . . 76
4.2.3 Detection of Wheel Liftoff . . . 80
4.2.4 Surface Variations - Transition between asphalt and gravel . . . 81
5 Conclusions and Future Work . . . 84
5.1 Conclusions . . . 84
5.2 Comments on Possible Error Sources . . . 85
5.2.1 Strain Gauge Bridge Circuit Installation . . . 85
5.2.2 GPS Lever Arm Effects and IMU misalignment . . . 87
5.2.3 GPS Latency . . . 88
5.2.4 Tire Model Inaccuracy . . . 89
5.2.5 Nonlinearity in steer angle at hand wheel (and at tires) . . . 89
5.2.6 Camber Thrust / Roll Steer compensation . . . 90
5.3 Future Work . . . 92
5.3.1 Intermediate Testing . . . 92
5.3.2 Implementing longitudinal force measurement methods . . . 93

5.3.3 Measurements on Varied Terrain and Surfaces 94
Bibliography 95
Appendices 98
A Prowler ATV Platform & Hardware 99
A.1 Vehicle Properties 99
A.2 Sensor Specifications 101
A.3 Computer System 103
B Circuit Diagrams 106

List of Figures

1.1 M.U.L.E. Unmanned Ground Vehicle 2

1.2 Research Motivation: ATV Rollover Prevention 3

2.1 The Lateral Bicycle Model 9

2.2 Various Tire Curves 10

2.3 Bicycle Model singularity at low velocity 12

2.4 Nonlinear Four Wheel Model Lateral Schematic 13

2.5 Vehicle Roll Model 15

2.6 Roll model free body diagram, showing sprung mass (left) and unsprung mass (right) 16

2.7 Vehicle Pitch Model 17

2.8 Quarter Car Suspension Model 18

2.9 Quarter Car Suspension Free Body Diagram 19

2.10 Half Car Suspension Model 20

2.11 Full Car Suspension Model 22

2.12 Suspension geometry and kinematic relationships showing undeflected (left) and deflected (right) 24

2.13 SAE Tire Coordinates 25

2.14 Comparison of various tire models. 27

2.15 Tire model - Effect of changing cornering stiffness, C_α 28

2.16 Pacejka and Dugoff Tire Models - Effect of varying F_z 29

2.17 Friction circle for F_z =3000 N and μ =0.87 29

2.18 SolidEdge model of prowler used to find inertias about primary axes. 32

2.19 Roll center height determination 33

2.20 Roll stiffness estimate using Ryu method[1] 35

2.21 Cornering stiffness calculation 37

2.22 Tire Comparison: All-trail or "Road" tire (left) vs. Off-road tire (right) . . . 38

2.23 Cornering stiffness values for various tires 38

2.24 Prowler ATV in the CarSIM Simulation Environment 39

2.25 Comparison of Vehicle Model to CarSIM Simulation - Sideslip 40

2.26 Comparison of Vehicle Model to CarSIM Simulation - Yaw Rate 40

2.27 Model Validation agains experimental data - Model Inputs 41

2.28 Model Validation agains experimental data with incorrect parameters - Angular Rates 42

2.29 Model Validation agains experimental data with incorrect parameters- Sideslip, Yaw Rate, and Lateral Velocity 42

2.30 Model Validation agains experimental data with incorrect parameters - Slip Angles 43

2.31 Model Validation agains experimental data - Angular Rates 44

2.32 Model Validation agains experimental data - Sideslip, Yaw Rate, and Lateral Velocity 44

2.33 Model Validation agains experimental data - Slip Angles 45

3.1 Suspension deflection potentiometer mounted parallel to the coil-spring assembly. 47

3.2 Lower Suspension A-Arm drawn in Solid Edge, in unloaded condition. 50

3.3 Lower suspension A-Arm loaded with a lateral load. 50

3.4 Upper Suspension A-Arm drawn in Solid Edge, in unloaded condition 51

3.5 Upper Suspension A-Arm loaded with a combined vertical and lateral load. . 51

3.6 Frequency Content of suspension deflection data 53

3.7 Data Acquisition Circuit showing PCB layout (left) and Schematic (right). (Shown full size in Appendix B) 54

3.8 Completed Data Acquisition Circuit housed in protective box. 54

3.9 Mounted Omega™ SGD-3/350-LY41 Strain Gauge on Chromoly (4130) Tubing 55

3.10 INA2126 Instrumentation Amplifier Circuit 56

3.11 MAX 680 Dual Charge Pump Voltage Converter Circuit 57

3.12 Instrumentation Amplifier and Signal Conditioning Circuit 59

3.13 Protective mounting of strain gauges. 60

3.14 Strain gauge mounting locations schematic. 61

3.15 Photo showing the mounting locations of the strain gauges. 61

3.16 Prowler shown on jackstands in order to isolate the sprung mass from the strain sensors and provide the initial offsets of the strain gauges 62

3.17 Static strain measurements of unloaded suspension components, (Top-Bottom: FL, FR, RR, RL tires) 63

3.18 Suspension Strain isolated from, then combined with the sprung mass 64

4.1 Prowler ATV Data Acquisition Flowchart 67

4.2 Septentrio GPS Antenna Mount 68

4.3 Crossbow IMU440 68

4.4 Steer Angle String Potentiometer 69

4.5 Advantech Ruggedized Computer for Data Logging 70

4.6 Prowler Data Collection - Transient Dynamic Maneuver 71

4.7 Prowler Data Collection - Constant Radius Turning 71

4.8 Steer Angle and Velocity for 50 ft. radius turn data run 73

4.9 Strain Gauge Lateral Force measurement for 50 ft. radius turn 73

4.10 Combined Strain Gauges measurement for 50 ft. radius turn 74

4.11 Vertical force measurement vs. Model forces for 50 ft. radius turn 76

4.12 Steer angle and velocity for sinusoidal steering data run 77

4.13 Strain gauge lateral force measurement for sinusoidal steering 78

4.14 Strain gauge lateral force measurement vs. model forces for sinusoidal steering 79

4.15 Vertical force measurement vs. model forces for sinusoidal steering 80

4.16 Front Wheel Strain Gauge Lateral Force Measurement vs. Total Vehicle Force for 50 ft. radius turn 81

4.17 Strain gauge lateral force measurement of surface transition between asphalt and gravel 82

5.1 Strain Gauge Bridge Circuit for measurement of Axial Strain Only (rejects bending strain) 85

5.2 Strain Gauge Bridge Circuit for measurement of Bending Strain Only (rejects axial strain) 86

5.3 Lateral deformation of an ATV tire during cornering 89

5.4 Effects of camber thrust and roll steer from suspension jounce and rebound . 91

5.5 Future Work: Intermediate testing of the Prowler suspension components . . 93

5.6 Future Work: Testing the Prowler ATV on various types of terrain and surfaces 94

A.1 Prowler ATV 100

A.2 Crossbow IMU440 101

A.3 Septentrio Three-Antennae PolaRx2e GPS System 103

A.4 Prowler Hardware and Component Case 104

A.5 Advantech Ruggedized Computer for Data Logging 104

B.1 Data Acquisition Circuit Schematic 107

B.2 Data Acquisition Circuit PCB layout 108

List of Tables

2.1 ATV Suspension parameters identified by Chang 31

2.2 Inertial ATV parameters identified by Warner 31

2.3 Prowler ATV measured parameters 34

2.4 Prowler ATV estimated parameters - roll and pitch stiffness and damping . . 35

2.5 Prowler ATV estimated parameters - roll and pitch stiffness and damping . . 35

3.1 Material properties 48

3.2 Strain circuit gain and filtering values 56

Chapter 1

Introduction

Improving Unmanned Ground Vehicle systems has been a major focus of both industry and government sectors in recent history. Tire and suspension forces are an integral part of the vehicle dynamic analysis needed for many of these systems to function. The tire forces are known to have a direct and dramatic impact on the stability of off-road vehicles. The tire contact patch is the critical vehicle-to-terrain interaction point. Having as much knowledge as possible about this junction of the system can provide information about limit handling (i.e. – how steep of a hill can this vehicle traverse, how slippery of a road can this vehicle turn on at a given velocity). ATV's, as indicated in their name All-Terrain Vehicles, are very capable of traversing very difficult and challenging terrain. Furthering the knowledge of off-road vehicle systems will allow for the vehicle to extend its performance capabilities and potentially traverse terrain previously thought impassable. There are many applications where navigation and path-planning can benefit from real-time knowledge of the tire and suspension forces. For example, allowing tire properties to be estimated would be critical in determining the speed with which a corner can be taken. Knowing this maximum attainable lateral force, and consequently a safe operating velocity can affect the desired trajectory of the vehicle while traversing terrain.

1.1 Motivation and Prior Work

Improving unmanned systems has been a major focus of both industry and government sectors in recent history. The US Army implemented the Future Combat Systems in 2003, with the goal of improving its battlefield capabilities. One of these directives was the development and deployment of unmanned vehicles, specifically ground vehicles. Though this

Figure 1.1: M.U.L.E. Unmanned Ground Vehicle

program was cancelled in 2009, many sections of the military continue to pursue advancements in the dynamic analysis and control of unmanned ground vehicles as part of their modernization, such as the Army's Brigade Combat Team Modernization (BCTM). The research presented in this thesis seeks to further investigate analysis in the areas related to improved understanding of unmanned ground vehicle dynamics and control.

Nearly every automobile manufacturer today incorporates some sort of stability control system into the standard equipment of their product. The benefits of stability control were so marked that in 2006, the National Highway Transportation Safety Administration required that all passenger cars, multipurpose passenger vehicles, trucks, and buses with a gross vehicle weight rating of 4,536 kg (10,000 pounds) or less be outfitted with an electronic stability control system [2]. There is significant literature available in the areas of vehicle state estimation and parameter identification, which has led to marked improvements in recent years toward safety systems that operate well in a variety of weather conditions, road parameters, as well as varying tire and vehicle types [10, 22, 30]. However, this prior research is heavily focused in the areas of passenger vehicles and vehicles that drive primarily on roads such as trucks and SUVs. The ATV and off-road industry sell and develop numerous vehicles each year, but very few of these systems incorporate an effective system to assist with stability control. The need for this research, demonstrated in Figure is compounded by the fact that ATVs and off-road vehicles tend to drive on terrains that are much more

Figure 1.2: Research Motivation: ATV Rollover Prevention

conducive to rollover situations, such as steep hills, muddy inclines, and rugged ground, as well as the vehicle setup, often having a high center of gravity due to ground clearance requirements. These driving conditions provide significant motivation towards developing knowledge and furthering improvement of ATV stability control systems. A key component of enhancing those vehicle stability control systems is accurate knowledge of the tire and suspension forces over a wide variety of suspension setups and terrain interactions.

On-road vehicles can be dramatically different in performance and handling characteristics when compared to small ATVs. However, many of the dynamic and kinematic estimation techniques used to ascertain information about the vehicle can be adapted to work for ATVs. Bevly, Travis, and Daily explored numerous methods to identify many critical vehicle parameters and vehicle states such as sideslip, roll angle, cornering stiffness, and slip angles [8, 7, 6, 11, 19, 20]. Accurately identifying vehicle parameters is critical to many estimation techniques, as many of these model based methods are sensitive to errors in the model, such as incorrect weight split [3].

Researchers have begun to address many of the issues associated with off-road vehicle dynamic analysis. Improved methods of identifying key parameters of specific types of ATV's, including side-by-side RUVs (Recreational Utility Vehicles) were shown in [29]. Warner's work showed that ATVs are significantly more sensitive to changes in parameters such as

CG (center of gravity) height, track width, tire properties, suspension properties, and driver interactions. Additional properties with the potential to vary dramatically are the intertial properties that affect the attitude dynamics of the vehicle. A method for identifying these inertial properties using a pendulum based technique and suspension response analysis is presented in [29].

Due to the very low operating pressure of many ATV tires, the contact patch is highly deformable and very difficult to model accurately. Further complicating this issue is the addition of system disturbances in the form of rocks, mud, sticks, and other types of irregular terrain that cause deformations in the tire contact patch which affect the tire dynamics and subsequently the handling properties of the vehicle. More commonly used models such as the point contact tire model do not sufficiently capture desired effects of the aforementioned scenarios. [9] expanded upon a method presented in [4] that incorporates a series of radial and interradial springs for modeling the highly deformable and nonlinear tires of typical ATVs . This work also developed methods to allow for the tire model to leave the ground, which frequently occurs during normal operation of ATVs in off-road environments.

Other researchers have attacked the difficult task of tire modeling through exploring new sensing techniques. One method attempted to capture ATV tire properties experimentally by changing the load and slip angle of the tire and measuring the force generated over varying surfaces, such as clay and gravel[21]. Capacitive-resistive sensors can be implemented into the tire to directly measure the deformations of the tire contact patch and calculate critical tire properties based off of those measurements [26]. Similarly, vision based tracking measurements can be used to capture the contact patch deformation [15] . Rather than directly attempting to sense the contact patch, other methods focus on trying to capture the forces as they are transferred from the tire to the wheel and suspension linkages. Ohori developed a "smart tire" with strain gauges mounted on each of 5 spokes of a vehicle wheel [23]. The smart tire was tested on a drum in a laboratory setting, but the results were shown

to be practically useful with the potential for future development of this data collection method for dynamic analysis.

Drawing on the many resources presented in this section, the goal of this thesis is to combine some of the methodologies and ideas presented above in an effort to analyze the tire and suspension forces experienced by UGVs and ATVs during dynamic maneuvers.

1.2 Contributions

The focus of the research presented in this thesis is the improvement of tire force estimation using strain gauge sensors and displacement sensors mounted on the suspension. To accomplish this, an investigation of off-road vehicle modeling must be done. A very accurate off-road vehicle model must be developed, and that developed vehicle model will be used to estimate tire forces based off of sensors already installed on the vehicle. In addition to the modeling contributions, this thesis presents a method to incorporate suspension strain gauge measurements to improve tire force estimation and decouple the forces at the tire contact patch into vertical, lateral, and longitudinal components.To that end, the following contributions are made:

- Developed a "full" vehicle model that attempts to completely capture the vertical and lateral tire forces at the tire contact patch, including effects from roll and pitch.
- Experimentally determined values of Prowler ATV parameters used in modeling and control algorithms.
  - Inertias
  - Cornering Stiffness for Multiple Tires
  - Roll Center (s) Height
  - Roll & Pitch Stiffness and Damping

- Developed a method for directly measuring forces in the suspension linkages using strain gauges and potentiometers.
- Developed a method to use the results of suspension force measurements to assist in tire modeling and tire curve analysis An analysis of a test vehicle platform is conducted and an accurate vehicle model is presented with accurately identified vehicle parameters.
- A proven design methodology for mounting, data acquisition, and integration of measurements of suspension strain and suspension deflection is presented.

1.3 Thesis Outline

Chapter 2 discusses of various vehicle models and their application to off-road vehicle modeling. Various tire models are compared in their usefulness and application to off-road performance. Additionally, suspension models are derived and compared. The chapter concludes with the development of the integrated model developed for this thesis, combining vehicle, suspension, and tire models into a single model for analysis. The model is validated against experimental data and CarSIM, a software that provides a very accurate simulation environment using very thorough parameters taken from the vehicle. Chapter 3 details the design methodology for measuring forces at the tire using two different sensing techniques: suspension deflection and strain gauges mounted on the suspension linkages. The hardware setup is presented, and data is collected and analyzed using the two different sensor sets. Chapter 4 shows experimental results and data from performing various types of dynamic maneuvers on normal terrain (level asphalt). Analysis of the results is provided and potential applications of the measurements are examined. Chapter 5 provides conclusions, commentary on possible sources of area, and areas for future work and improvement.

There are also appendices that highlight the Prowler ATV data collection platform and the full sensor specifications of the test platform as well as the circuit diagrams of the data acquisition system.

Chapter 2

Modeling

A very accurate vehicle model can dramatically improve the performance of vehicle estimation and control algorithms. In fact, many models and estimation techniques require a very accurate and thorough knowledge of vehicle parameters and states to operate. However, many of these values can be difficult to measure, and even sometimes difficult to calculate or estimate within the model. In addition to the difficulty of finding the values, the math required on some of the more complex models can be computationally intensive which can make algorithms virtually ineffective to implement in a real-time environment. A much simpler vehicle model will not accurately capture the total effect of the vehicle but can iterate quickly and has real-time capabilities. Therefore, it is important to consider these tradeoffs between simplicity, speed, and model accuracy when looking at vehicle parameters and models. Because the ultimate direction of this research is application in a real-time, real-world environment, the most complicated model that accurately captures the suspension and tire force dynamics while still allowing for a reasonably fast iteration to allow for real-time implementation is the desired model. While the specifications for how fast "real-time" is for this application may vary depending on the desired control strategy, an iteration time of roughly 0.01 - 0.1 seconds could be considered reasonable for most implementations. This is not a design constraint so much as a general theme and consideration in the development of this vehicle model.

2.1 Vehicle Modeling

To begin a discussion on vehicle modeling, the simplest model is usually a good starting point. From there, additional parameters, degrees of freedom, and constraints can be applied

to account for additional dynamics and characteristics as needed. In vehicle modeling literature, the de facto standard is the two wheel bicycle model. The bicycle model is a relatively simple model that works well in low dynamics environments. Varying dynamic maneuvers will affect the need for more complex models as many vehicle systems are highly nonlinear and require detailed models to accurately capture dynamics. Lower order and lower degree of freedom models are often not desirable for applications involving high speeds, large slip angles, weight transfer, and large accelerations [27]. Some applications of this thesis involve relatively low speeds, low accelerations, and low slip angles so many of the model simplifications and linearizations presented in this chapter may be utilized in those situations. Of note, all models are developed based on a specific test platform, the Prowler All-Terrain Vehicle. A detailed look at the Prowler ATV is presented in Appendix A.

2.1.1 Bicycle Model

Due to its relative simplicity and ease of use, the bicycle model is one of the primary tools used in ground vehicle modeling [8]. It can be used as a kinematic or kinetic model, or both, depending on the needs of the model. The model is formed by lumping the inner and outer front axle components together and the inner and outer rear axle components of a four-wheeled vehicle together to form one front and rear axle. In both kinematic and kinetic bicycle models, the central point for summation of forces and moments is the Center of Gravity (CG) of the vehicle. This is located some distance (a) from the front axle and some distance (b) from the rear axle. Lateral and longitudinal tire forces at both tires drive the dynamics of the model. The velocities at each wheel are also taken into account, thus providing additional parameters known as slip angles (α) at each tire. These slip angles are the difference in the direction the wheel is facing (heading) and the direction of the wheel velocity vector. Additionally, there is a slip angle (β)of the total vehicle which is similarly defined as the difference between the vehicle heading and the vehicle velocity vector (course). Figure 2.1 shows the lateral bicycle model, including each of the above defined variables.

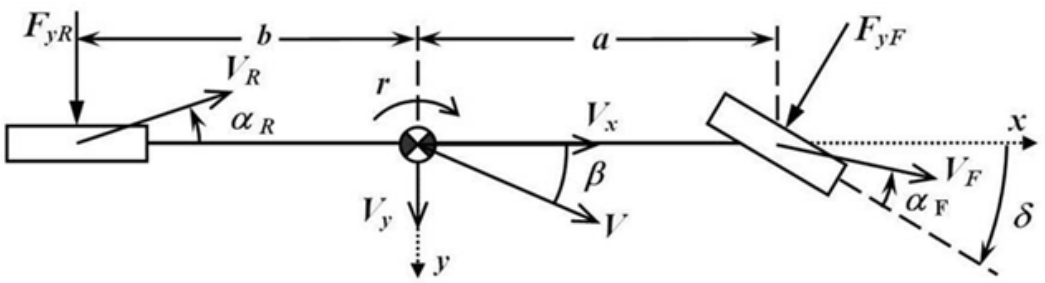

Figure 2.1: The Lateral Bicycle Model

Finding the sum of the forces of the CG in the y-direction and the sum of the moments about the vertical z-axis gives the lateral dynamics equations of motion for the model.

$$\sum F_y = m\ddot{y} = F_{yF}\cos(\delta) + F_{yR} + F_{xF}\sin(\delta) \tag{2.1}$$

$$\sum M_z = I_z\ddot{\psi} = aF_{yF}\cos(\delta) + aF_{xF}\sin(\delta) - bF_{yR} \tag{2.2}$$

As seen from the free body diagram, while the steer angle is the primary input to the model, it is the tire forces that truly drive the dynamics of the system. Tire force models will be discussed in more detail in Section 2.3, but it is important to note that for the bicycle model, the tire forces frequently operate in a region of the tire curve that can be approximated by a linear relationship, as seen in Figure 2.2.

This linear relationship between the cornering stiffness (C_α) and slip angle (α) at the tire is shown in Equations (2.3) and (2.4). Note that the sign convention is such that it associates positive forces with negative slip angles.

$$F_{yf} = -C_{\alpha f}\alpha_f \tag{2.3}$$

$$F_{yr} = -C_{\alpha r}\alpha_r \tag{2.4}$$

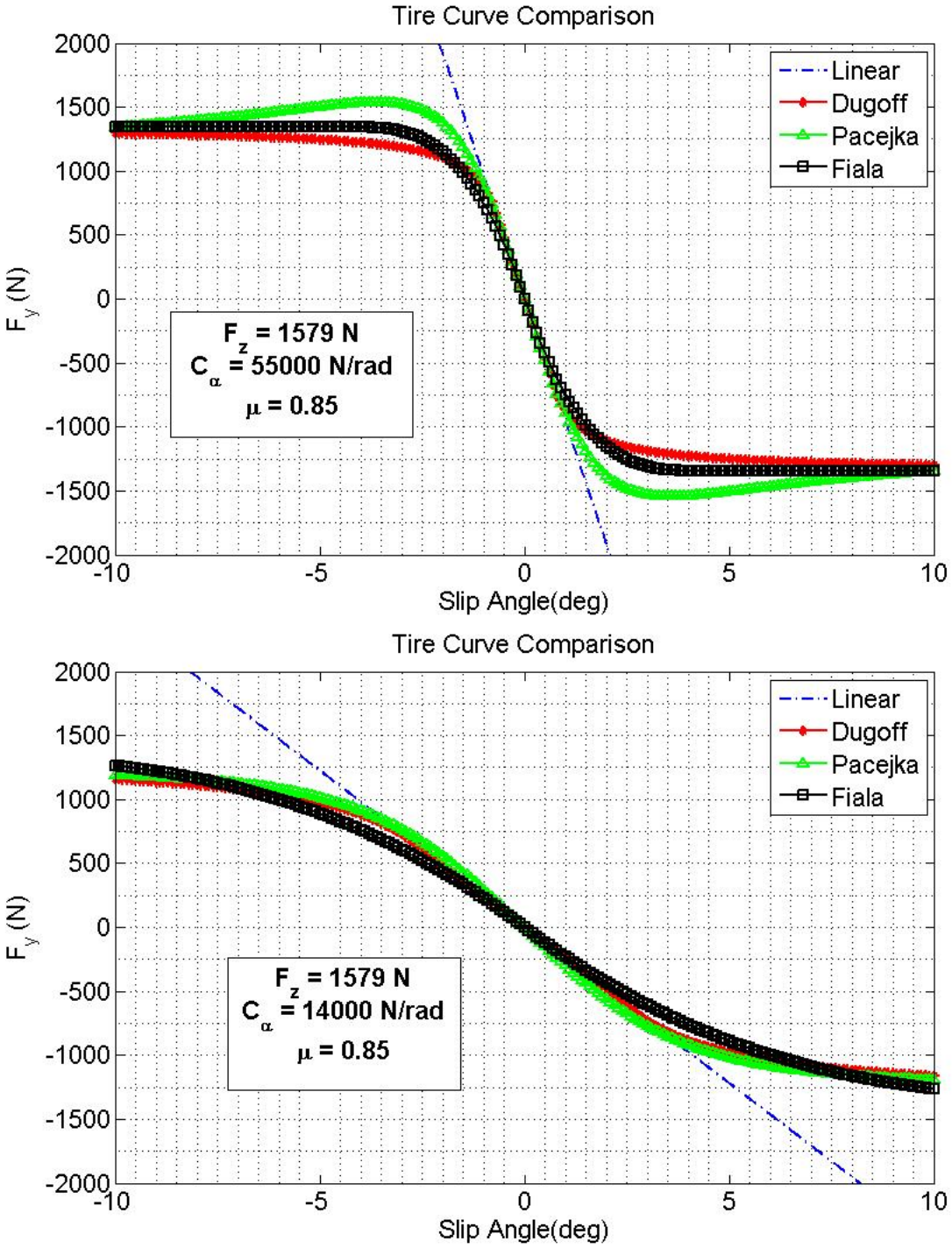

Figure 2.2: Various Tire Curves

Using the linear tire force relationships, assuming small angles, linearizing about the vehicle states, and solving for yaw acceleration, $\dot{r}$, and sideslip rate,$\dot{\beta}$, the equations can be placed into a state space form, as shown in Equation (2.5).

$$\begin{bmatrix} \dot{\beta} \\ \dot{r} \end{bmatrix} = \begin{bmatrix} \frac{-C_{\alpha f}-C_{\alpha r}}{mV} & \frac{-aC_{\alpha f}+bC_{\alpha r}}{mV^2} - 1 \\ \frac{-aC_{\alpha f}+bC_{\alpha r}}{I_z} & \frac{-a^2C_{\alpha f}-b^2C_{\alpha r}}{I_z V} \end{bmatrix} \begin{bmatrix} \beta \\ r \end{bmatrix} + \begin{bmatrix} \frac{C_{\alpha f}}{mV} \\ \frac{aC_{\alpha f}}{I_z} \end{bmatrix} \delta \tag{2.5}$$

The linear bicycle model operates on the assumption that linearization holds based on the small angle approximation. However, it is important to note that often in experimental use of ATVs, and more specifically the test platform used for data collection in this research, many of the steer angles and sideslip angles approach 40 deg and therefore invalidate the assumption of small angles for some of the maneuvers performed later in this thesis. Additionally of note is the dependency of velocity on the bicycle model. In deriving the bicycle model, it is inherently assumed that the velocity is constant. The bicycle model can be used in simulation for varying velocities by calculating the A and B matrices at each step using the current vehicle velocity state and then propagating the states using the linear simulation toolbox in MATLAB, or by simply propagating the equations of motion and integrating the derivatives using simple trapezoidal integration. Using experimental steer angle and velocity measurements, the bicycle model was simulated in MATLAB to validate the bicycle model. One problem that quickly became apparent was the negative effects of low velocity. Due to the fact that the velocity is effectively a parameter in the denominator of the terms of the A matrix, low values of velocity can cause numerical issues when the velocity value falls below a certain threshold, as seen in Figure 2.3. There is also a singularity in the model when $V = 0$ m/s. In order to account for this singularity, a threshold was selected to prevent the model from becoming unusable when blending the model with experimental data.

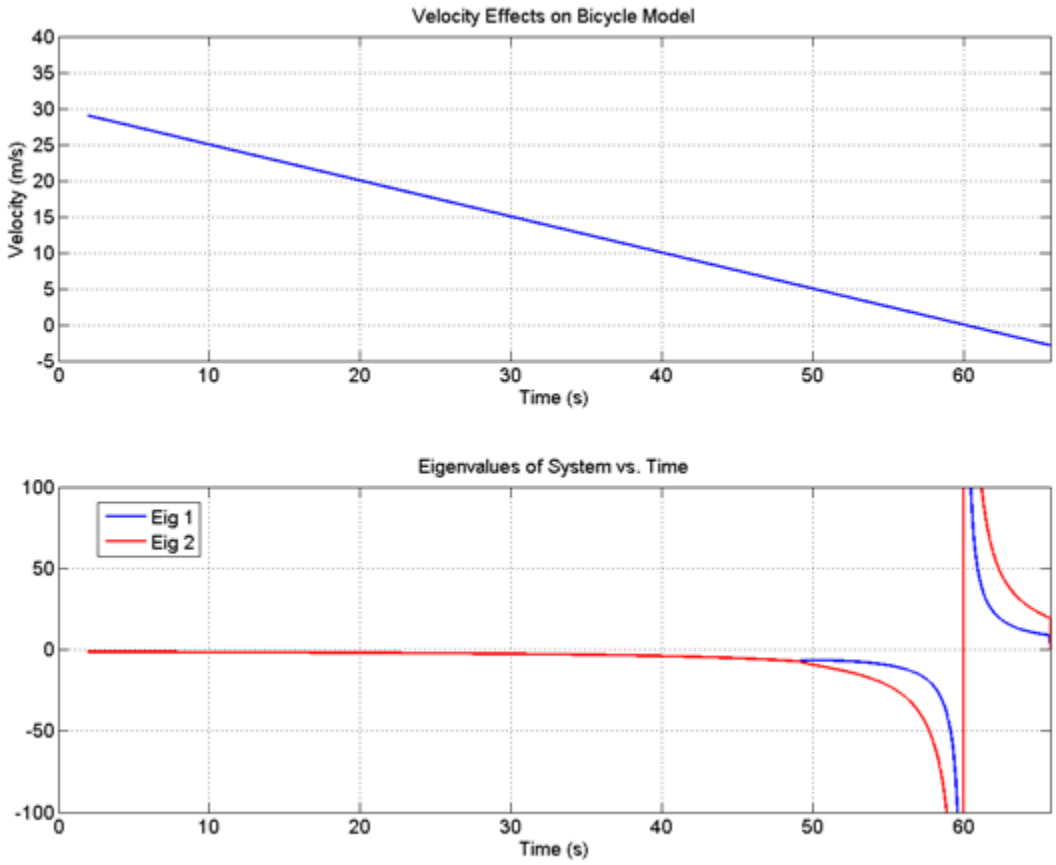

Figure 2.3: Bicycle Model singularity at low velocity

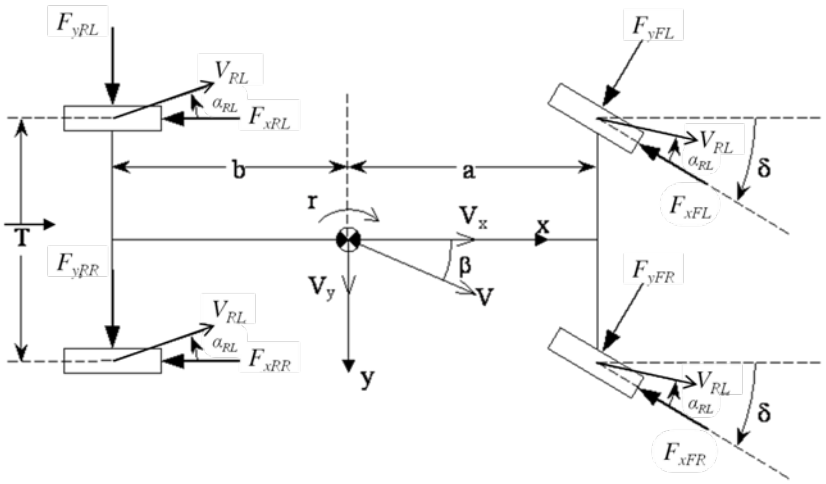

Figure 2.4: Nonlinear Four Wheel Model Lateral Schematic

2.1.2 Nonlinear Four Wheel Vehicle Model

When more complex analysis of dynamics is desired, modifications must be made to the vehicle model to incorporate these dynamics. The bicycle model is very simplistic and has limitations that can prevent this additional needed analysis, such as neglecting the roll and weight transfer between inner and outer wheels. Also, as discussed in the previous section, due to the potential for large angles of vehicle attitude (sideslip, roll, pitch, and yaw) as well as model inputs (steer angle), there exists the possibility of the linearization assumptions of small angles to break down. To account for these angles and add additional levels of complexity for force analysis including weight transfer and nonlinear tire models, the following section details the derivation of a nonlinear 4-wheel vehicle model. This model will be comprised of a lateral model combined with a roll and pitch model.

Figure 2.4shows the lateral yaw dynamics about the vehicle z-axis.

Summing the forces and moments about the CG gives the following lateral equations of motion.

$$\sum F_y = m\ddot{y} = (F_{yFL} + F_{yFR})\cos\delta + (F_{xFL} + F_{xFR})\sin\delta + (F_{yFL} + F_{yRR}) \tag{2.6}$$

$$\sum M_{CG} = I_z\ddot{\psi} = a(F_{yFL}\cos\delta + F_{yFR}\cos\delta - F_{xFL}\sin\delta - F_{xFR}\sin\delta)$$
$$-\tfrac{t_F}{2}(F_{yFL}\sin\delta - F_{yFR}\sin\delta - F_{xFL}\cos\delta + F_{xFR}\cos\delta) - b(F_{yRL} + F_{yRR}) - \tfrac{t_R}{2}(F_{xRL} - F_{xRR}) \tag{2.7}$$

Note that this model assumes that the steer angle is the same on both the front and left sides of the front axle. Also note that the direction of steer angle is defined positive to the right, such that a positive steer angle generates a positive yaw rate.

The sideslip angle, β, is the angle between the vehicles actual velocity vector, V, and the longitudinal velocity component, V_x. The GPS definition of sideslip is also useful for this analysis, and can be defined as the GPS course measurement, ν, minus the GPS heading measurement, Ψ, as shown in Equation 2.8.

$$\beta = \nu - \Psi \tag{2.8}$$

This slip angle will be a critical component of both the model and the experimental data. Using the sideslip, the slip angle at each of the wheels can be deterimined using Equation 2.9.

$$\begin{aligned} \alpha_{fL} &= \tan^{-1}\left[\frac{V\sin\beta + ra}{V\cos\beta + r\frac{t_f}{2}}\right] - \delta_f \quad \alpha_{fR} = \tan^{-1}\left[\frac{V\sin\beta + ra}{V\cos\beta - r\frac{t_f}{2}}\right] - \delta_f \\ \alpha_{rL} &= \tan^{-1}\left[\frac{V\sin\beta - rb}{V\cos\beta + r\frac{t_r}{2}}\right] - \delta_r \quad \alpha_{rR} = \tan^{-1}\left[\frac{V\sin\beta - rb}{V\cos\beta - r\frac{t_r}{2}}\right] - \delta_r \end{aligned} \tag{2.9}$$

Looking at the other degrees of freedom, the roll of the vehicle can be defined as the angular orientation about the vehicle x-axis. Figure 2.5shows the roll dynamic model. The mass is treated as an elevated mass that rotates about a defined point called the roll center. this roll center is not a stationary point, and must be calculated by looking at the suspension geometry. As the suspension geometry changes, the roll center location also changes. This point is physically important because it is the point where forces at the tire act through the body in the roll coordinate frame. Although the roll center is not stationary, assuming it to be in the centerline of the vehicle and constant simplifies the model and is assumed for this

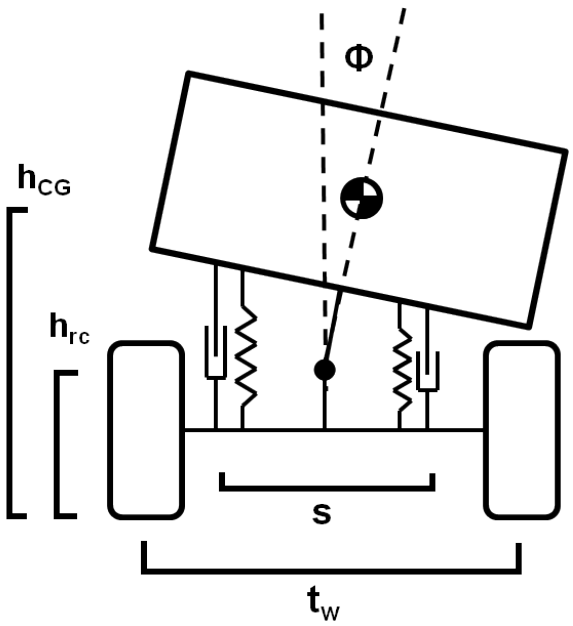

Figure 2.5: Vehicle Roll Model

work. Note the height of the roll center, h_{rc}, and the height of the center of gravity, h_{cg}, are not co-located.

Separating the unsprung mass, m, and the sprung mass, M, the free body diagram is seen in Figure 2.6.

Summing the moments of the sprung mass about the roll center yields the roll equations of motion, Equation 2.10.

$$\sum M_{rc} = I_x\ddot{\phi} = -B_\phi\dot{\phi} - K_\phi - m\ddot{y}h_1 cos\phi + mgh_1 \sin\phi - M_{arb} \tag{2.10}$$

Note that in this model, the force from the suspension spring and dampers are lumped into a singular roll stiffness for simplification. However, these parameters B_ϕ and K_ϕ account for the suspension spring and damping values, tire spring and damping values, and kinematic relationships of the suspension all in one term . Also note, $h_1$is the difference between the center of gravity height, h_{cg}, and the roll center height, h_{rc}.

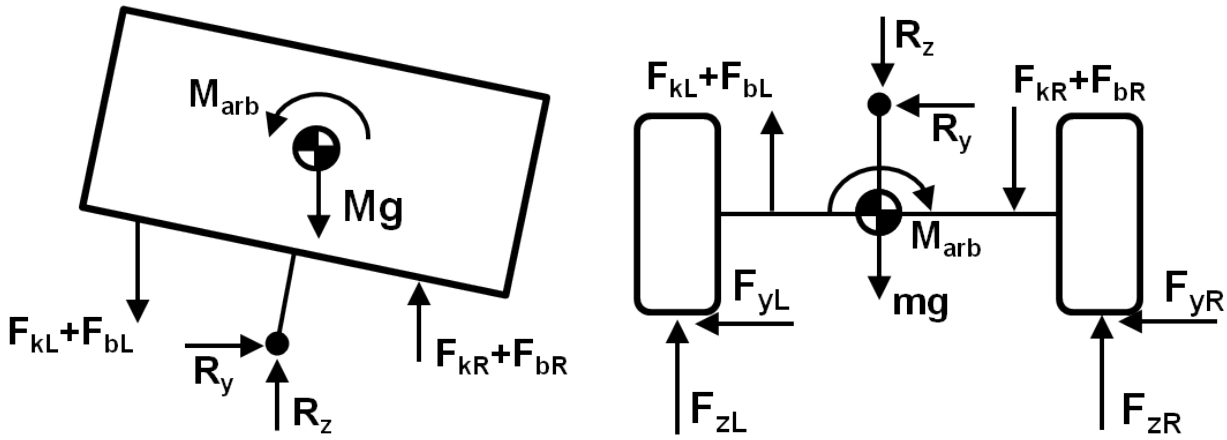

Figure 2.6: Roll model free body diagram, showing sprung mass (left) and unsprung mass (right)

In looking at the roll model, realtionships for the lateral weight transfer, ΔF_z, can be found by summing the forces about the roll center for the unsprung mass. This yields the relationship in Equation 2.11.

$$\sum M_{rc} = I_x\ddot{\phi} = 0 = \frac{t}{2}(F_{zL} - F_{zR}) + h(F_{yL} + F_{yR}) + B_\phi\dot{\phi} + K_\phi + M_{arb} \tag{2.11}$$

Summing the forces in the y-direction for both the sprung and unsprung masses and equating the reaction forces at the roll center give the following relationship.

$$-m\ddot{y} = -(F_{yL} + F_{yR}) \tag{2.12}$$

Substituting Equation 2.12 into Equation 2.11, and solving for the front and rear individually, the following equations are obtained for the lateral weight transfer due to vehicle roll.

$$\Delta F_{zf} = [B_{\phi f}\dot{\phi} + K_{\phi f}\phi + h_f m(\dot{V}sin\beta + V\dot{\beta}cos\beta + rVcos\beta)]/t_f \tag{2.13}$$

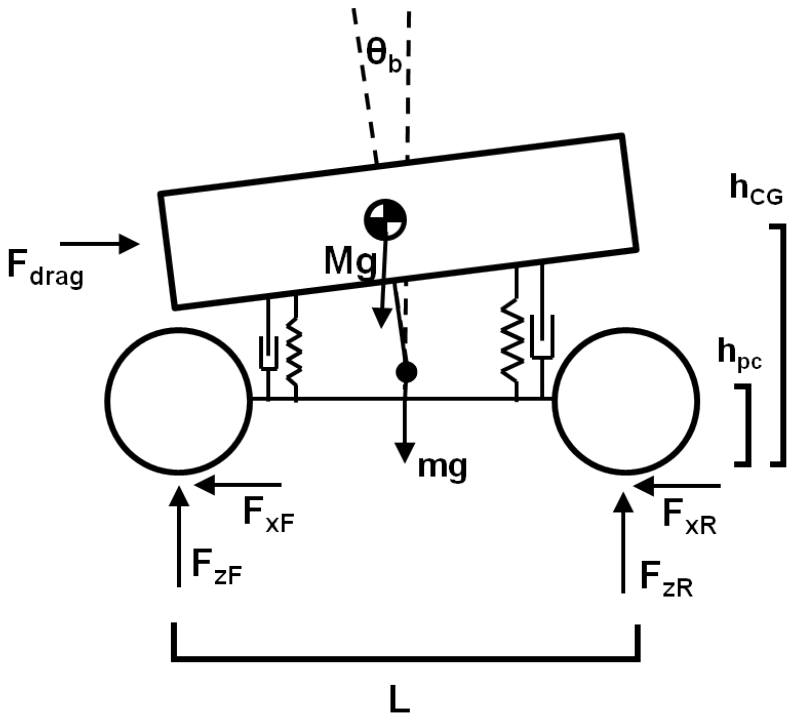

Figure 2.7: Vehicle Pitch Model

$$\Delta F_{zr} = [B_{\phi r}\dot{\phi} + K_{\phi r}\phi + h_r m(\dot{V}sin\beta + V\dot{\beta}cos\beta + rVcos\beta)]/t_r \tag{2.14}$$

Finally, the model for the final degree of freedom of the vehicle model, pitch, is shown in Figure 2.7. The pitch motion is defined about the vehicle y-axis.

The pitch equations of motion are derived analogous to the roll equations of motion, simply changing the subscript labeling to match the pitch coordinates.

$$\sum M_{pc} = I_y\ddot{\theta} = -B_\theta\dot{\theta} - K_\theta - m\ddot{x}h_1 cos\theta + mgh_1 \sin\theta \tag{2.15}$$

Like the roll model, this model also lumps the force from the suspension spring and dampers into a singular pitch stiffness and pitch damping for simplification. These values of roll and pitch stiffness and damping will be estimated using experimental data from the vehicle in Section 2.4.

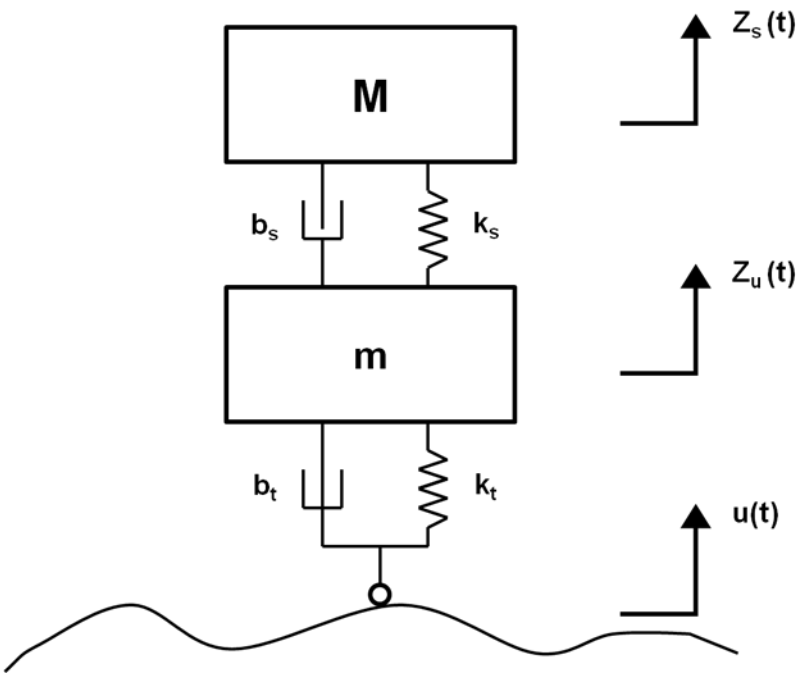

Figure 2.8: Quarter Car Suspension Model

2.2 Suspension Modeling

2.2.1 Quarter Car Model

The quarter car suspension model looks at an individual wheel assembly and the vertical travel of a sprung mass (representing the vehicle) and an unsprung mass (representing the tire) mass. This is the simplest of all suspension models used for analysis, but also provides the least amount of information to the overall state of the total vehicle. The primary input is the road surface and the output is the acceleration, velocity, and position of the sprung (vehicle) and unsprung (tire) mass. The model has two degrees of freedom, one representing the motion of the tire and the other representing the motion of the sprung mass (vehicle body). Figure 2.8 shows the quarter car suspension model.

The free body diagram of a quarter car suspension is seen in Figure 2.9.

Where:

$$F_{bs} = b_s(\dot{z_u} - \dot{z_s}) \tag{2.16}$$

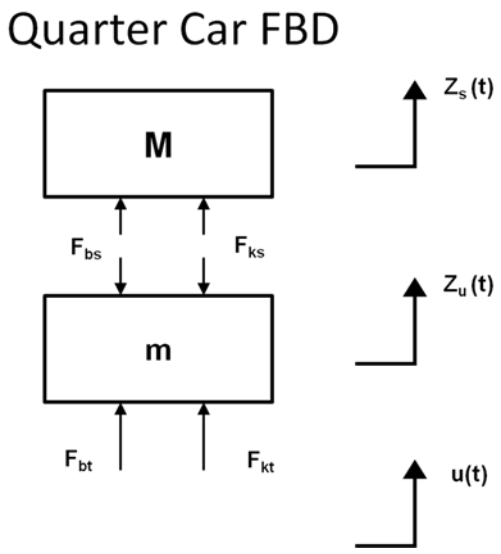

Figure 2.9: Quarter Car Suspension Free Body Diagram

$$F_{bt} = b_t(\dot{u_s} - \dot{z}_u) \tag{2.17}$$

$$F_{ks} = k_s(z_u - z_s) \tag{2.18}$$

$$F_{kt} = k_t(u_t - z_u) \tag{2.19}$$

This creates a first order state matrix where:

$$[\mathbf{x}] = \begin{bmatrix} x_s \\ x_u \\ z_s \\ z_u \end{bmatrix} \tag{2.20}$$

The system can now be written in state space representation. Summing the forces and moments from the free body diagram of Figure 2.9, the following equations of motion are derived:

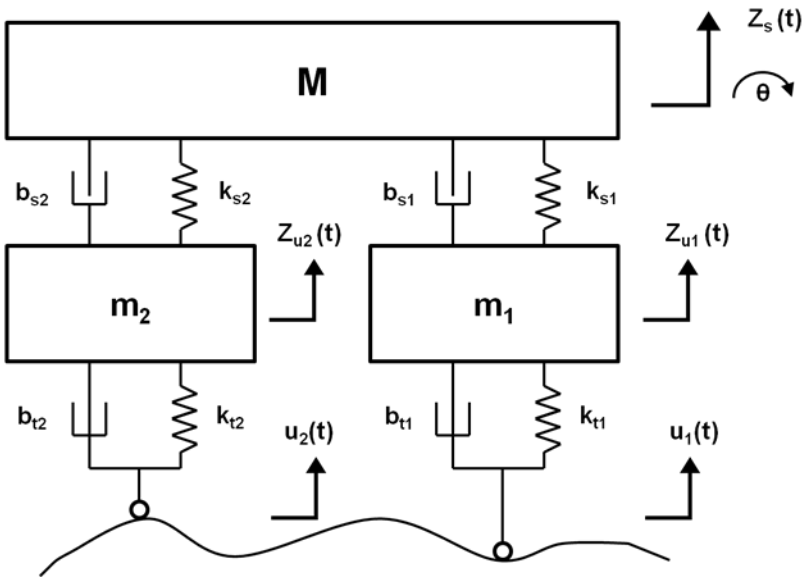

Figure 2.10: Half Car Suspension Model

$$[\dot{\mathbf{x}}] = \begin{bmatrix} \frac{-b}{m} & \frac{b}{m} & \frac{-k_s}{m} & \frac{k_s}{m} \\ \frac{b}{m} & \frac{-b}{m} & \frac{k_s}{m} & \frac{-(k_s+k_t)}{m} \\ 1 & 0 & 0 & 0 \\ 0 & 1 & 0 & 0 \end{bmatrix} [\mathbf{x}] + \begin{bmatrix} 0 \\ \frac{k_t}{m} \\ 0 \\ 0 \end{bmatrix} u \tag{2.21}$$

In developing the free-body diagram for the quarter car suspension, it is important to note the relative motions between the ground (u), the unsprung mass (z_u), and the sprung mass (z_s). These relative motions and their respective velocities will impact the forces of the dampers and springs connected to the masses.

2.2.2 Half Car Model

The half car model is similar to the quarter car model, but includes the addition of an extra degree of freedom (θ) which accounts for the pitch of the vehicle. The model can be used as a horizontal model, looking at only the front or rear axle, for example. However, the more common use of the model is in the longitudinal frame.

Including an additional state to account for the added degree of freedom, the state vector can be defined as:

$$[\mathbf{x}] = \begin{bmatrix} x_1 \\ x_2 \\ x_3 \\ x_4 \\ z_1 \\ z_2 \\ z_s \\ \theta \end{bmatrix} \tag{2.22}$$

Summing the forces and moments from the free body diagram of the half car model, the equations of motion can be derived. Because of the introduced pitch equations, the half car model is nonlinear, unlike the previous quarter car model. However, the angle can reasonably linearized about an operating point of $\theta = 0$ deg. This approximates the trigonometric functions to:

$$\sin\theta \approx \theta \tag{2.23}$$

$$\cos\theta \approx 1 \tag{2.24}$$

A 0 deg operating point can be assumed to be valid because the roll of the body in the body coordinate frame is relatively low. A vehicle does not typically experience more than 10 deg to 15 deg of body roll in normal maneuvers. There can be cases in extreme off-road environments where this assumption may no longer be valid. It should be noted that this body frame roll angle assumption does not limit large angles of road bank and road grade.

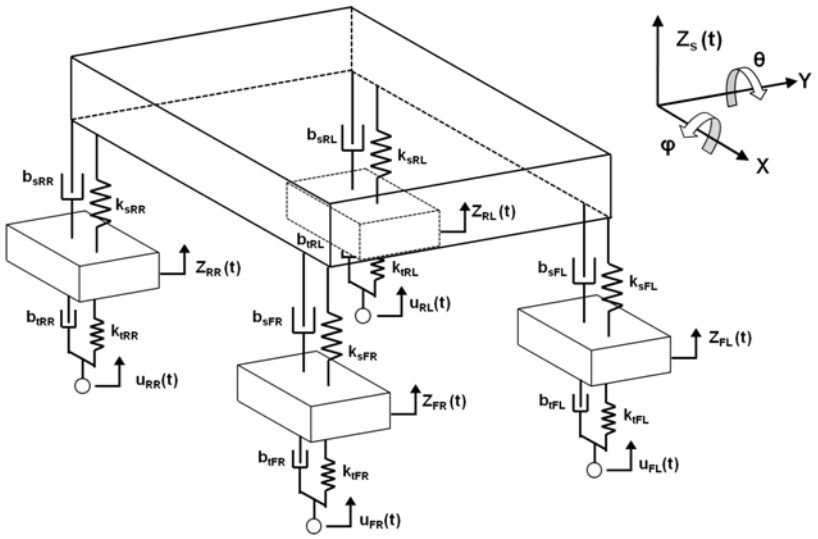

Figure 2.11: Full Car Suspension Model

However, the body frame does not directly see these large angles and therefore the small angle assumption will still remain valid.

2.2.3 Full Car Model

Similar to the half car model, the full car model is also nonlinear due to the combined pitch and roll equations of the model. Figure 2.11 shows the full car model and its coordinate frame. The same small angle approximation is still valid in this case however, thus allowing for linearization about an operating point of $\theta = 0$ deg.

Developing the free body diagram and summing the forces and moments gives the equations can be place in linearized state space format in a similar fashion to the quarter car and half car models. The full equations are then integrated into the vehicle model.

2.2.4 Kinematic Suspension Effects

It is important to take into account suspension geometry and kinematic relationships when modeling suspension components. There are multiple linkages and the spring and damper can be attached in a number of positions depending on the desired performance characteristics. The model is intended to resemble the suspension on the test vehicle as

closely as possible. First, a kinematic suspension model is developed, which translates vertical motion and forces at the tire contact patch into motion and forces as it relates to the body through the installation ratio. Secondly, this model is incorporated / nested into a full vehicle suspension model to account for the total vehicle states. Using the geometry from Figure 2.12, the vertical force introduced into the system can be related to the deflection of the suspension spring assuming that the suspension acts like a linear spring with a stiffness of (k_s).

Assuming the linear spring force, we can write F_z in terms of the spring stiffness and the deflection.

$$F_z = k_t \Delta z_u \tag{2.25}$$

Looking at the geometry of the upper a-arm from z_u and Δl, the relationship can be written as Equation 2.26.

$$\Delta z_u = (a+b)\frac{\Delta l}{a} \tag{2.26}$$

Substituting Equation 2.26 into Equation 2.25, the following relationship is obtained to relate the vertical force at the tire, F_z, to the suspension deflection, Δl. Note that for the prowler, a=5 inches and b=6.5 inches, which gives a ratio of 2.3.

$$F_z = \frac{(a+b)}{a} k_s \Delta l = 2.3 k_s \Delta l \tag{2.27}$$

To verify this, the Prowler was placed on jacks therfore isolating the suspension components and guaranteeing that $F_z = 0N$. Then, the Prowler was lowered off of the jacks and allowed to come to rest on the ground. The deflection change during these two static points should be equal to the F_z that was applied to the vehicle, or the percentage of the total weight resting on each wheel. When comparing these deflections, an effective spring stiffness of 158,780 N/m was calculated. When compared to the manufacturer provided value of 65,000 N/m per spring (for the suspension spring), the ratio is equal to 2.44. This proves

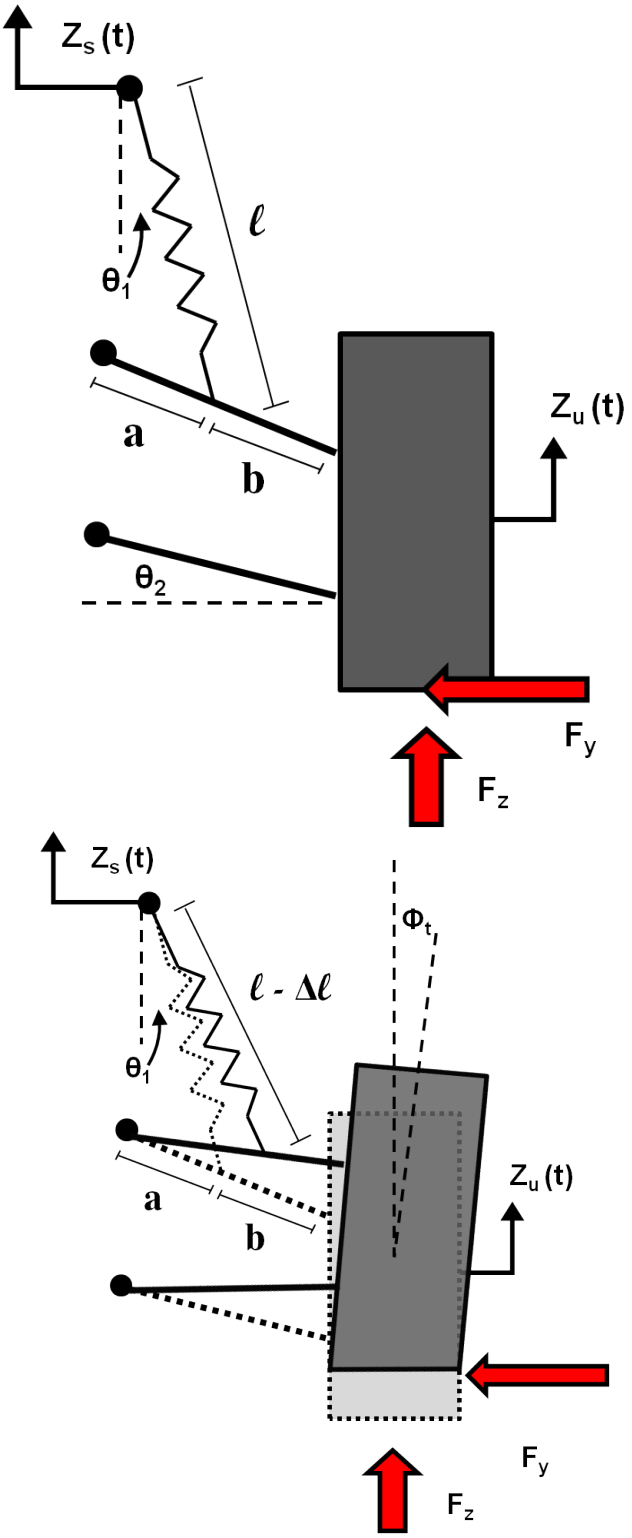

Figure 2.12: Suspension geometry and kinematic relationships showing undeflected (left) and deflected (right)

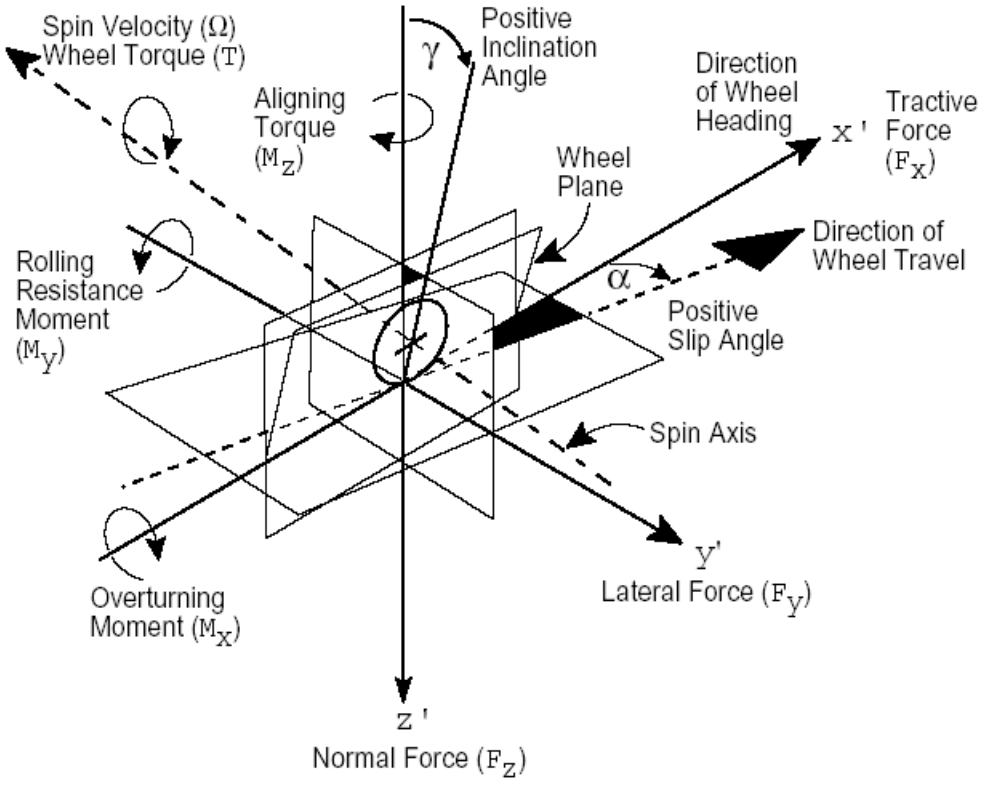

Figure 2.13: SAE Tire Coordinates

that the kinematic relationship developed will adequately translate the deflection from the sensor into the vertical tire force at the wheel.

2.3 Tire Modeling

Figure 2.13 shows the SAE tire coordinate system. The only interaction between the external world and the vehicle goes through the contact patch of the tire, making it a critical component in any dynamic vehicle maneuver. However, the tire is nonlinear in nature and can be difficult to model accurately. Most models rely on fitting numerous empirical data sets for very specific conditions. When those conditions change, the model fidelity can sometimes suffer. Additionally, many models are based off of tires with very similar charateristics. ATV tires have dramatically different characteristics from passenger tires, and even SUV tires. For this reason, a valid and accurate tire model is critical to accurate vehicle dynamics estimation

and analysis, especially on off-road vehicles in off-road environments where tire parameters and environmental conditions can change very quickly.

As with any tire model, the key aspect is the interaction between the road and the tire, known as the contact patch. Tremendous amounts of research have been dedicated to the analysis, characterization, and data extraction of this critical vehicle component [9, 17, 18, 20, 28]. One of the most important areas of study is based on the frictional relationship between the tire and the road. The friction, or "grip", of a tire is a key component to the capabilities of a vehicle. In off-road vehicles, tires are much more heavily dependent on the type of terrain. For example, the interaction between wet grass, sand, and rocks are dramatically different for the same off-road tire. For this thesis, the contact patch itself is not analyzed. However, the force analysis techniques presented later in this thesis will be an effort to provide knowledge of the forces at this contact patch, specifically as they relate to the dynamics and handling of the vehicle.

In order for a tire to generate a force on a surface, there must exist some form of slip. In the lateral direction, this term is simply known as the slip, lateral slip, or α. The primary goal of any tire model is to relate this slip angle to the lateral force availabe for that tire. Many different models exist that look at many different methods to establish this relationship, be it model matching to empirical data or analytical derivation. Typically, the tire model is used to generate a profile, or tire curve, of the expected behavior of the tire. The simpliest of these models assumes a linear relationship between the lateral force and slip angle. It can be expressed using a constant called the cornering stiffness, C_α,as seen in Equation 2.28.

$$F_y = C_\alpha \alpha \tag{2.28}$$

Various tire models were considered and explored, including the Pacejka and Dugoff models [12], a radial interradial spring model [4], and a parametric based model [5]. Another model, the Fiala, or exponential tire model, also works well for ATV tires[21]. Figure 2.14 shows a comparison of some of these models.

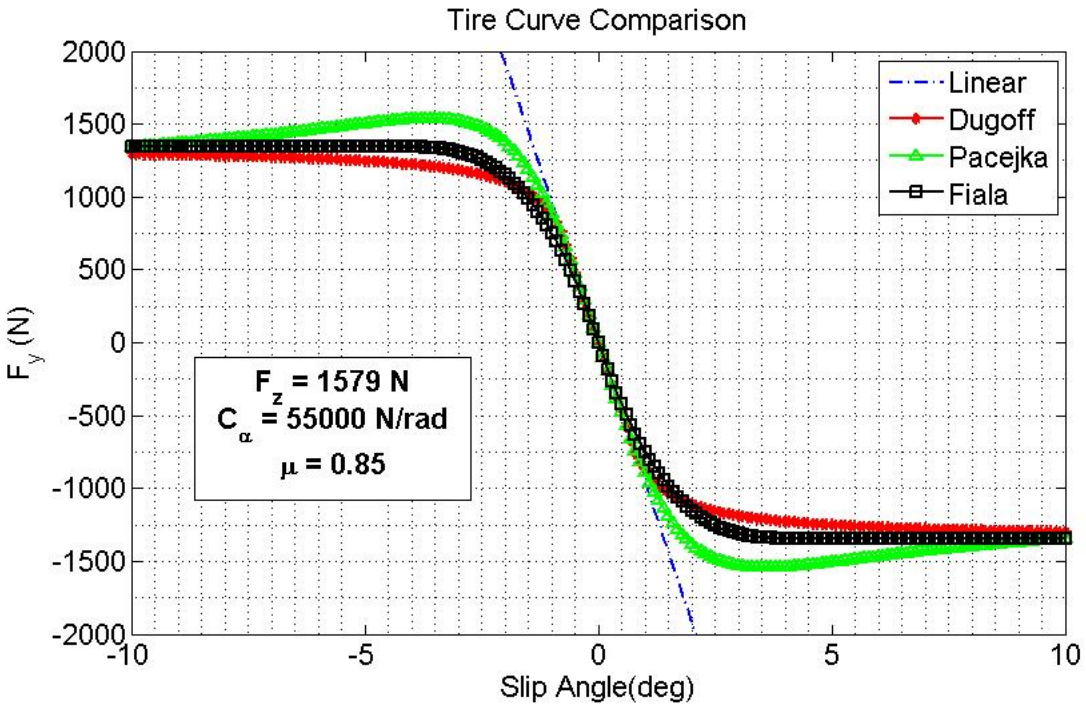

Figure 2.14: Comparison of various tire models.

Initially, the simple linear tire model was developed and used for analysis in this thesis. After analyzing data, it was discovered that ATV tires become nonlinear even with very small slip angles and and it is nearly impossible to capture the dynamics using linear tire assumptions (small slip angles). As seen in Figure 2.15, the model is nonlinear even for very small angles and can only be linearly approximated within ± 2 deg. This is due to the smaller F_z and $C_\alpha$values of ATV's which has a "flattening" effect of the tire curve.

Additionally, note the variations of the slope of the linear parts of the graph in Figure 2.16. This slope is the value of the cornering stiffness, which is normally assumed to be constant in many vehicle modeling applications. However, the Prowler ATV has a much higher tendancy to roll and pitch, thus affecting the weight transfer and subsequently the normal force at each tire. This frequently changing normal force causes the cornering stiffness values to change within a wide range of values during maneuvers that would normally be classified as "low" dynamics.

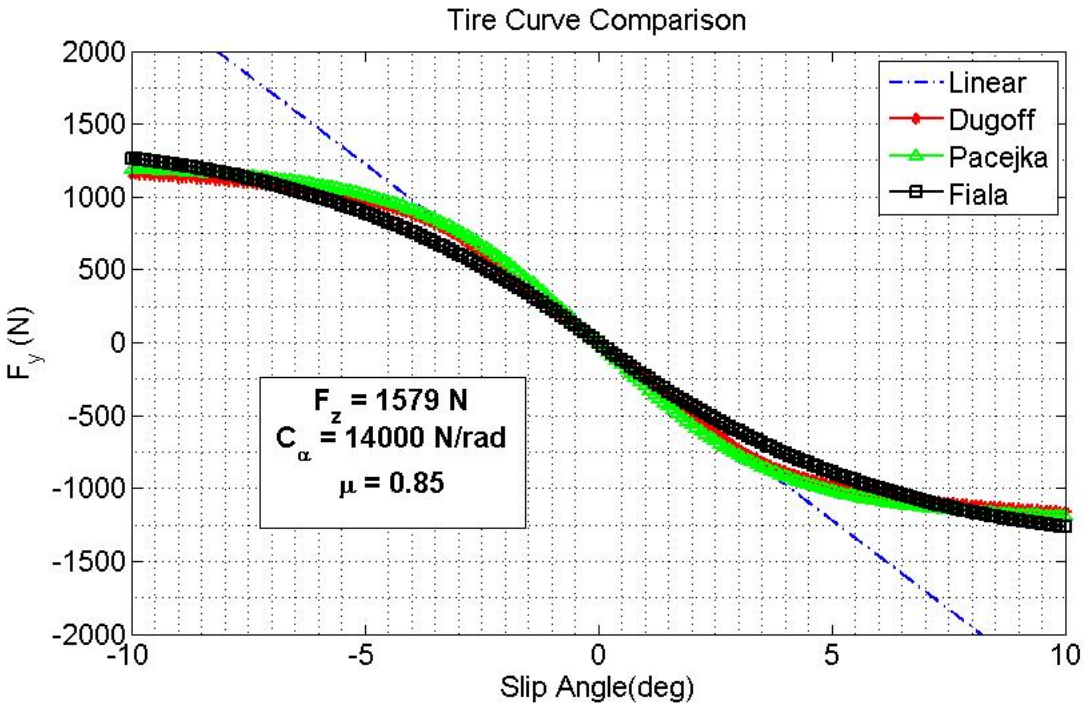

Figure 2.15: Tire model - Effect of changing cornering stiffness, C_α

Another aspect in tire modeling involves the coupling of lateral, longitudinal, and vertical forces. In reality, all three of these forces coexist on the tire contact patch, but often many models and analyses neglect some number of the components. One way to look at coupling effects of the forces is through the friction circle. The friction circle (or friction ellipse) concept requires the vector total of the lateral and longitudinal tire forces to lie within this maximum limit of the tire for a given F_z and μ.The maximum traction limit of each tire is dictated by the vertical load, F_z, and the coefficient of friction, μ, between the tire and the road. This effectively "limits" the total available force generated at the tire in the lateral and longitudinal direction. A plot of the friction circle is shown in Figure 2.17. Note that in extreme cases of longitudinal tire force, the lateral force is limited to a much lower value and vice versa. Physically, this means that during heavy acceleration or braking, the turning ability of the vehicle is greatly diminished.

The friction circle is critical in acceleration and braking when lateral and longitudinal forces are both present in large amounts. However, the work in this thesis attempts to

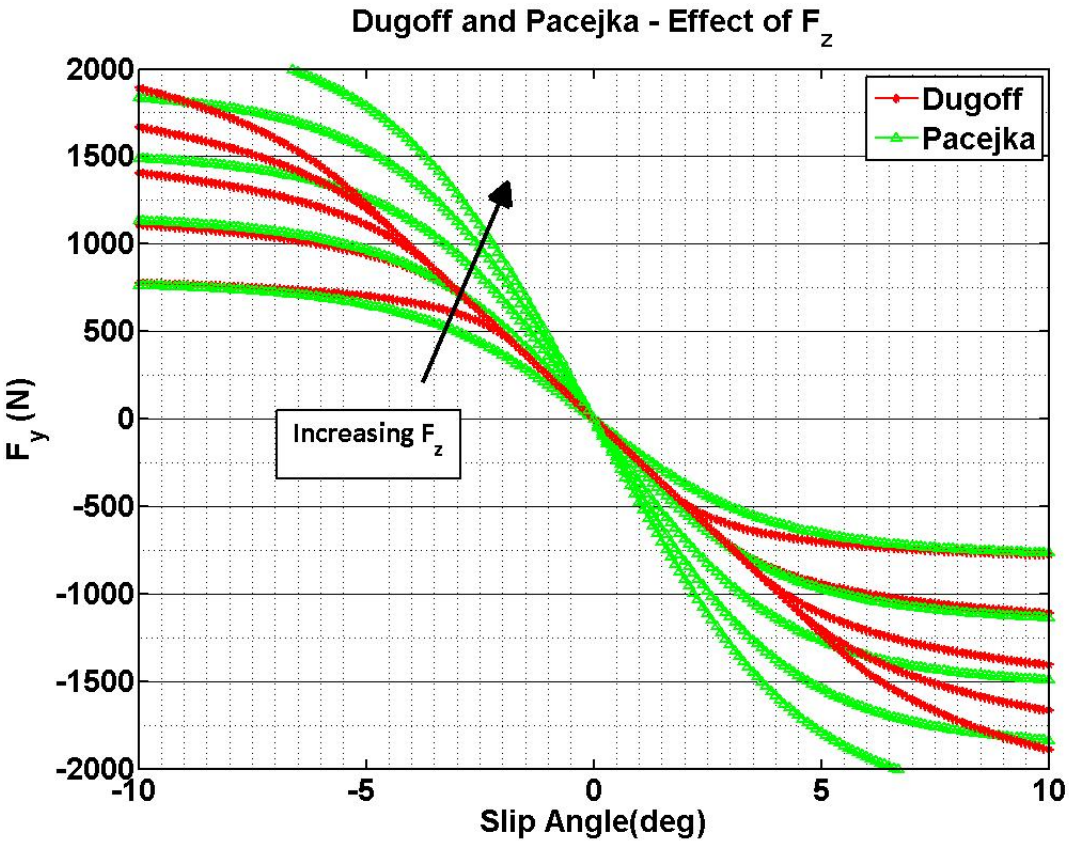

Figure 2.16: Pacejka and Dugoff Tire Models - Effect of varying F_z

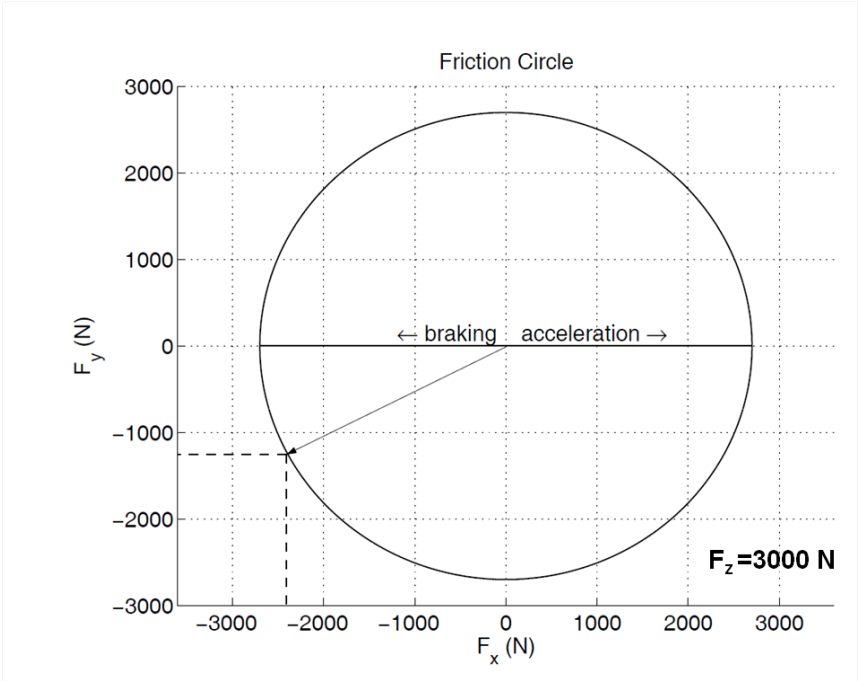

Figure 2.17: Friction circle for F_z =3000 N and μ =0.87

capture only the lateral dynamics and therefore many of the experiments are designed to run at a constant velocity with very low forces in the x-direction. However, should further analysis be conducted, it is recommended that friction circle analysis be included for this work.

The tire model is one of the most critical aspects of any vehicle model, as it is the primary interaction between the model and the physical world. Therefore, much of the model accuracy depends on a valid and appropriate tire model. A more thorough analysis of tire modeling and examination of various ATV tires would certainly yield better results and a more accurate model. However, the analysis of tire model performance as it related to the research goals presented in Chapter 1 quickly extended beyond the scope of the thesis. The exponential model has been shown to be valid for large slip angles, and for that reason provides a suitable choice for the analysis presented in this thesis.

2.4 Vehicle Parameter Identification

After developing a vehicle model, it is then important to identify the vehicle parameters that are critical to the model accuracy. Many vehicle parameters are difficult to measure or calculate, and a number of techniques can be employed to find appropriate values. To begin, a literature search was conducted to examine parameters used by researchers performing work on similar vehicles.

2.4.1 Vehicle Inertia

A good approximation for the inertia of a vehicle given the mass and weight split is found in [6]. Using Equation 2.29 and the measured values from the Prowler ATV of $m = 644.1kg$, $a = 0.89m$, and $b = 0.79m$, the inertia of the Prowler ATV can be approximated as 452 $kg \cdot m^2$.

$$I_z \approx m \times a \times b \tag{2.29}$$

The values related to suspension and tire parameters presented in Table 2.1 were shown in [9]. An analysis using pendulum techniques and novel measurement methods provided the values listed in Table 2.2 [29].

Table 2.1: ATV Suspension parameters identified by Chang

Parameter	Symbol	Value (units)
Sprung Mass ($\frac{1}{4}$ car model)	m_s	53.61 kg
Unsprung Mass (($\frac{1}{4}$ car model)	m_u	23.24 kg
Suspension Spring Stiffness	k_s	8265.5 $\frac{N}{m}$
Suspension Damping	b_s	640 $\frac{N \cdot s}{m}$
Tire Spring Stiffness	k_t	30922 $\frac{N}{m}$
Tire Damping	b_t	1500 $\frac{N \cdot s}{m}$

Table 2.2: Inertial ATV parameters identified by Warner

Parameter	Symbol	Value (units)
Roll Inertia	I_x	213.4 $kg \cdot m^2$
Pitch Inertia	I_y	445.7 $kg \cdot m^2$
Yaw Inertia	I_z	453.9 $kg \cdot m^2$
CG Height	h_{CG}	0.579 m
Weight	W	6421 N

After discovering commonly used values, additional measurements and calculations were made to try and identify as many parameters as accurately as possible. For example, solid modeling tools provide a useful method for determining the inertias of a vehicle about its primary axes. Building a model of the test platform in the SolidEdge design environment allowed for the identification of the inertial values used in the model. The model was constructed based on real materials and physical measurements of the vehicle. Compensating for the weight of components such as the tires, batteries, engine, and other weighted components allows for an accurate representation of the CG location and the inertial values of the vehicle, as seen in Figure 2.18.

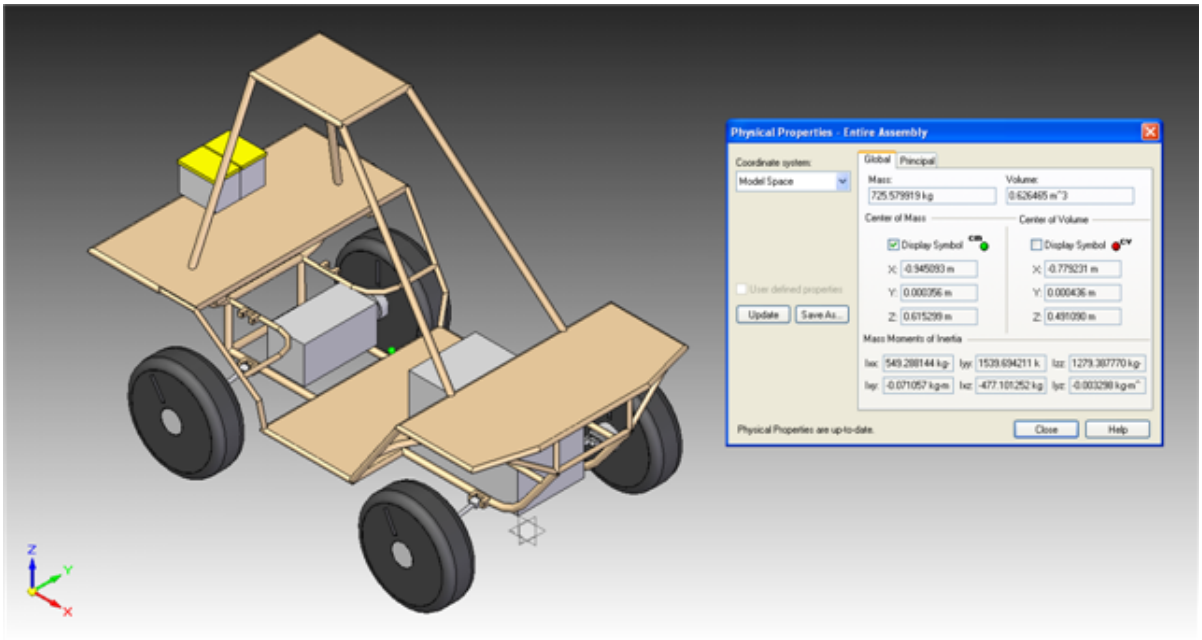

Figure 2.18: SolidEdge model of prowler used to find inertias about primary axes.

2.4.2 Roll Center Height

Solid Edge also proved to be a useful tool for establishing the roll center height of the vehicle. The roll center can be found by determining the virtual reaction point of the suspension. This is an imaginary point extended out from the suspension a-arms. The roll center is then found by extending a third line from the tire-ground contact point to the virtual reaction point, and measuring the height where that line crosses the centerline of the vehicle. In the case where the a-arms are parallel and the virtual reaction point is at infinity, simply extending a line that is at the same angle as the parallel suspension arms will determine the roll center height. This analysis must be done for both the front and the rear suspensions, and then using the wheelbase and the weight split of the vehicle, the roll center at the CG can be calculated. Figure 2.19 highlights the process of geometrically determining the roll center.

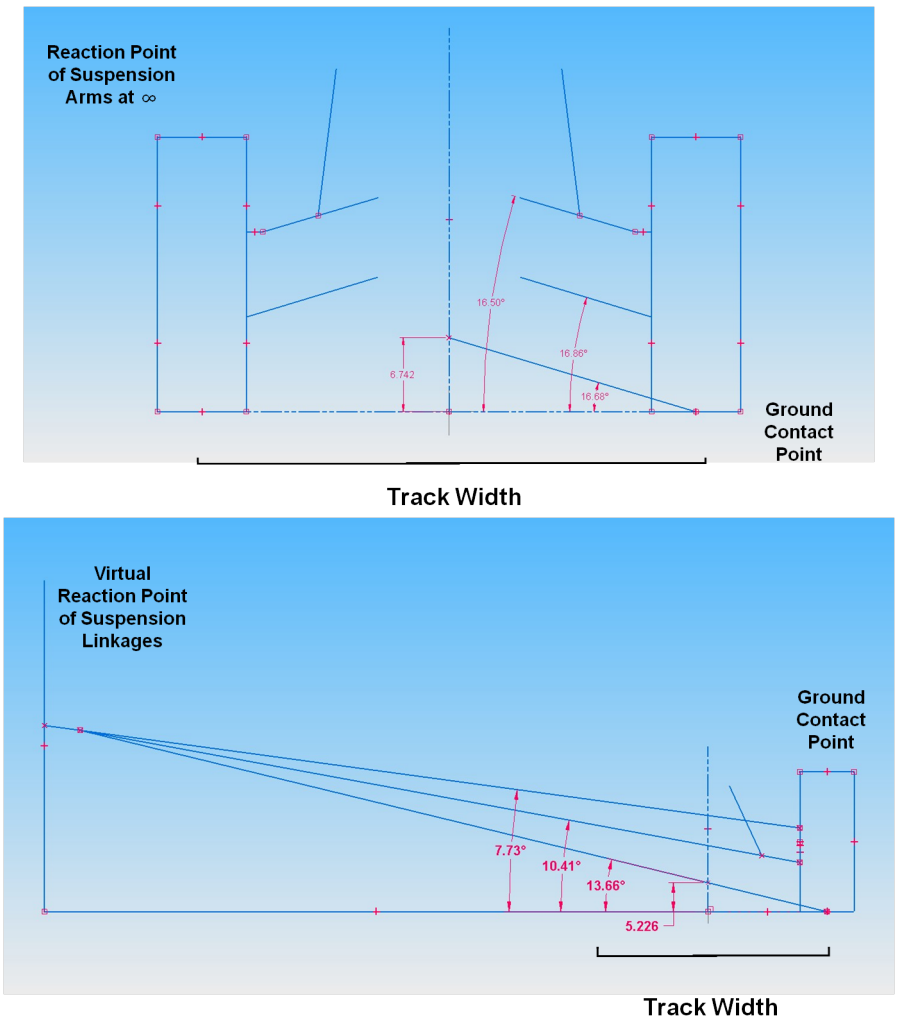

Figure 2.19: Roll center height determination

2.4.3 Measured Parameters

Further analysis of initial static data sets and static calculations of the prowler yielded a table of relevant parameters used in the vehicle model, listed in Table 2.3.

Table 2.3: Prowler ATV measured parameters

Parameter	Symbol	Value (units)
Mass	m	644 kg
Roll Inertia	I_x	549 $kg \cdot m^2$
Pitch Inertia	I_y	1539 $kg \cdot m^2$
Yaw Inertia	I_z	1279 $kg \cdot m^2$
CG Height	h_{CG}	0.579 m
Weight	W	6318 N
Front Axle Distance from CG	a	0.839 m
Rear Axle Distance from CG	b	0.6081 m
Wheelbase	L	1.4478 m
Front Track Width	t_f	1.143 m
Rear Track Width	t_r	1.092m
Front Distance b/w Suspension Components	S_f	0.6858m
Rear Distance b/w Suspension Components	S_r	0.7366m
Roll Center Height	h_{rc}	0.155 m
Pitch Center Height	h_{pc}	0.3 m

2.4.4 Roll and Pitch Parameters

Many of the parameters critical to accurately modeling the prowler cannot be measured directly. Instead they must be estimated or solved for using the dynamic equations of motion. This can be a useful method of analysis and allows for a more complete and thorough list of parameters. For example, Ryu presents a method in [1] that looks at comparing empirical datasets using measurements of roll, roll rate, pitch, pitch rate, lateral acceleration, and longitudinal acceleration to estimate these parameters using a least squares fit of roll moment vs. the roll angle and roll rate, shown in Figure 2.20.

Performing this analysis on the Prowler ATV yielded the results presented in Table 2.4.

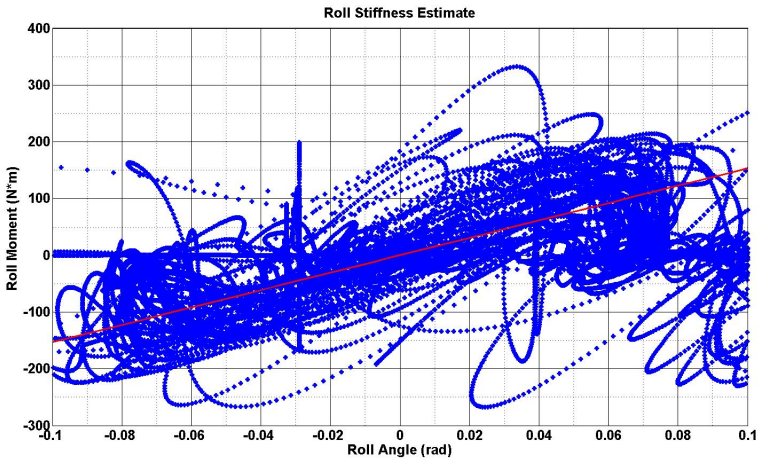

Figure 2.20: Roll stiffness estimate using Ryu method[1]

Table 2.4: Prowler ATV estimated parameters - roll and pitch stiffness and damping

Parameter	Symbol	Value (units)
Roll Stiffness	K_ϕ	2743 Nms/rad
Roll Damping	B_ϕ	203.8 Nm/rad
Pitch Stiffness	K_θ	3153 Nms/rad
Pitch Damping	B_θ	824.03 Nms/rad

However, implementing these values into the Prowler model did not improve the performance of the model and caused irregular behaviors. It is unknown why these estimates do not perform well, but searching for an alternative method provided the following equation from Gillespie [14].

$$K_\phi = 0.5 K_s s^2 \tag{2.30}$$

In this equation, $K_s$is provided by the manufacturer to be 65,000 N/m and s is the distance in meters between the suspension components. Using this formula for both the pitch and roll calculations, the parameters listed in Table 2.5 were calculated.

Table 2.5: Prowler ATV estimated parameters - roll and pitch stiffness and damping

Parameter	Symbol	Value (units)
Roll Stiffness	K_ϕ	15285.5 Nms/rad
Pitch Stiffness	K_θ	67392 Nms/rad

These two methods produced dramatically different estimates for the same parameter, and their effects on the model are equally dramatic. It is unknown as to the cause to the potential errors in these two values. However, some value had to be chosen in order to proceed with the validation of the model. Using various iterations of "tuning" the model, final values were selceted that lie somewhere in between the extremes of the values presented by the two estimation methods. The model could be improved by further improvements to the estimation of these model parameters.

2.4.5 Cornering Stiffness

One of the most critical parameters to lateral vehicle dynamics is the cornering stiffness. Recall from Section 2.3 that the cornering stiffness, C_α, is one of the key elements in tire curve identification as it relates the slip angle and lateral force in the linear region of the tire curve.

A first attempt at estimating the cornering stiffness was done using a recursive least squares algorithm based on a simple estimator using measurements of lateral acceleration and yaw acceleration differentiated from a rate gyro. However, this yielded poor results, likely due to invalid assumptions on the data such as constant longitudinal velocity and constant steer angle. A more effective method found in [8] calculates the cornering stiffness using dynamic equations of motion, assuming that the sideslip angle is either known or can be estimated. In the case of this thesis, there is a "truth" measurement of the sideslip angle from the three-antenna GPS system discussed in Section 4.1. Using this measurement and solving Equation 2.31, the cornering stiffness can be directly solved for.

$$\begin{aligned} C_{\alpha r} &= \frac{mVr}{(\frac{b}{a}+1)\alpha_r} \approx \frac{mVr}{(\frac{b}{a}+1)(\beta-\frac{br}{V})} \\ C_{\alpha f} &= \frac{bC_{\alpha r}}{a\alpha_f} \approx \frac{bC_{\alpha r}(\beta-\frac{br}{V})}{a(\beta+\frac{ar}{V}-\delta)} \end{aligned} \tag{2.31}$$

Performing this analysis on experimental data yieled the results shown in Figure 2.21. The data presented is from a run in which a 50 ft. constant radius turn was driven at an

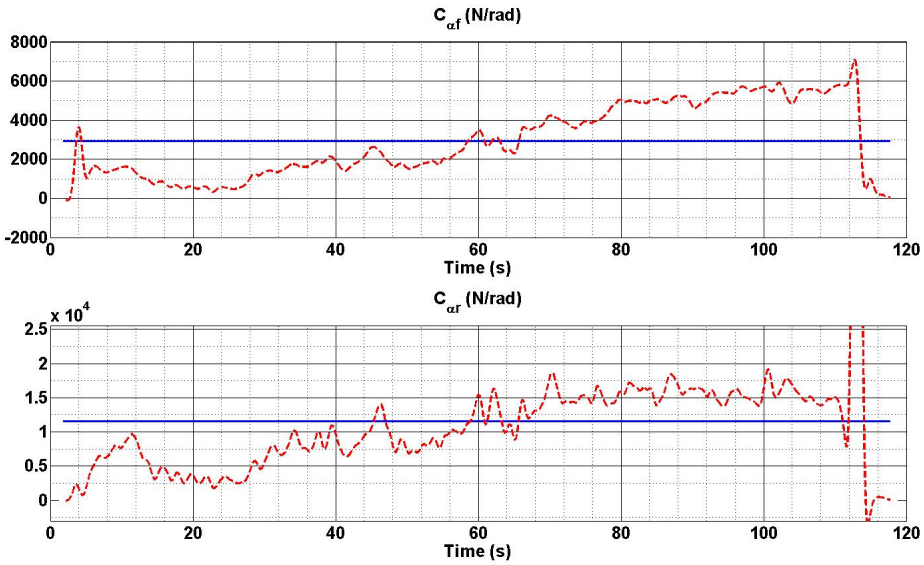

Figure 2.21: Cornering stiffness calculation

increasing velocity. The red line represents the solution for C_α for each time step. The blue line is the mean of the data over the time period.

As can be seen in the plot, the cornering stiffness does not appear to be constant. As the vehicle increases speed later in the run, it is observed that the cornering stiffness increases. This is supported by results presented in [24], where it is shown that conlinearities of the contact patch and the variations of grip conditions can cause variations in the cornering stiffness. They also present a method to adapt these values online. However, for the developed model, a constant value of C_α is necessary for comparison of the model to the expected forces. Therefore, the mean value is taken from Figure 2.21 (the blue line). It is assumed that this is a valid approximation since the values correspond to similar values presented in literature for like vehicles. Figure 2.22 shows the two tires used for the analysis in this thesis. Figure 2.23 shows the values used as the cornering stiffness for two sets of tires used in this thesis.

Figure 2.22: Tire Comparison: All-trail or "Road" tire (left) vs. Off-road tire (right)

	Pressure (p.s.i.)	$C_{\alpha f}$ (N/rad)	$C_{\alpha r}$ (N/rad)
Road	12	5975	17076
Off-Road	4	3124	13886

Figure 2.23: Cornering stiffness values for various tires

2.5 Model Validation

After developing the vehicle model, it is important to validate the model against "truth" data or a high fidelity simulation to ensure that the model has been correctly developed to capture the actual dynamics of the system. The solid model of the Prowler developed in SolidEdge and shown in Figure 2.18 was imported into the CarSIM simulation environment. Through careful measuring of vehicle parameters such as mass, weight, weight split, suspension geometery, steering ratio, and tire properties, the CarSIM model was able to be constructed in a way that is very physically similar to the actual ATV test platform. The CarSIM software is incredibly customizeable and allows for nearly every types of vehicle input parameters. To this end, the Prowler ATV was extensively measured and the data was incorporated into CarSIM to compare against a one of the many "standard" vehicle options within CarSIM. As stated in the motivation, much research is done in passenger vehicles and trucks as far as vehicle dynamics and analysis. But the CarSIM software setup for ATVs and small UGVs is relatively untapped. Using a "Small SUV" setup may be an acceptable

Figure 2.24: Prowler ATV in the CarSIM Simulation Environment

substitute for taking the time to measure and compare all of the various dimensional and performance specifications of the prowler.

When comparing the simulation environment to the full model developed in Section 2.1, the model shows a relatively good fit to the simulation data. Figure 2.25 and Figure 2.26 show the sideslip and yaw rate from a run consisting of a sinusoidal steering input at a constant velocity. It is important to note however, that the primary difference between the CarSIM simulation data and the model is the difference in tire models. The exponential tire model was not implemented into CarSIM, and the default tire model of a "small SUV" was used. This tire model is not entirely accurate for the Prowler, as shown in the previous section. This is most likely the reason for the discrepancy between the blue, full nonlinear vehicle model, and the red CarSIM data. Note, there is a numerical issue in the model at low speeds which causes the spike seen at 15 seconds.

The validation of CarSIM shows that the derived equations are in fact valid when compared to the simulation environment. However, comparing the model to experimental data would yield a far more accurate representation of the model accuracy, since the goal is to fully capture the vehicle behavior. Further validation was performed against experimental data collected from the Prowler ATV. It is assumed that since the developed vehicle model

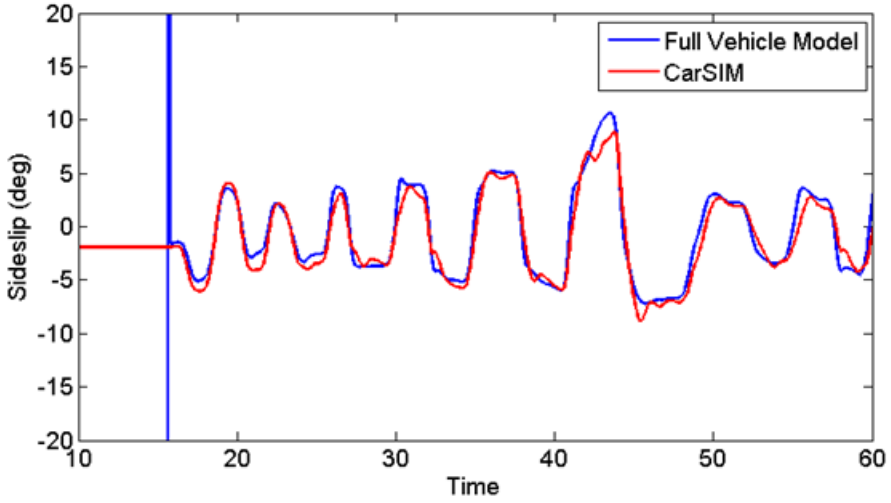

Figure 2.25: Comparison of Vehicle Model to CarSIM Simulation - Sideslip

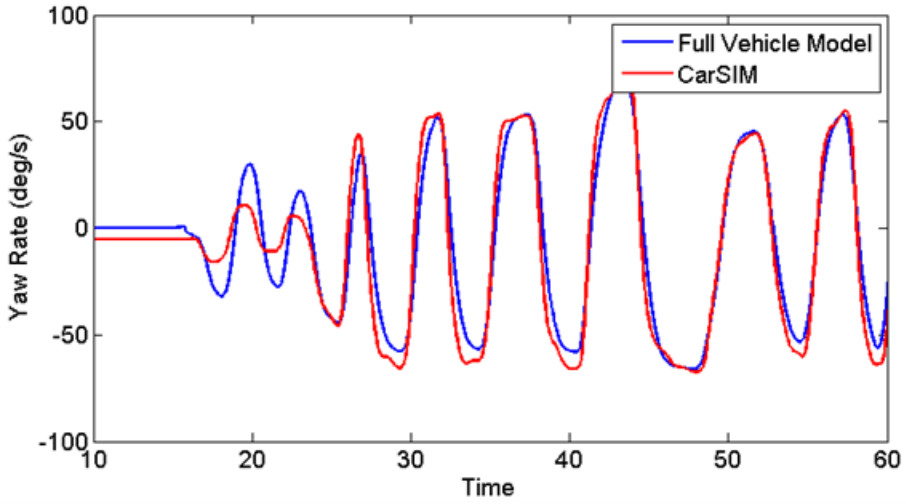

Figure 2.26: Comparison of Vehicle Model to CarSIM Simulation - Yaw Rate

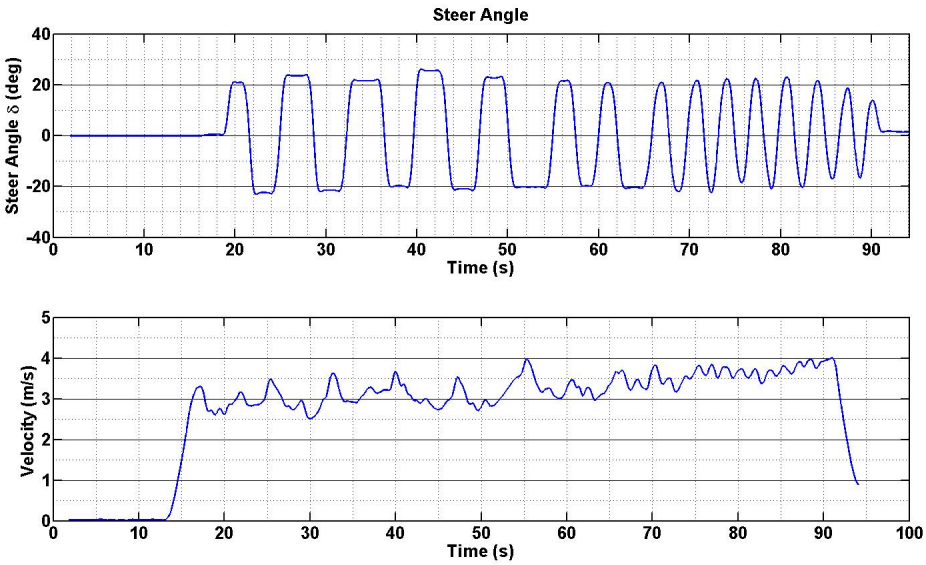

Figure 2.27: Model Validation agains experimental data - Model Inputs

matches the experimental data well, then the correct analysis of vehicle dyanmics has been applied. This also shows that valid parameters have been selected for the vehicle model. Initially, the model had the correct trends and magnitudes as the data, but there were distinct differences in the behavior of the model vs. the experimental data. Figure 2.27 shows the inputs to the model. The inputs for this run are a sinusoidal steer angle at roughly two different frequencies, seen from 18 to 65 seconds and then from 65 to 90 seconds. The velocity was held to as close to constant as possible. Figures 2.28, 2.30, and 2.29 show the model fit against the data.

Of note, the large error seen from 0-15 seconds can be attributed to the fact that using differential GPS measurements, a heading measurement cannot be accurately obtained at low velocities. This causes the measurement to be wildly erratic until the vehicle begins moving, which occurs at roughly 17 seconds during this run. The correct trends and magnitudes appeared to be close. However, there was obvious error and distinct differences between the model behavior and the experimental data. It was hypothesized that this descrepancy was due to incorrect parameters used in the model. Once the parameters had been improved, as

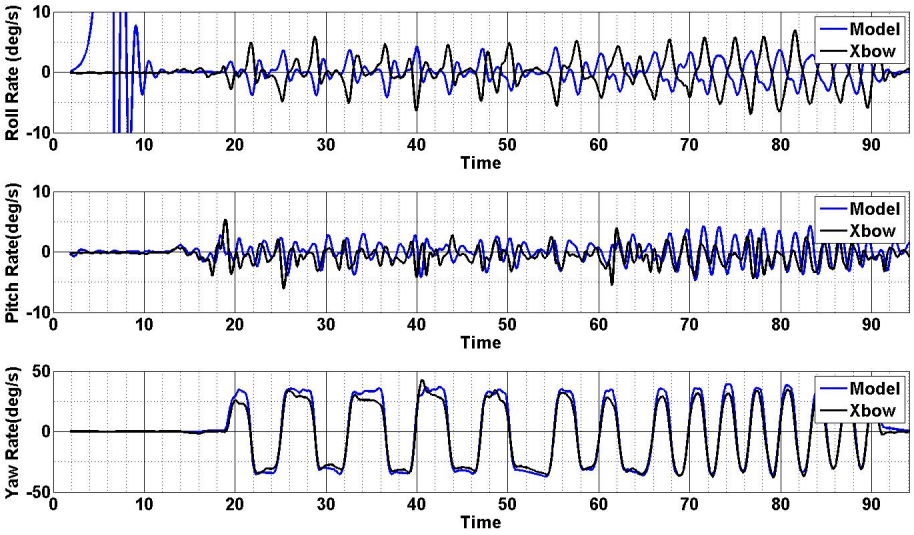

Figure 2.28: Model Validation agains experimental data with incorrect parameters - Angular Rates

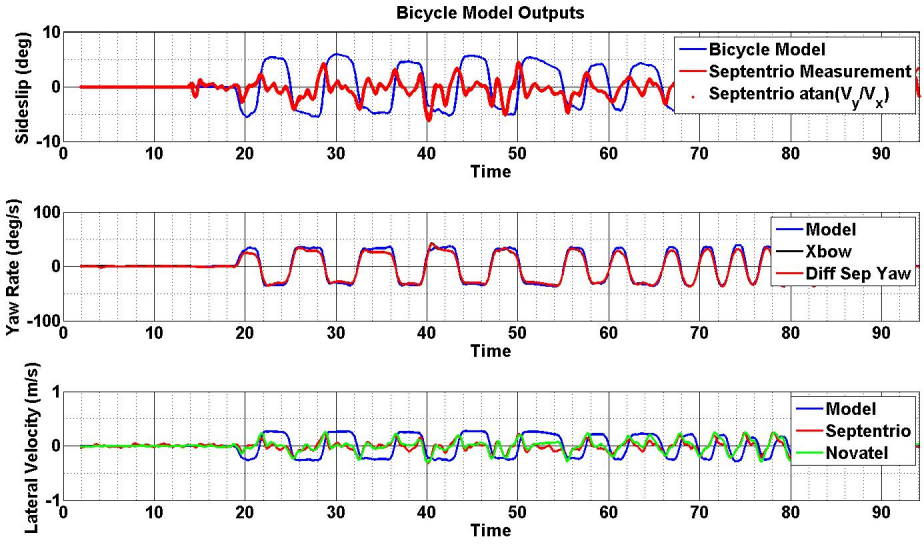

Figure 2.29: Model Validation agains experimental data with incorrect parameters- Sideslip, Yaw Rate, and Lateral Velocity

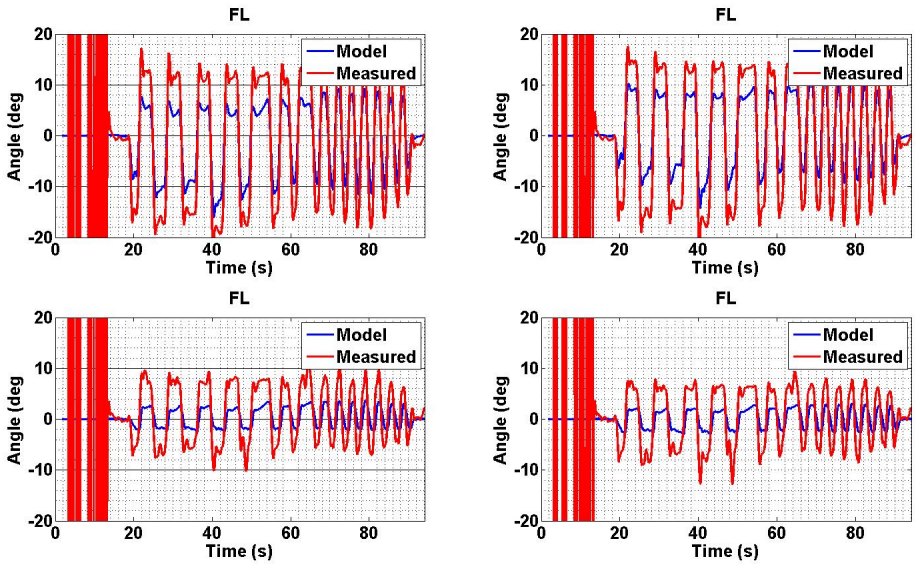

Figure 2.30: Model Validation agains experimental data with incorrect parameters - Slip Angles

discussed in Section 2.4, the model showed a much better fit to the experimental data, as seen in the Figures 2.31, 2.32, and 2.33.

While the fit is visually good, there are still many improvements that may be made to these parameters that would yield better results. Additionally, there are many possible sources of error in both the data collection and the model that could potentially account for the discrepancies seen in some of the validation plots. A discussion of some of these error sources is included in Chapter 5. For example, there are non-trival errors in the yaw rate and sideslip measurements of the model caused by errors in the assumption that C_α is linear, which does not hold true in the experimental data.

In this chapter, various vehicle models were considered and compared for their application towards modeling the test platform used for this research. A nonlinear 4 wheeled model is presented that takes into account roll, pitch, and yaw of the vehicle in an attempt to capture the tire forces at the contact patch of the tire. Various tire models were compared, and the fiala, or elastic, tire model was chosen for its accuracy in the prescence of high values of tire slip angle. Various vehicle parameters relevant to the model were considered and

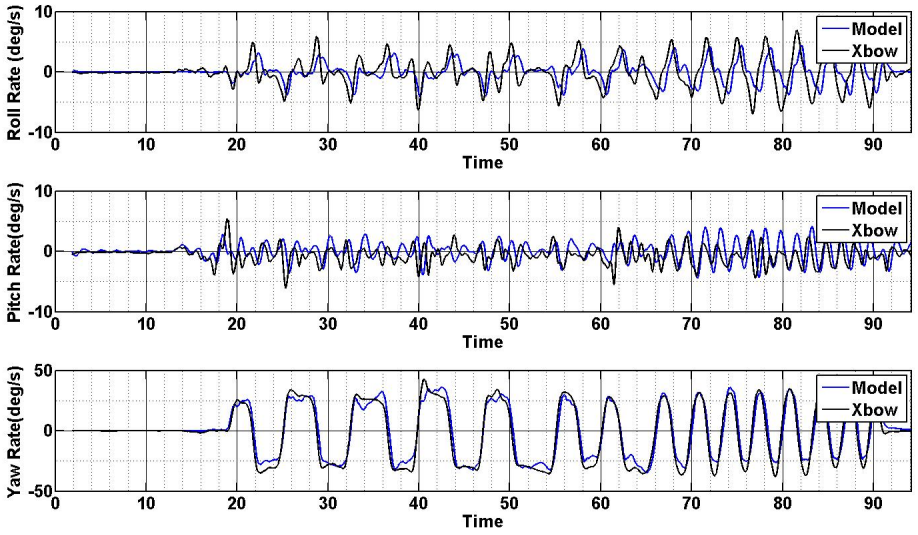

Figure 2.31: Model Validation agains experimental data - Angular Rates

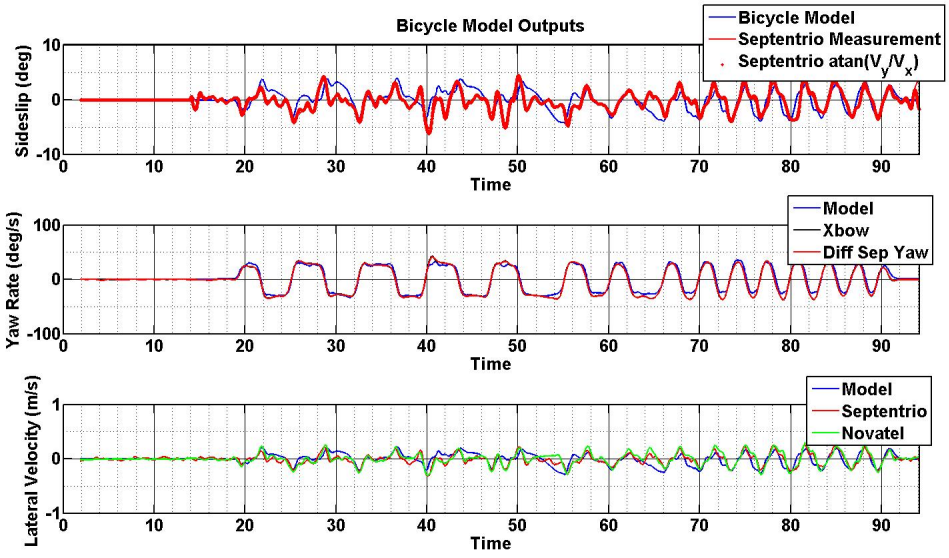

Figure 2.32: Model Validation agains experimental data - Sideslip, Yaw Rate, and Lateral Velocity

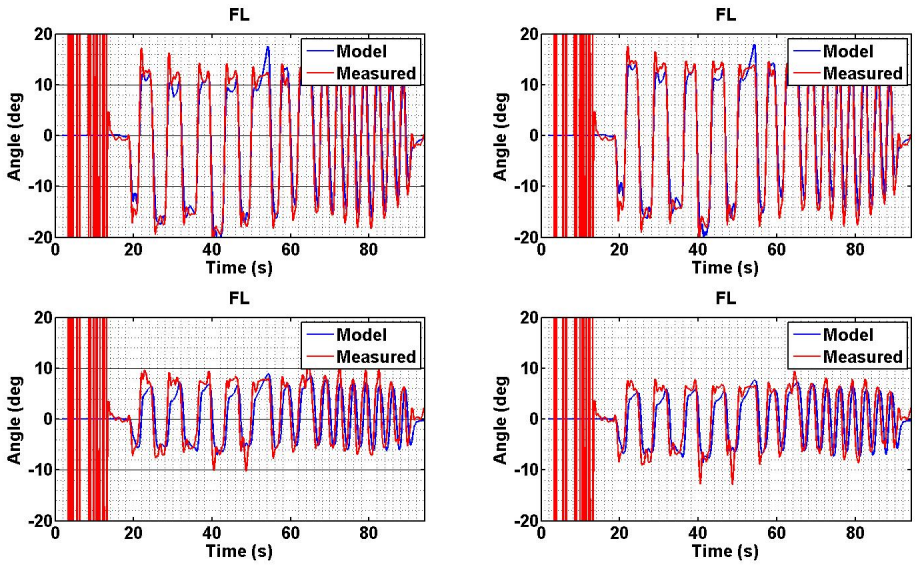

Figure 2.33: Model Validation agains experimental data - Slip Angles

methods to analyze and identify those parameters are presented. Finally, this model was shown to be sufficiently validated, thus providing a method to obtain expectations of results for experimental data acquisition. This model will be the baseline against which the strain gauges and suspension deflection potentiometers are compared to determine their validity as a tool for measuring vehicle dynamic forces.

Chapter 3

Vehicle Force Measurements Using Suspension Deflection and Strain

Having developed the models and completing sufficient validation of those models, it is important to consider the feasibility and develop a system of analysis using suspension deflection and strain gauge methods for force measurement. This chapter details the methodology presented to capture the measurements of vertical and lateral force. Sensors are examined and mounting solutions are presented. Also, hardware installation, signal processing, and calibration results are presented.

3.1 Deflection

The coil-spring assembly pictured in Figure 3.1 consists of a spring wrapped around a damper. Recall from Section 2.2.4 that the suspension analysis becomes nonlinear when analyzing the model between F_z and the deflection of the sprung mass. However, if a measurement of the deflection of the spring were measured directly parallel to the spring, then that measurement can be related to the force at the wheel. This measurement can be accomplished by mounting a linear potentiometer to the coil-spring assembly, as showin in Figure 3.1. Using the value from the potentiometer, and given the stiffness of the spring, the force carried by this member of the suspension linkage can be approximated using the method developed in Section 2.2.4. Using this potentiometer, the deflection of the coil-spring assembly can be measured directly and then used to assist in the estimate of vehicle roll, ground roll,

The linear potentiometer used is the Celesco MLP-125. It is a ruggedized (IP67) potentiometer due to the fact that the mounting location is highly susceptible to water and dirt exposure. The PIC18F2580 Microcontroller from Microchip was selected as the primary

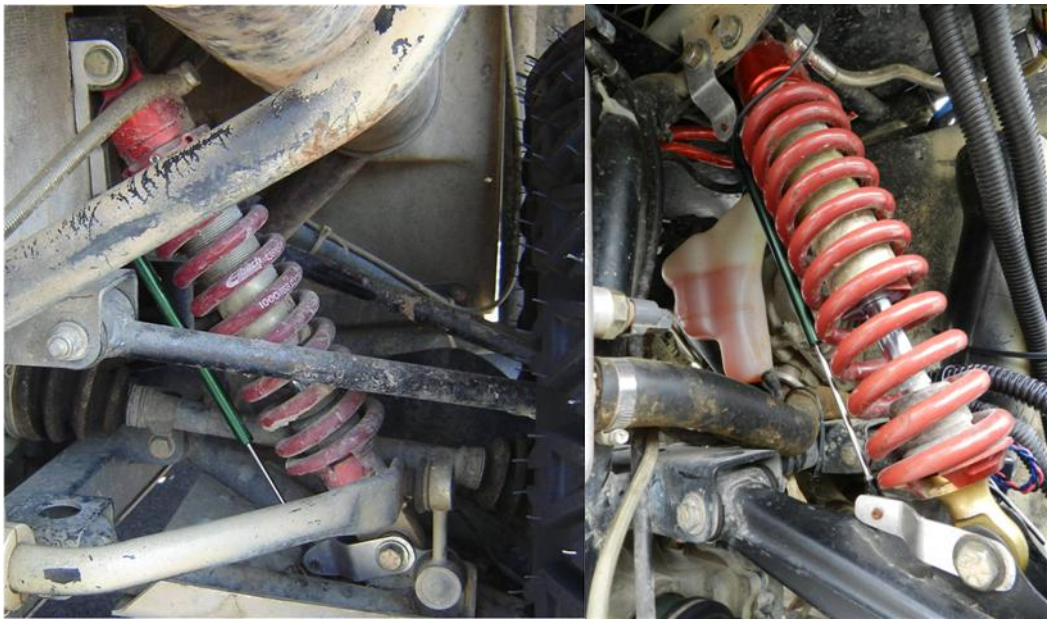

Figure 3.1: Suspension deflection potentiometer mounted parallel to the coil-spring assembly.

data acquisition tool for the suspension potentiometers. This very capable PIC has up to 10 A/D channels, as well as a built in A/D module with a user-defined sample rate. It also has a built in CAN module that transmits and receives CAN messages. CAN, or Controller Area Network, is a well-defined and well-documented protocol for transmission of data in vehicle systems. It has been proven thoroughly in industry, and as such is a reliable method for interfacing these sensors and data acquisition circuits. More detail of these circuits will be discussed in the following sections.

3.2 Strain Theory and Strain Gauges

The concept of strain (ε) is the driving mechanism behind strain gauges. Strain, and stress (σ), are mechanical properties of all materials under loading. Stress is defined as an internal resistance to forces, while strain is the displacement and deformation that occurs. Even more specifically strain is defined as the change in length per unit of length ($^{\Delta L}/_{L}$). Strain is a dimensionless quantity, but is usually expressed in terms of in/in or mm/mm. It also tends to be very small in magnitude and is often referenced in terms of micro strain

($\mu\epsilon$), which is 10^{-6}mm/mm. Strain can be either a positive or negative value, depending on whether the loading and consequent change in length is in the compressive or tensile direction. Often, the shape or structure of a material will cause strain in multiple directions. For example, stretching a small rod such as a suspension arm would not only cause the rod to lengthen axially, but would also cause the diameter of the rod (or cross sectional width) to decrease. This deformation in the direction perpendicular to the applied force is known as transverse strain and is related to the axial strain by a ratio called Poisson's Ratio (ν). This ratio is formally defined as the negative ratio of the transverse strain to the axial strain and is specific to the material being loaded.

$$\nu = -\frac{\Delta\epsilon_{transverse}}{\Delta\epsilon_{axial}} \tag{3.1}$$

Equally important in strain analysis is Youngs Modulus, also called the Elastic Modulus or Modulus of Elasticity. It is defined as the ratio of tensile stress to tensile strain, or:

$$E = \frac{\sigma_{tensile}}{\epsilon_{tensile}} \tag{3.2}$$

Some typical values of Poisson's Ratio and Young's (Elastic) Modulus for various materials are presented in Table 3.1.

Table 3.1: Material properties

Material	Poisson's Ratio, ν	Elastic Modulus, E $(GPa.)$
Aluminum (2024-T4)	0.32	73.0
Aluminum (6061)	0.32	71.7
Steel - 1018	0.285	206.8
Steel - 4130	0.28	190.0
Steel - 304 SS	0.25	193.0

The material used in the test vehicle frame for validation of the methods and algorithms in this thesis is Chromoly, an alloy of steel containing Chromium and Molybdenum. The values of Poisson's ratio and Youngs Modulus referred to in this work are the properties of Chromoly, also known as 4130 steel, from Table 3.1.

Using Equations 3.2 and 3.1, a relationship between strain and force can be developed. Given that stress is the axial force applied to a member divided by the cross sectional area, or:

$$\sigma_{axial} = \frac{F_{axial}}{A} \tag{3.3}$$

The relationship between strain and force can be written as:

$$F = EA\epsilon \tag{3.4}$$

This relationship allows the force to be determined within a structural member, such as the suspension a-arm, with a measurement of the strain within that member. In order to obtain the measurement of strain directly, a sensor called a strain gauge can be used.

A strain gauge exploits the principle of electrical resistance as a way to gauge the deformation of materials and therein determine the loads induced within the material. This aspect of strain gauges is especially useful in applications where it is necessary and/or beneficial to know specific loading data. Strain gauges can determine miniscule strain on micro-electrical components, as well as determine the fatigue and stress of a bridge many miles long. They can also detect strain over long periods of time, or at incredibly fast sampling times.

3.3 Strain Suspension Forces

Using a simple Finite Element Analysis module in Solid Edge, a mockup of the suspension was created and loaded to determine both the range of stresses that could potentially be experienced within the suspension linkages, as well as a visual confirmation of stress/strain behavior of the components. The solid model was developed using hand measurements of the actual A-Arm components on the Prowler ATV test platform. Also, material properties of the 4130 (Chromoly) steel were included in the simulation environment.

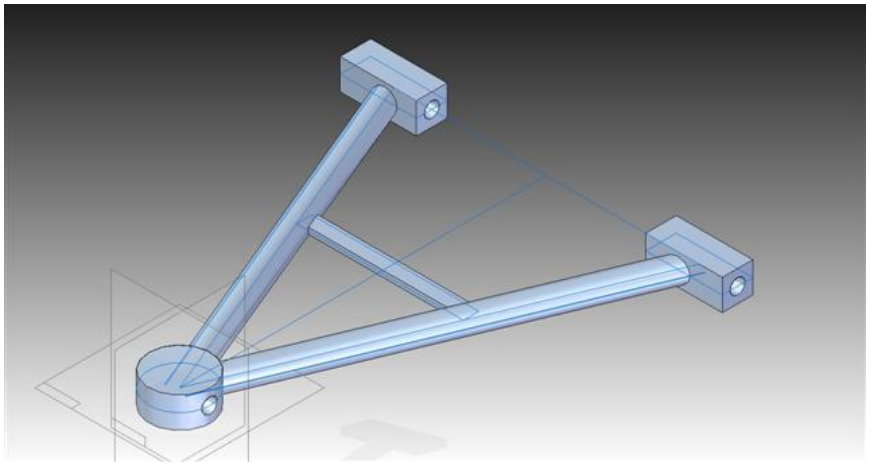

Figure 3.2: Lower Suspension A-Arm drawn in Solid Edge, in unloaded condition.

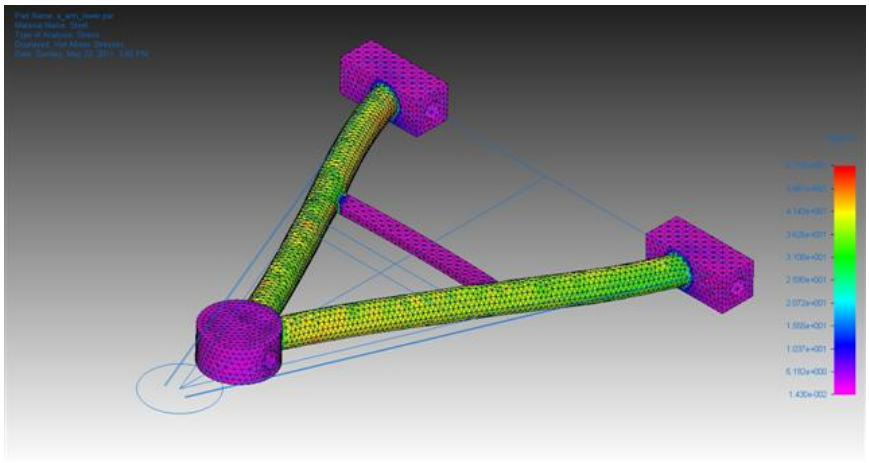

Figure 3.3: Lower suspension A-Arm loaded with a lateral load.

In Figure 3.2, a load of 2000 N is applied in the lateral direction, while in Figure 3.3, the lateral load is also combined with a vertical load of 500 N.

In Figure 3.3, a load of 2000 N is applied in the lateral direction, while in Figure 3.5, the lateral load is also combined with a vertical load of 500 N.

The results of this simulation suggest that the order of stress induced by reasonable forces in these linkages should be on the order of 180 - 200 MPa, which corresponds to a strain value on the order of 10 $\mu\varepsilon$. More details on this calculation and the use of these values as design considerations are discussed in Sections 3.2 and 3.4. But the primary purpose of this simulation is to establish the range of expected values for selecting the appropriate strain

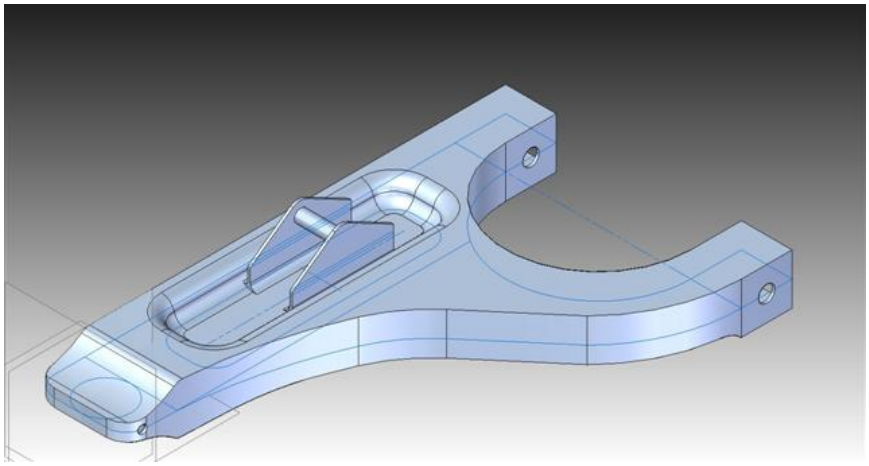

Figure 3.4: Upper Suspension A-Arm drawn in Solid Edge, in unloaded condition .

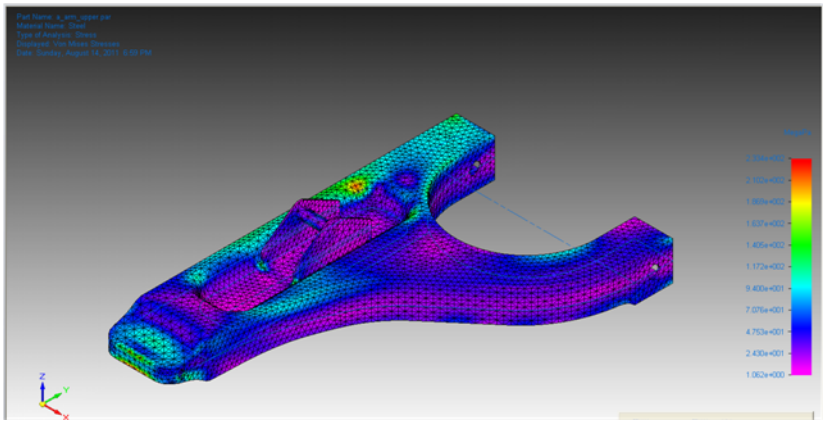

Figure 3.5: Upper Suspension A-Arm loaded with a combined vertical and lateral load.

gauge and the location to place the strain gauge. Based off of this simulation analysis, the location of the strain gauges was selected to be on the lower A-arms halway between the joints, as well as only on the upper portion of the upper A-arm near the base where the wheel connects.

3.4 Strain Gauge Selection and Circuit Design

The PIC18F2580 Microcontroller from Microchip was also selected as the primary data acquisition tool for the strain gauges. Since there are 4 strain bridges on each wheel, there must be at least this many A/D pins available on the PIC. Commonly, in normal driving conditions, a suspension mode operates on the order of 1 Hz to 20 Hz [16, 31]. Despite going up to 20 Hz, more common frequency content of suspension data would be expected around the area of 2-6 Hz, as this is typically the design goal for human ride comfort [13]. Furthermore, looking at frequency content of deflection data taken from the deflection sensors described in Section 3.1, it can be seen that most of the suspension dynamics appear to fall within this range of low ($<$ 20Hz) range, as shown in Figure 3.6.

It is important to set the sample rate at a minimum of twice the maximum frequency present to prevent aliasing of the data and ensure that the dynamics are fully captured. For convenience, a sample rate of 100 Hz is selected to coincide with the data transmission rate of a CAN bus over which the data will be collected. This sample rate is well above the minimum sample rate needed to fully capture the dynamics of the suspension.

The data acquisition circuit design was completed using a circuit designed in PCB Artist software and then manufactured by Advanced Circuits. The primary design of the circuit board was for implementation into an on-board vehicle CAN bus. The test platform already had multiple sensors and controllers installed and interfaced to a singular CAN bus, as is common in many commercial vehicles today. The CAN protocol allows for very rapid and reliable data transmission and acquisition. Figure 3.7 shows the layout for the circuit board

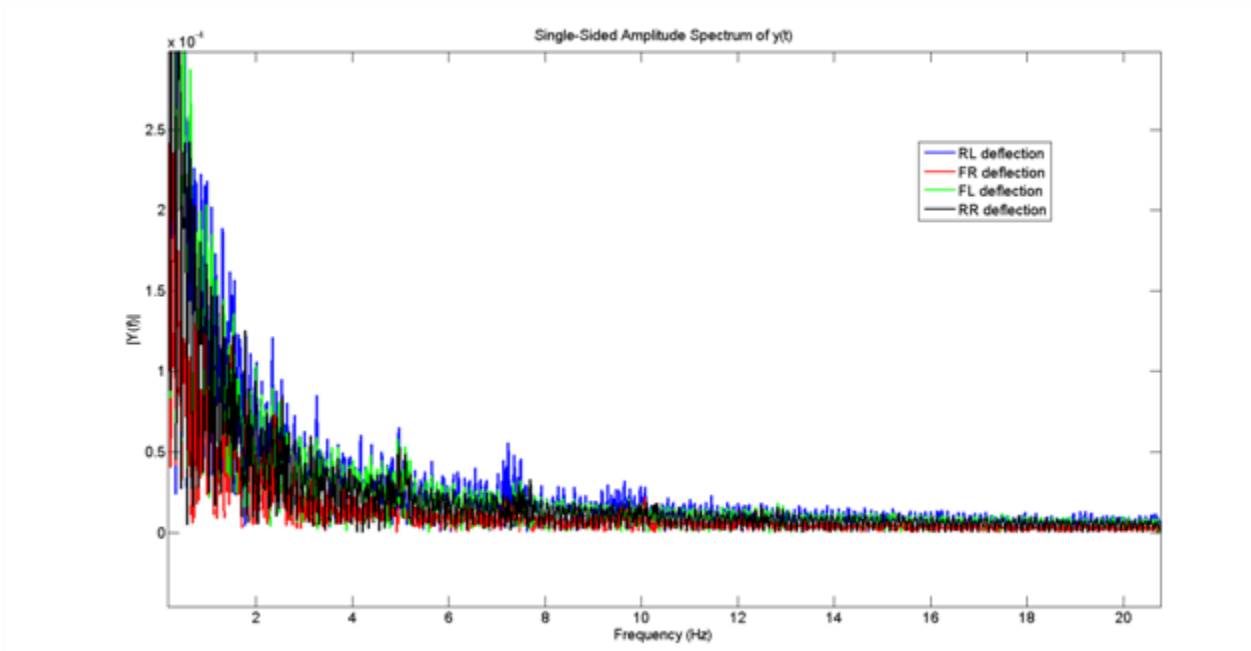

Figure 3.6: Frequency Content of suspension deflection data

and Figure 3.8 shows the protective enclosure used to house the circuit and provide the connections. Appendix B contains higher resolution versions of these images for reference.

For this application of measuring the loading of the suspension arms of an off-road vehicle, it is important and necessary to select a strain gauge that is durable and, like the A/D module, operates fast enough to capture desired dynamics of the vehicle suspension. Most strain gauges can operate at sample rates many orders beyond the desired range of vehicle suspension applications. Therefore, a general purpose gauge will be acceptable for this application and the sample rate of the suspension strain gauges will be set manually by the A/D module in the PIC data acquisition circuit. Additionally, this strain gauge was primarily selected to be a low cost implementation. Because the strain of the suspension is relatively low, this allows for nearly any strain gauge with relatively low yield strain to be mounted. The selected strain gauge was the SGD-3/350-LY41 from Omega™ Engineering [?], with a unit cost of $4.90 per gauge. This is a 350Ω resistance strain gauge with a grid length of 3mm. The gauge was applied to the suspension components using the TT300

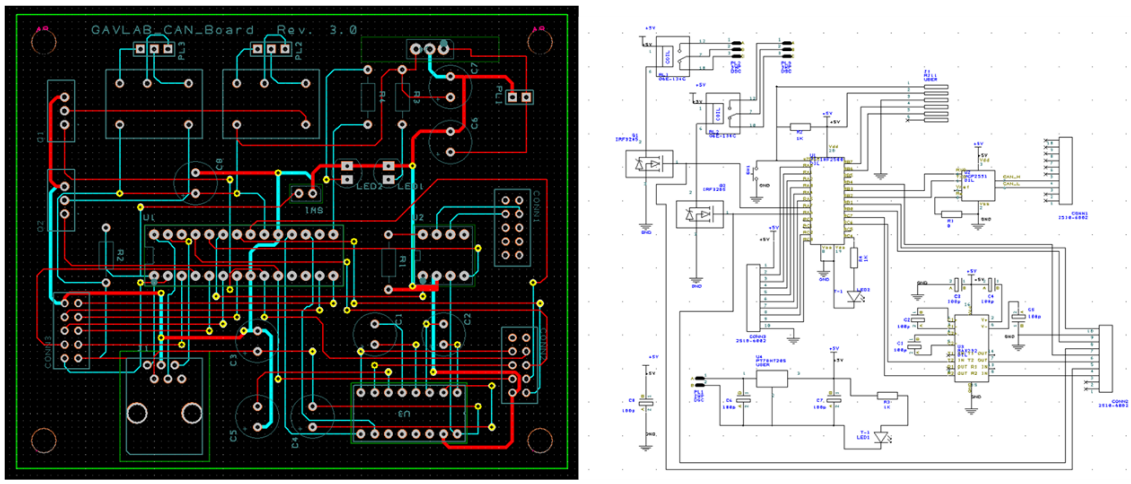

Figure 3.7: Data Acquisition Circuit showing PCB layout (left) and Schematic (right). (Shown full size in Appendix B)

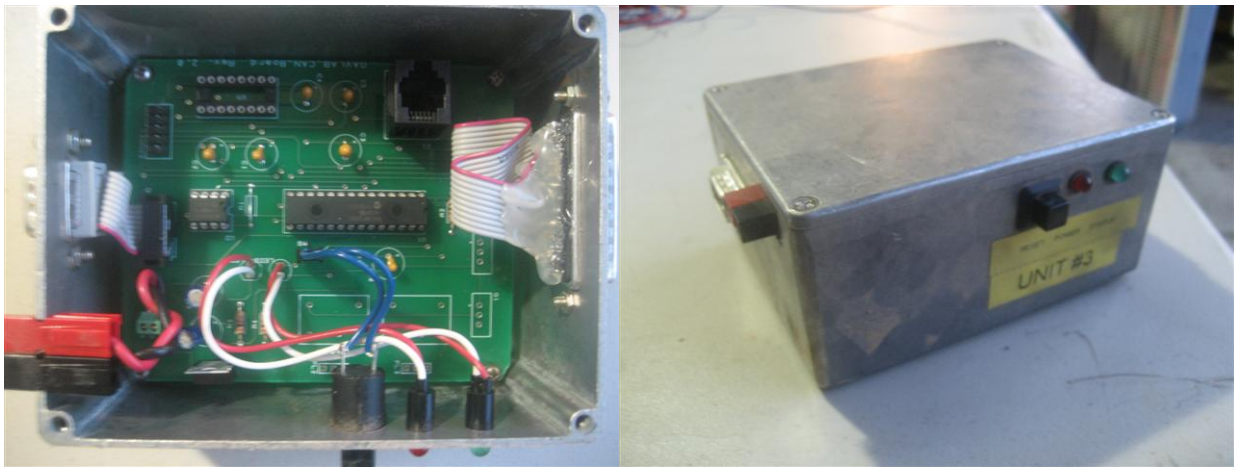

Figure 3.8: Completed Data Acquisition Circuit housed in protective box.

Figure 3.9: Mounted Omega™ SGD-3/350-LY41 Strain Gauge on Chromoly (4130) Tubing

adhesive kit, also from Omega™ Engineering. Site preparation on the suspension components involved cleaning, removing the paint, filing a small flat area to mount the gauge, and sanding progressively from 150 grit to 400 grit sandpaper to prepare the surface. Additionally, acid cleansing of the metal and base neutralization was necessary to prepare the surface for sufficient bonding with the resin.

Because of the relatively small values of strain, signal conditioning was necessary to amplify the voltage signal coming from the strain gauge. An instrumentation amplifier IC was selected from Texas Instruments™ (INA2126). This chip contains dual channel, built in op-amp circuits which allows for gains ranging from 5 to 10000 depending on an external resistance setting between pins 1 and 8 . Figure 3.10 shows the internal circuit for the instrumentation amplifier.

The gain of the IC circuit is set by:

$$G = 5 + \frac{80k\Omega}{R_G} \tag{3.5}$$

with the resistance, R_G, being the selectable parameter. Because the strain expected in this application is roughly 500 - 1000 $\mu\varepsilon$, this corresponds to expected values of roughly 5 - 20 mV. In order to read these values in from an A/D converter, the voltage needs to be

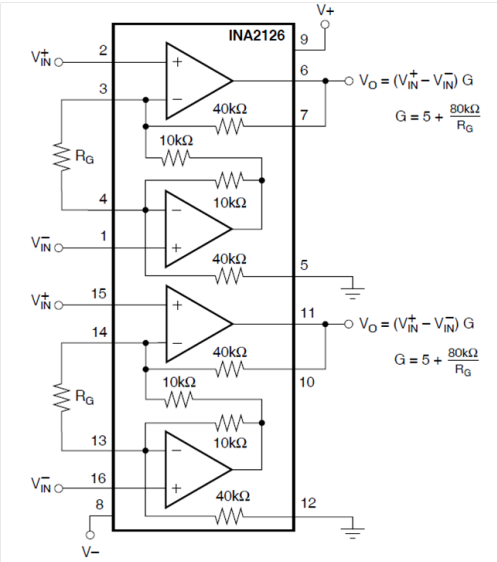

Figure 3.10: INA2126 Instrumentation Amplifier Circuit

in the range of 0V to +5V, thus setting the desired gain at approximately 233. For this gain, a resistance value of 350Ω is required. However, because of the varying geometries and thicknesses of the suspension linkages, some of the gains were set to 100Ωto give a gain of 805. Table 3.2 shows a full listing of the gains, channel connections, and filtering capacitors used for each individual circuit.

Table 3.2: Strain circuit gain and filtering values

CAN Box	CH	Location			Gain Resistor	Power Line Filtering Capacitor	Signal Line Filtering Capacitor	Channel	Output Wire Color	Bridge	Bridge Resistor Tolerance	Potentiometer adjuster?
					(Ω)	(uF)	(uF)	(2126INA)				
1	0	Front	Left	Upper A-Arm	100	100	100	A	Blue w/ tape	quarter	0.10%	yes
	1	Front	Left	Steer Tie Rod	350	100	100	B	blue	quarter	0.10%	no
	2	Front	Left	Lower A-Arm Front	350	220	100	A	green	half	1%	no
	3	Front	Left	Lower A-Arm Rear	350	220	100	B	blue	half	1%	no
3	0	Front	Right	Upper A-Arm	100	220	100	B	blue	quarter	0.10%	no
	1	Front	Right	Steer Tie Rod	350	220	100	A	green	quarter	0.10%	no
	2	Front	Right	Lower A-Arm Front	350	220	100	A	green	half	1%	no
	3	Front	Right	Lower A-Arm Rear	350	220	100	B	blue	half	1%	yes
4	0	Rear	Left	Upper A-Arm Front	100	220	100	A	green	half	0.10%	no
	1	Rear	Left	Upper A-Arm Rear	100	220	100	B	blue	half	1%	no
	2	Rear	Left	Lower A-Arm Front	100	220	100	A	green	half	1%	no
	3	Rear	Left	Lower A-Arm Rear	100	220	100	B	blue	half	1%	no
5	0	Rear	Left	Upper A-Arm Front	100	220	100	A	green	half	1%	no
	1	Rear	Left	Upper A-Arm Rear	100	220	100	B	blue	half	1%	no
	2	Rear	Left	Lower A-Arm Front	100	220	100	A	green	half	0.10%	yes
	3	Rear	Left	Lower A-Arm Rear	100	220	100	B	blue	half	mixed	no

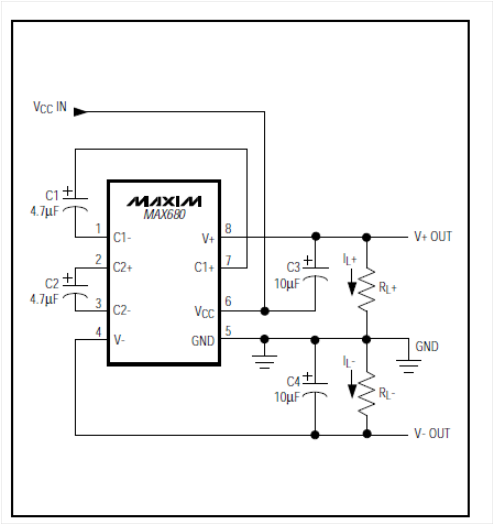

Figure 3.11: MAX 680 Dual Charge Pump Voltage Converter Circuit

Low resistor values required for high gain can make wiring resistance important. Sockets add to the wiring resistance, which will contribute additional gain error in gains of approximately 100 or greater. Since the application of this thesis requires a gain of upwards of 233 and 805, this socket and wire resistance will contribute significant errors to the system. This circuit could be improved greatly for much better performance on future implementation of this system.

The instrumentation amplifier requires both a positive and negative voltage supply for correct operation. The MAX680, from Maxim IC™, a dual charge-pump voltage converter was selected to provide this voltage supply.

This power supply chip performed poorly during the initial hardware testing phase. However, due to cost and time constraints, additional chips were not purchased and methods to improve the performance of this chip were examined and implemented. The primary problem with this power supply was a significant amount of noise which in turn invalidated the operation of the instrumentation amplifier. Additionaly, inconsistencies arose between the positive and negative voltage outputs of the chip on the scale of 1V to 2V. Further testing showed that the cause of these issues may have been a noisy power supply line coming from the vehicle power system. This problem was solved by implementing larger capacitors to

help filter the voltage supply. Referring to Figure 3.11, the designed application of this chip calls for 4.7 μF capacitors on the incoming power supply lines. Increasing these capacitors by a factor of 10, to 47 μF, showed marked improvement in the operation of the amplifier. Furthermore, filtering capacitors were implemented on the power lines and the output signal lines of the INA2126. A viable concern of implementing these types of hardware filters is inducing lag in the data measurement. However, because the desired dynamic measurements are at a relatively low frequency, the induced lag did not prove to be a significant source of error. The filtering also proved to be necessary when examining initial measurements with an oscilliscope. Before filtering, the amplified strain measurements were indistinguishable within the noise of the strain gauges and resistors. Once the filters were implemented, the system output was reasonable and corresponed to expected values. For purposes of ensuring that dynamic measurements were not eliminated from the data, a simple calculation of the bandwidth of the system was performed. Using a simple equation for an RC filter shown in Equation 3.6, and knowing the pin resistance of 80 Ω and the signal filtering capacitor of 100 μF, the cutoff frequency of the filter can be found as roughly 19.9 Hz.

$$f = \frac{1}{2\pi RC} \tag{3.6}$$

Recall from Figure 3.6 that most of the desired dynamics of the suspension fall well under 20 Hz. Therefore, it can be concluded that this filtering will not eliminate any of the desired dynamics to be captured.

Figure 3.12 shows the completed signal conditioning circuit that was designed and implemented on perforated solder boards. The bridges can be seen on the right of the photograph, while the filtering capacitors, power supply, and instrumentation amplifier chip can be seen on the left. The circuit was placed securely in a project box to allow the circuit to be mounted closely to the strain gauges on the a-arms. Long lead wires can be a large source of error and noise in strain measurement applications, so placing the bridge as physically close as possible to the active gauge reduces this potential source of error. Also, because of the

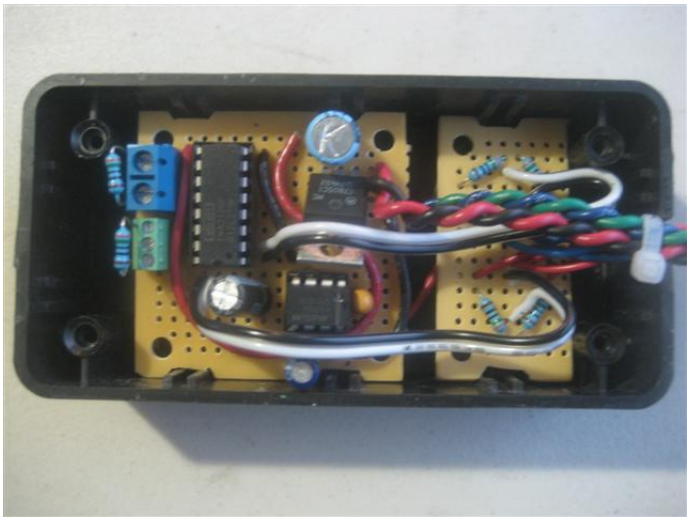

Figure 3.12: Instrumentation Amplifier and Signal Conditioning Circuit

nature of where the box is mounted on the ATV, the project boxes protect the circuit from dust and water which could damage the circuit.

3.5 Suspension Strain Gauge Mounting

Due to the nature of the vehicle and the location of the mounting, it is important to consider a method to ensure that the strain gauge will not become dismounted from the suspension arm. Special precautions and considerations must be made to ensure the valid operation of the strain gauge during the period of data collection. Hot glue (which is relatively inert) was used to provide protection around the gauge, as well as strain relief for the wires attached to the strain gauge. Additionally, a protective layer of tape was applied to ensure that the gauges were not affected during driving manuevers.

Strain gauges were placed on the upper and lower A-Arms of the vehicle in the front suspension. Due to the geometry of the a-arm, only one gauge was mounted on the upper a-arm, and two gauges were mounted on the lower a-arm. The configuration of these gauges allows for the measurement of the normal forces at the tires and the axial loading of the suspension arms during lateral manuevers.

Figure 3.13: Protective mounting of strain gauges.

A gauge was mounted on the steering tie rod between the steering rack and the wheel. This gauge was placed to measure the steering alignment torque as well as the lateral forces resisting steering of the vehicle. Additionally, as noted in Figure 3.15, the suspension deflection linear potentiometer can be seen mounted in the direction of the suspension coil-spring assembly.

Once properly mounted and installed on the vehicle, it is necessary to take appropriate calibration and validation data that allows the user to confirm the correct operation and mounting of the strain gauges. Static data was taken in a number of loading conditions to ensure that proper mounting and operation was achieved.

The first calibration was done with the vehicle sitting on a set of jackstands with the sprung mass of the vehicle isolated and removed from the a-arm loading, as demonstrated in Figure 3.16.

Figure 3.17 shows the non-zero values of the initial offsets, or biases in the gauge. These values could be due to an initial imbalance in the bridge resistance or could be caused by variations in the temperature effects on the resistors. Biases could also be due to varying weights of the unsprung masses (the tire and wheel assemblies) which were not on the a-arm

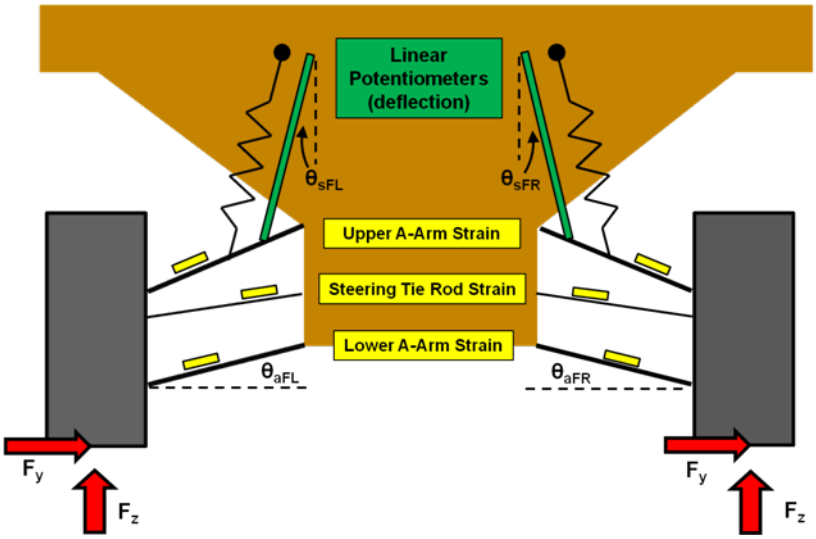

Figure 3.14: Strain gauge mounting locations schematic.

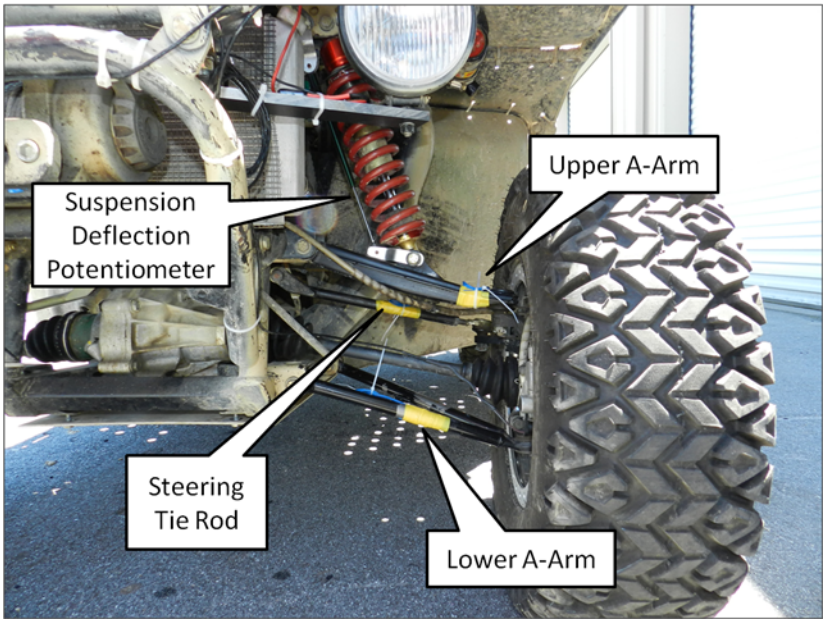

Figure 3.15: Photo showing the mounting locations of the strain gauges.

Figure 3.16: Prowler shown on jackstands in order to isolate the sprung mass from the strain sensors and provide the initial offsets of the strain gauges

during strain gauge mounting. This additional 20 kg of weight would be enough to show up as a bias in this static test. However, regardless of the cause of the offset, the goal of this research is to show the changes in strain due to various dynamic maneuvers and forces, so the static baseline will be acceptable as long as the values are calibrated in the software to compensate for these initial biases. Also of note, in the front right tire there appears to be a drift that is not apparent in the other sensors. Because this is isolated to one wheel, it is believed to be an incorrect circuit wiring issue. However, even in the presence of these errors, the sensors appear to be operating within a reasonable "zero loading" condition. This leads to the conclusion that the sensors are properly mounted and the data acquisition is correctly installed.

After taking static data, a run was recorded when the prowler was lowered off of the jackstands and the weight of the sprung mass was placed onto the suspension components. This effect can be seen below in Figure 3.18. Additionally in this figure, a distinct jump in the data can be seen before and after the point where the vehicle was lowered off of the jacks. This effect is caused by turning the steering wheel to the left and then to the right while the vehicle was isolated on the jacks, and then the same steering maneuver (left then right) was performed again with the vehicle resting statically on all four wheels. Turning

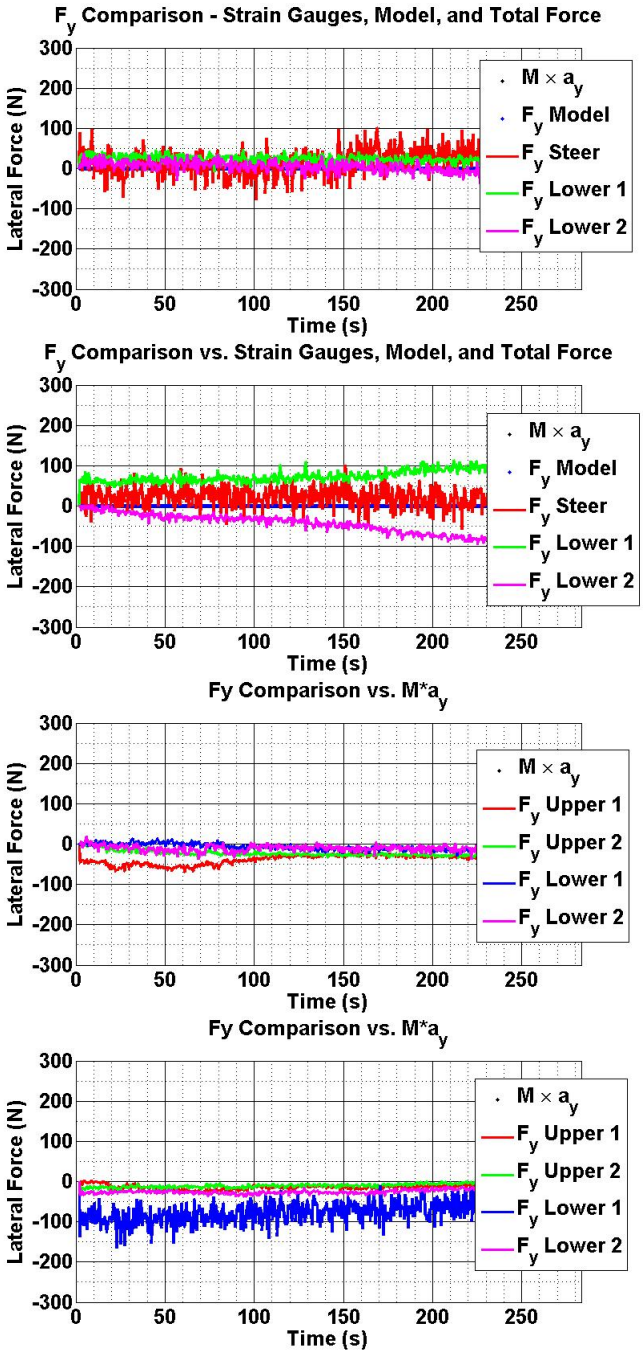

Figure 3.17: Static strain measurements of unloaded suspension components, (Top-Bottom: FL, FR, RR, RL tires)

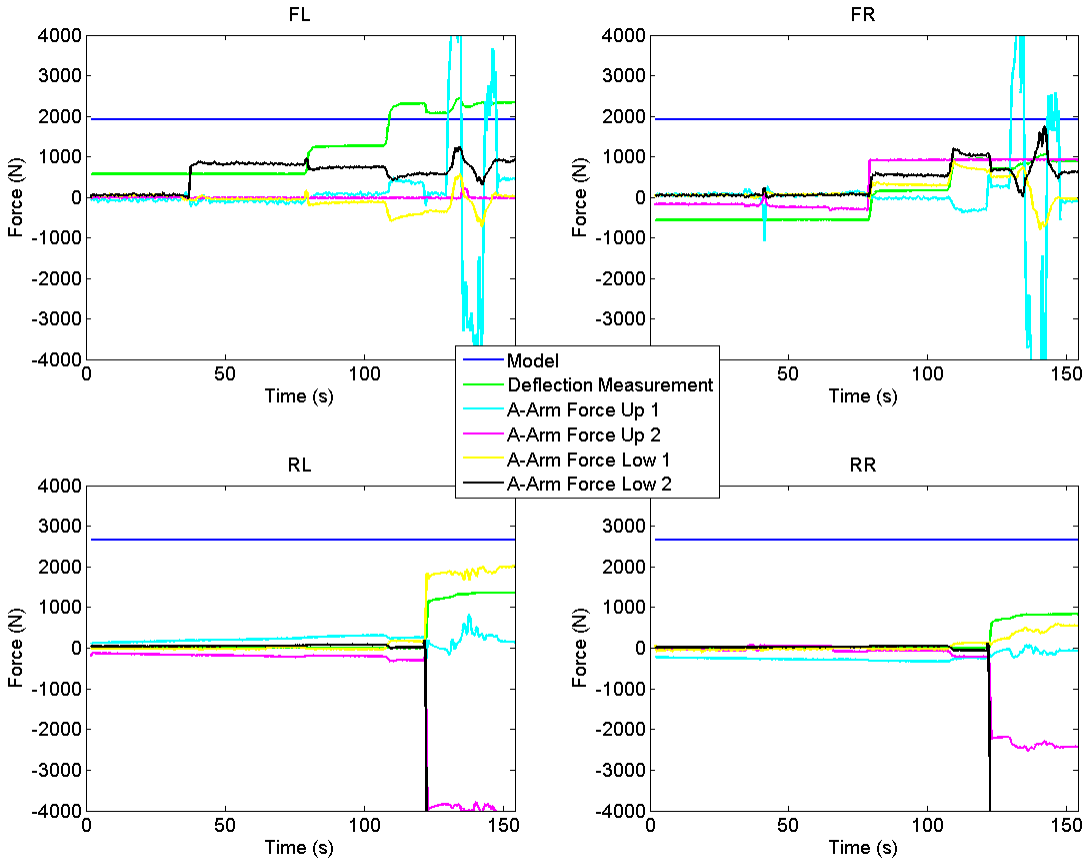

Figure 3.18: Suspension Strain isolated from, then combined with the sprung mass

the steering wheel was done to validate the direction of strain gauge compression / tension to the appropriate reading of the A/D value as well as to show any induced strain on the A-arm linkages caused solely by turning the steering wheel.

From Figure 3.18, it can be seen that the front is lowered down off of the jackstands first at around 70 seconds and then the rear at around 120 seconds. The teal line labeled "a-arm Force Up 1" is actually the channel that corresponds to the strain gauge mounted on the steering tie rod on the front of the vehicle. After the vehicle was lowered off of the jackstand, the steering wheel was turned all the way to limit left, then limit right, then back to zero steer angle. The force induced in the steering tie rod to turn the wheels can clearly be seen. The green line, labeled "Deflection Measurement" is the vertical force felt by the coil-spring

assembly, calculated from the linear spring model of the suspension stiffness and deflection measurement. The navy blue line is the "model," which is a constant for this maneuver. Because the vehicle remains static, there are no dynamics for the model to capture, so the blue line simply represents the static vertical force (or weight) should be on each wheel.

This chapter proposes a novel method to measure the vertical and lateral forces of a ground vehicle. The vertical forces are measured using a suspension potentiometer mounted to the coil-spring assembly of the test platform. The lateral forces are measured using strain gauges mounted directly to the suspension linkages and interfaced to a data acquisition circuit. Analysis and considerations of mounting the strain gauges are given and a method to extract data from these sensors using a PIC micro controller and amplifier circuit is presented. Data was collected and the strain gauges and deflection potentiometers were shown to be operating correctly.

Chapter 4

Experimental Results and Analysis

This chapter shows the data collection process and presents results from various data runs of the Prowler ATV on a closed course. The chapter begins with an introduction to the experimental setup of the test platform. Then, results are presented from the force measurements and analysis is given as to the reasonableness of these results. Various data runs, including driving straight, constant radius turning, and sinusoidal steering are examined. An application of force measurement is shown in the ability to detect when two-wheel liftoff will occur. Additionally, a test was performed to determine if the force measurements alone can detect a dramatic change in driving surface. This test involved a maneuver during which the vehicle was driven onto a gravel surface with dramatically different frictional properties.

4.1 Experimental Setup

The first step of the experimental setup was the implementation of the strain and deflection sensors described in the previous chapter. However, these sensors only provide a fraction of the necessary measurements needed to validate this work. An entire system of sensors was developed, installed, and interfaced onto the Prowler ATV test platform. Figure 4.1 gives an overall flowchart of the data acquisition setup.

In order to obtain velocity and attitude measurements of the vehicle, the Septentrio GPS system was used. The Septentrio is unique in that it is a 3-antenna GPS system. This allows for the use of the 3 position estimates to calculate a full attitude solution, assuming the antennas are mounted in a fixed, known location. This configurable location allows for many different mounting possibilities. To obtain the highest possible resolution and minimize the attitude errors, the largest possible baseline between the antennas is recommended. For

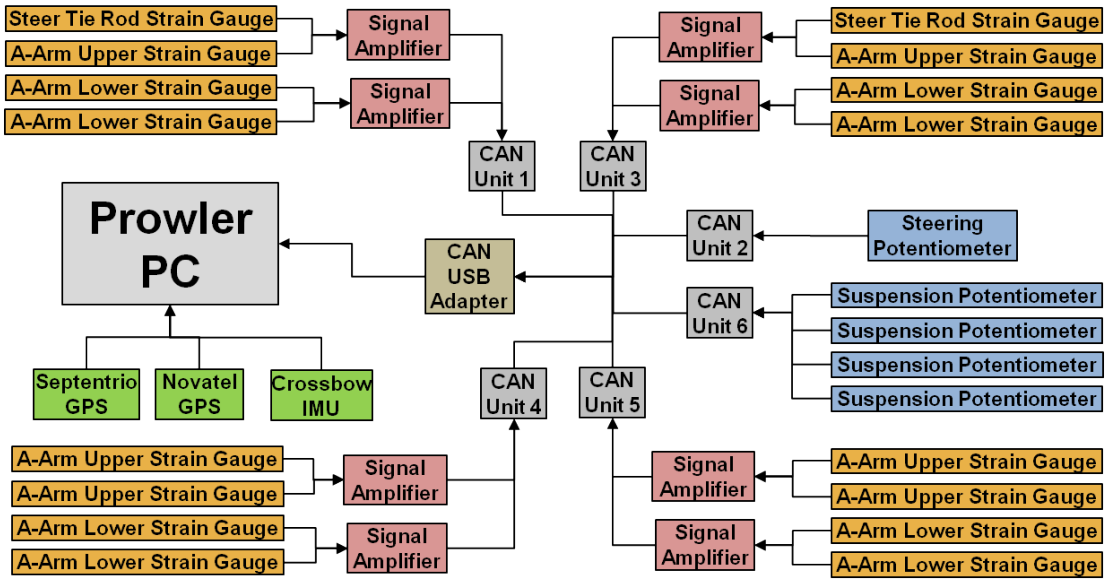

Figure 4.1: Prowler ATV Data Acquisition Flowchart

this reason, a custom aluminum mounting rack was made to extend the antennas far beyond the body of the vehicle. Figure 4.2shows the Septentrio mounted on the top of the Prowler ATV.

A 6 degree-of-freedom Crossbow Inertial Measuring Unit (IMU) was used to provide the angular rates of the body using rate gyroscopes and the accelerations of the vehicle in the 3 coordinate axes. The Crossbow, shown in Figure 4.3, provides data at a configurable output rate and is interfaced through a serial RS232 connection. The mounting of the IMU presented an issue, as it is desirable to physically locate the IMU at the center of gravity (CG) of the vehicle as this is a critical point in the analysis of vehicle forces and moments. However, the CG of the Prowler is not precisely known. Additionally, the area where the CG is estimated to be is largely inaccessible and near an exhaust vent which creates heating issues for the sensor. Thus, the IMU was mounted behind the seat of the vehicle, and dynamic relative acceleration equations were implemented to "translate" the IMU to the CG despite being mounted elsewhere.

Finally, a string potentiometer was implemented to provide the final needed measurement of the steer angle for model validation and force measurement. Various methods of

Figure 4.2: Septentrio GPS Antenna Mount

Figure 4.3: Crossbow IMU440

Figure 4.4: Steer Angle String Potentiometer

acquiring steer angle were explored, including mounting linear potentiometers to the steering tie rod of each wheel, similar to how the potentiometers are mounted along the axis of the coil-spring assembly of the suspension. However, wrapping the string potentiometer around the steering column proved to be a much simpler and more cost-effective implementation. The Celesco MT3-A, a very rugged and durable sensor shown in Figure 4.4, was selected and mounted to the steering column of the prowler such that it wraps around the column as the steering wheel is turned. The steering angle potentiometer was calibrated using a set of mechanical turn plates under each wheel and recording the A/D measurement of the potentiometer with the observed steer angle at the wheel.

Along with the sensors and data acquisition circuits described in Chapter 3, these sensors were integrated onto a singular computer for data collection. MOOS software architecture was used for the sensor interfacing and data logging code. This module based architecture was developed at the Massachusetts Institute of Technology. It allows for various sensors to be added and removed from a system with minimal code changes, as well as providing a common method for data logging and timestamping amongst sensors data received at multiple frequencies. The actual code was written in C++ and installed onto an Advantech ARK5260 ruggedized PC, shown in Figure 4.5.

Further details on the sensor specifications and test setup can be found in Appendix A.

Figure 4.5: Advantech Ruggedized Computer for Data Logging

The tests were conducted at the National Center for Asphalt Testing (NCAT) test track skidpad. The test area is a large, relatively flat asphalt area. There is a slight road grade and irregular pavement in some areas. However, despite these irregularities, it is an adequate proving ground for the validation of the work in this thesis. Furthermore, the model attempts to compensate for the road grade. While the exact value of the road grade is not known, nor constant, the model shows that given accurate road bank and grade information, these effects could be either incorporated into the model or removed from the experimental data.

Various driving maneuvers were performed and a large number of data sets were collected for analysis. The runs were chosen specifically to excite various dynamics of the vehicle. For example, the sinusoidal steering input is a good test to estimate and analyze lateral dynamics, while the launch-braking sequence is geared towards analysis of the longitudinal dynamics. Figure 4.6 shows the Prowler ATV completed a transient dynamic maneuver. The cones in the picture allow for multiple repeated data runs while attempting to hold parameters like road bank and road grade constant from run to run.

Figure 4.7 shows the Prowler performing a steady state turn at a constant radius. This test is often used to calculate and calibrate various vehicle models as it allows for the steady state calculation of many vehicle parameters such as roll stiffness, cornering stiffness and understeer gradient.

Figure 4.6: Prowler Data Collection - Transient Dynamic Maneuver

Figure 4.7: Prowler Data Collection - Constant Radius Turning

4.2 Force Measurements Results

Using the algorithms and methodologies provided in the previous chapter, the measured forces are compared against both the validated model and against experimental data. As an overall general comment on the results, the fit and trends of the data from the strain and displacement sensors match the expected values from the model quite well. There are however, variations that can be attributed to various sources of error in both the modeling and the data collection. Some of these possible error sources are discussed in Chapter 5. Also of note, two different tires were analyzed, but not all of the sensors were operational during the testing with the "Road" (All-trail) tire. All of the runs presented in this section were performed with the "Off-Road" tires presented in Figure 2.22 from Section 2.4.5.

4.2.1 Constant Radius Turn

A 50 ft. radius circle was created and marked off with paint. A human driver was used to attempt to steer the vehicle in a clockwise direction (right-hand turn) along the circumference of the circle, as seen in Figure 4.7. Figure 4.8 shows the measured steer angle and velocity profile for this run.

In looking at the outputs for the strain gauges for this run, it can be seen that the gauges follow an expected trend of the forces. The forces start out relatively low, considering that the run starts with very little lateral dynamics. However, as speed increase, the roll of the vehicle increases and weight transfer takes place. The total lateral force increases, as seen in Figure 4.9.

When compared to the forces expected from the model, the data also trends well. The trends and the magnitudes match well, although there are slight differences in certain areas. Note that the forces from the gauges appear to be greater than the values expected from the model. This is most likely due to the fact that the strain gauges are also picking up components of the vertical force in the suspension linkage while the model is resolved into the purely lateral force of the tire. The key point of analysis to take away is the trend of the

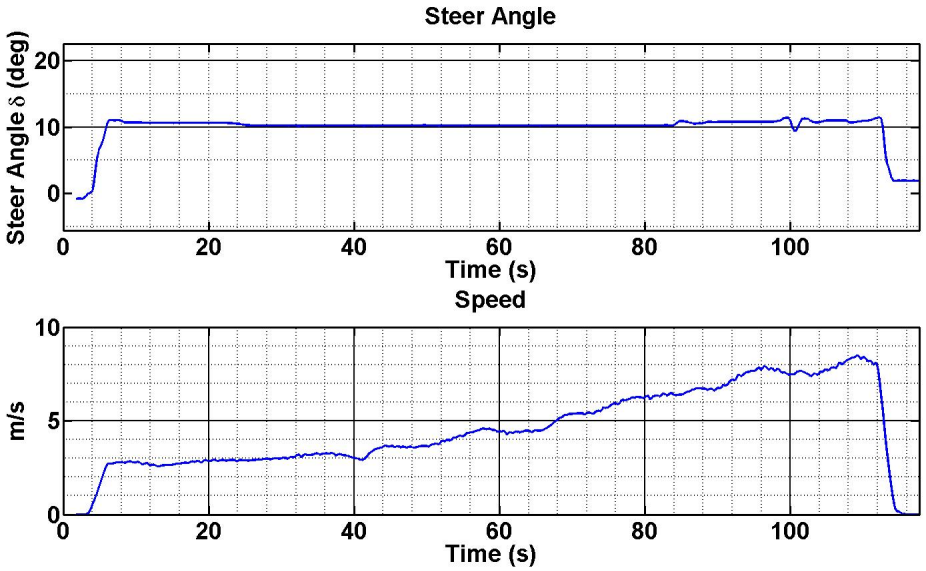

Figure 4.8: Steer Angle and Velocity for 50 ft. radius turn data run

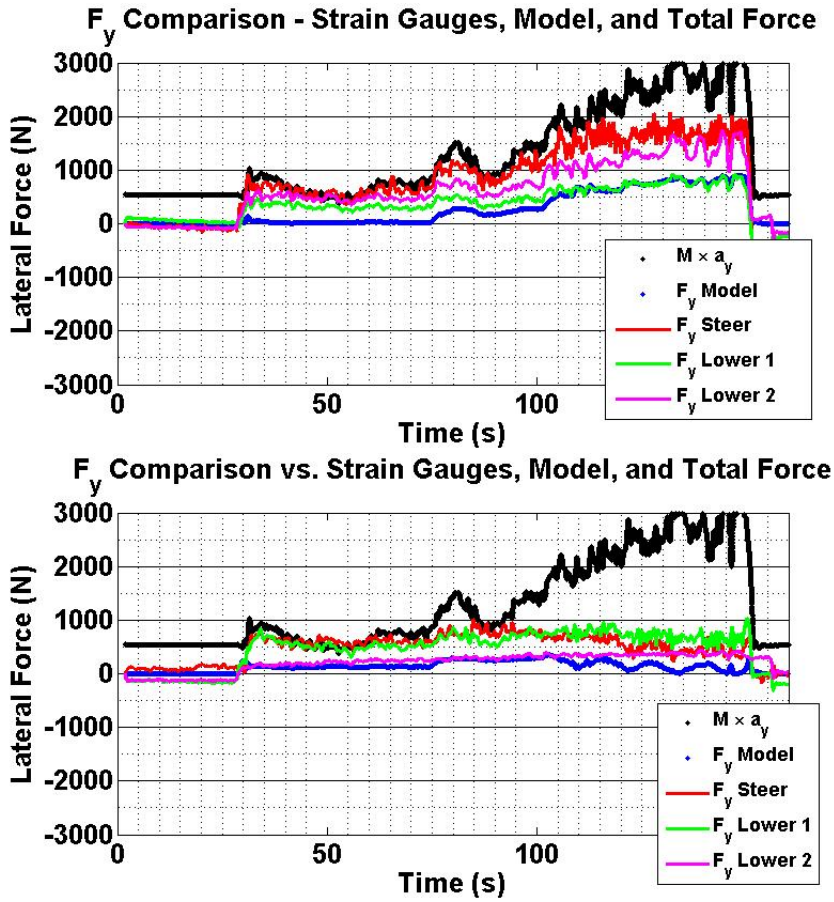

Figure 4.9: Strain Gauge Lateral Force measurement for 50 ft. radius turn

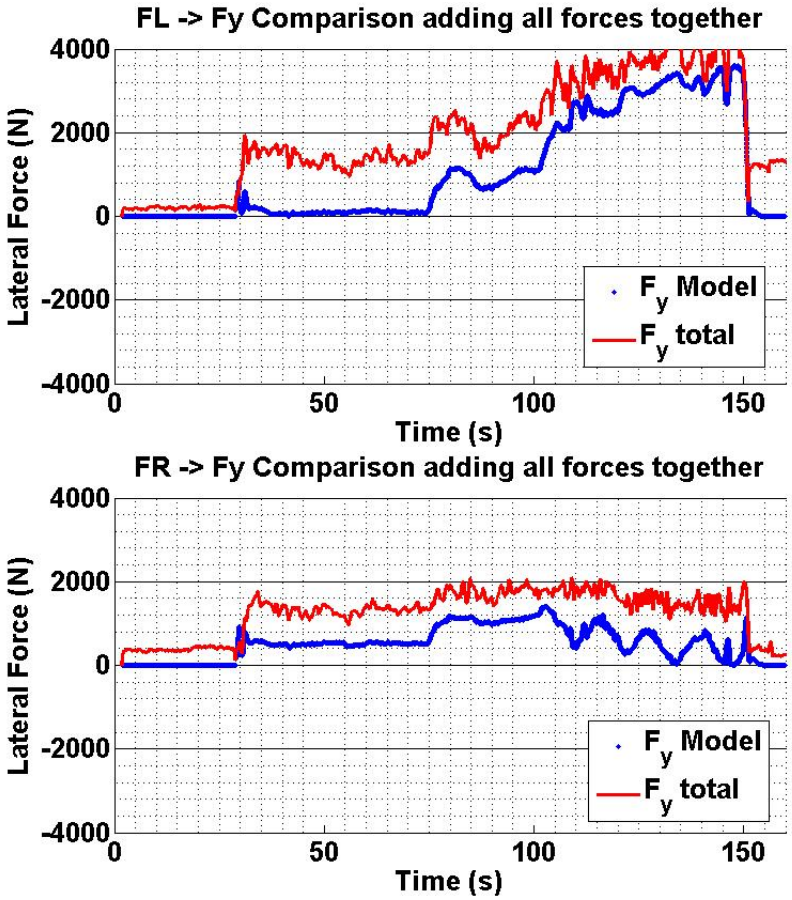

Figure 4.10: Combined Strain Gauges measurement for 50 ft. radius turn

data and whether or not the strain gauges capture the same dynamics as the model and the lateral acceleration, which the strain gauges appear to do well.

Another point of analysis to consider is when the values of the strain gauges for each wheel are added together. Theoretically, all of the force at the contact patch must be transmitted to the vehicle through the suspension mechanisms. Assuming that all of this force is captured by the strain gauge, then combining all the gauges to get a "total force" should give the net magnitude of the force for each wheel. Figure 4.10 shows this combined gauge analysis. As expected, the magnitudes and trends are close to the expected value for the model.

While the trends appear to match, and the magnitudes are of the correct order, it should be noted that there is still a significant difference between the value of the modeled forces

and the total force as measured by the strain gauges. There are two potential sources of this discrepancy. First, not every suspension linkage was able to be accounted for. On the front suspension, the upper a-arm strain gauge was not responsive and it is believed this sensor does not work. The rear suspension also has a linkage that had no gauge mounted to it due to accessibility issues. It is very possible that the lateral force carried in these members could account for the difference between the model and measured forces. Secondly, some of the gauges had a sign error due to incorrect wiring of the bridge completion circuit. Ideally, a positive value of strain would correspond to a compressive force and a negative value of strain would correspond to a tensile force. However, some of the gauges were wired in such a way that this sign convention could not be verified. This error caused some of the values for the gauges to appear to have the incorrect sign, thus indicating an incorrect force. It is believed that this problem was resolved in the post-processing of data. However, there was no way to verify the correct force in each linkage as it corresponds to the actual contact patch force. The methodology to further examine this problem and develop a more thorough and complete solution is described in Section 5.3.1.

Looking at the deflection measurements from the experimental data, it can be seen that the data matches both the trend and magnitude of the expected vertical forces of the model well, as seen in Figure 4.11.

The general trend of all four wheels follows the expected model, and shows the effect seen when the vehicle rolls to the left and the right side wheels begin to experience a much lower vertical force as they lift off of the ground. Eventually, the force in the front tire approaches zero normal force which corresponds to lifting off of the ground. Notice that the back wheel does not encounter the lower force values because of the weight split of the vehicle. There is more weight on the rear axle which makes it much more difficult for the rear wheel to lift of versus the front wheel.

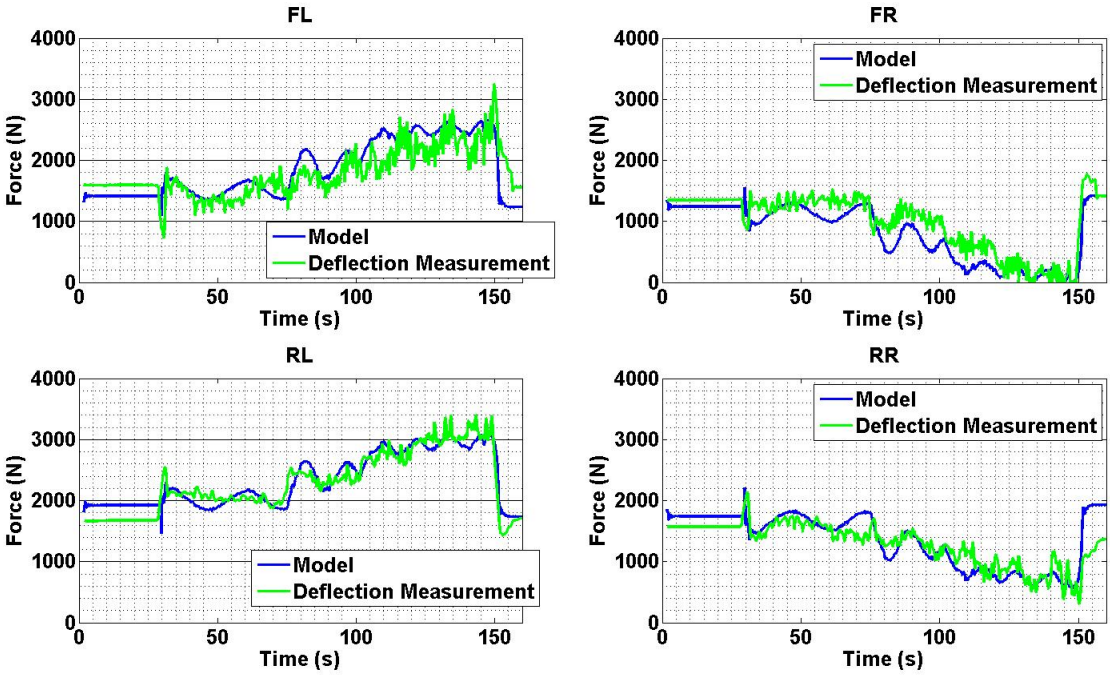

Figure 4.11: Vertical force measurement vs. Model forces for 50 ft. radius turn

4.2.2 Sinusoidal Steering Input

To test the transient dynamics, the Prowler was driven at an attempted constant velocity and a sinusoidal input was applied by a human driver to the steering wheel. As such, this is not a perfect sinusoidal input. However, this input is sufficient to excite the transient lateral dynamics and determine the strain gauges and potentiometers ability to capture the dynamics. Figure 4.12 shows the steering profile and velocity profile for this data set.

Looking at the data from the strain gauges, it can be clearly seen that the dynamic forces of the vehicle have been captured. The magnitudes and trends match what would be expected from the total lateral acceleration and the modeled forces, as seen in Figure 4.13. As described in the previous section, the sign errors of the strain gauges relating to compressive and tensile forces are believed to be corrected. However, further testing should be done before this conclusion can be guaranteed.

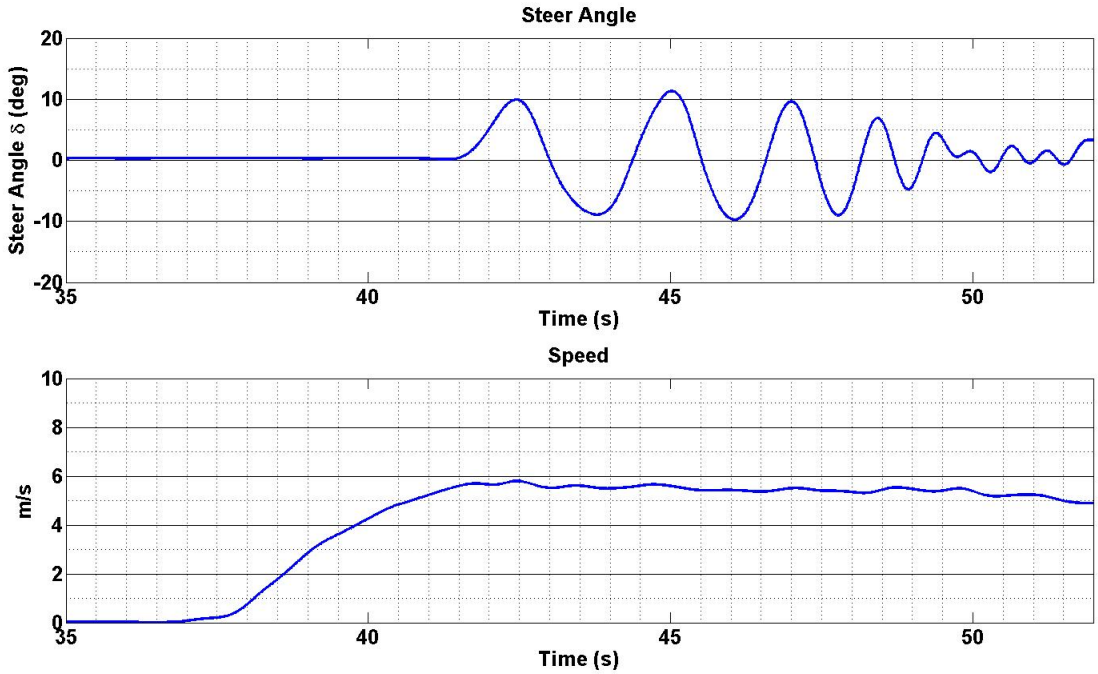

Figure 4.12: Steer angle and velocity for sinusoidal steering data run

Using the same method described in the previous section, combining the gauges to get a "total force" of the wheel can be seen in Figure 4.14. This data trends correctly with the expected model forces and the magnitude is also within a reasonable limit.

Looking at the deflection measurements from the experimental data, it can be seen that the data matches fairly well in regards to the trend and magnitude of the expected vertical forces of the model, as seen in Figure 4.15. There is however noticeable error at the peak measurements of the dynamic maneuver. This could be due to unmodeled effects such as the effects of suspension jounce and camber thrust. Also possible is the fact that the suspension deflection measurements do not account for all of the vertical force during highly dynamic maneuvers where some of the vertical force can appear as a lateral force to the strain gauge due to the roll of the vehicle. Future work involving methods to combine the strain and suspension deflection into an estimation scheme taking into account the roll of the vehicle would potentially help to resolve this problem.

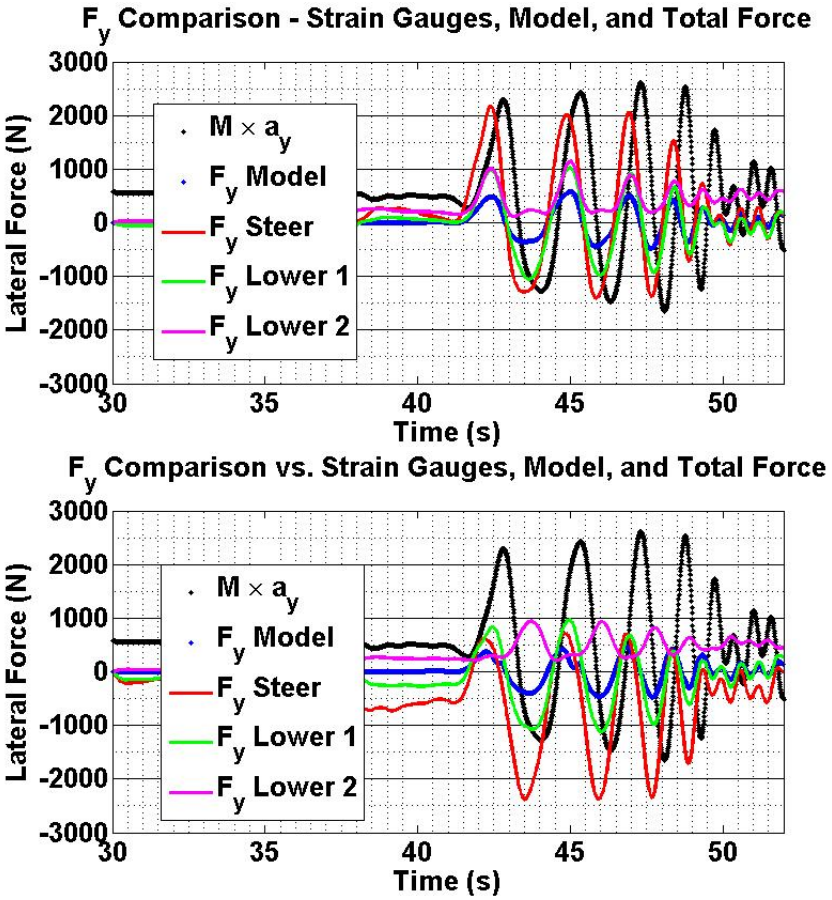

Figure 4.13: Strain gauge lateral force measurement for sinusoidal steering

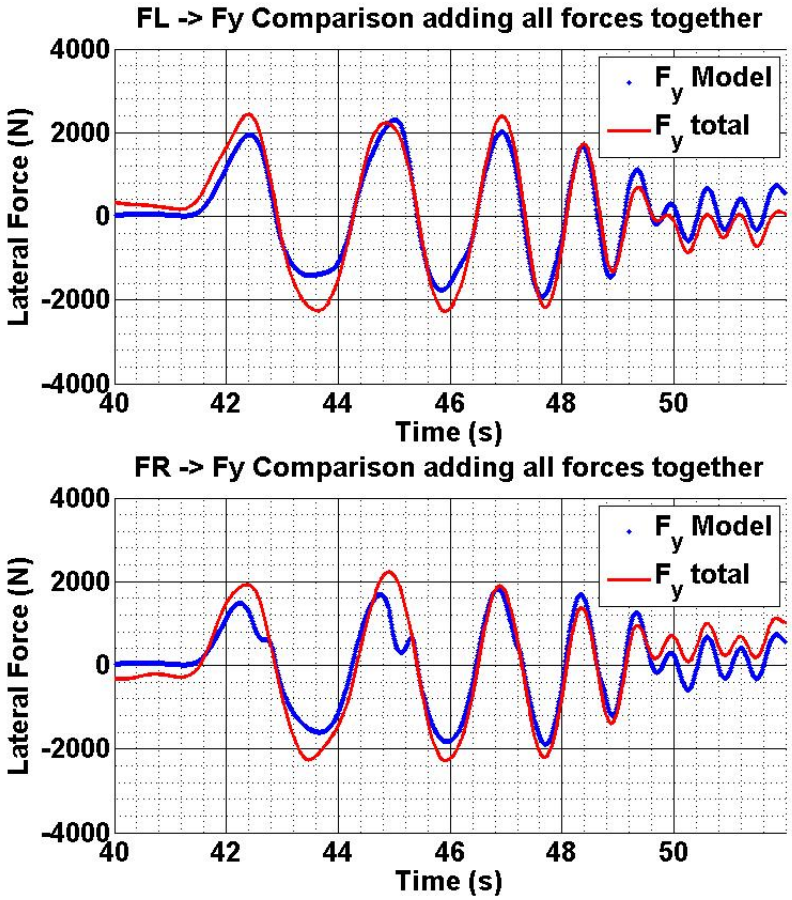

Figure 4.14: Strain gauge lateral force measurement vs. model forces for sinusoidal steering

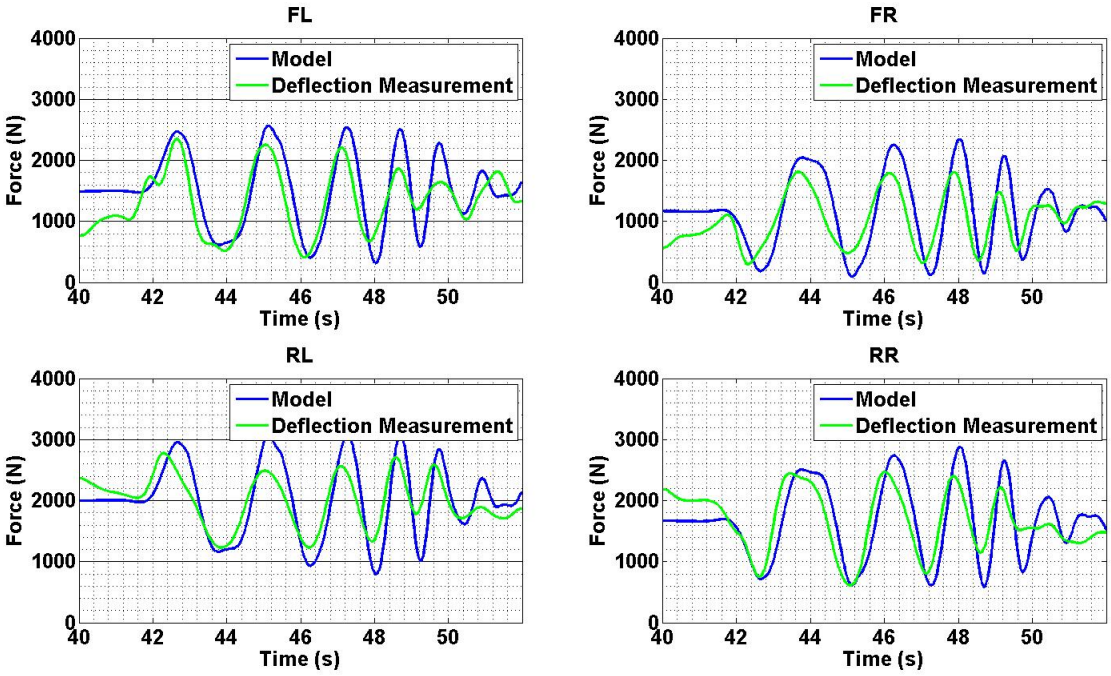

Figure 4.15: Vertical force measurement vs. model forces for sinusoidal steering

4.2.3 Detection of Wheel Liftoff

One potential application of this methodology using strain and deflection sensors is the ability to detect two wheel liftoff. This phenomena occurs prior to vehicle rollover, and systems that can accurately predict this event can be valuable in preventing vehicle rollover. Using data from a different run performing a 50 ft. radius turn at a constantly increasing velocity, Figure 4.16 shows a plot of the measured force in the front left (left) and front right (right) steering tie rod measurement against the mass times lateral acceleration, assumed to be the total force of the vehicle using Newton's 2nd law. The strain data had to be scaled to match the total force data, since the strain measurement here is in fact not the total force. However, this analysis is relevant as it shows the variations in the trend between two different types of measurements, the accelerometer and the strain gauge.

Looking at the 80 second mark of the plot, it can be seen that the force in the right (inner) tire begins to decrease while the force in the left (outer) tire continues to increase. Physically, this represents the wheel on the right "lifting-off" the ground as the vehicle

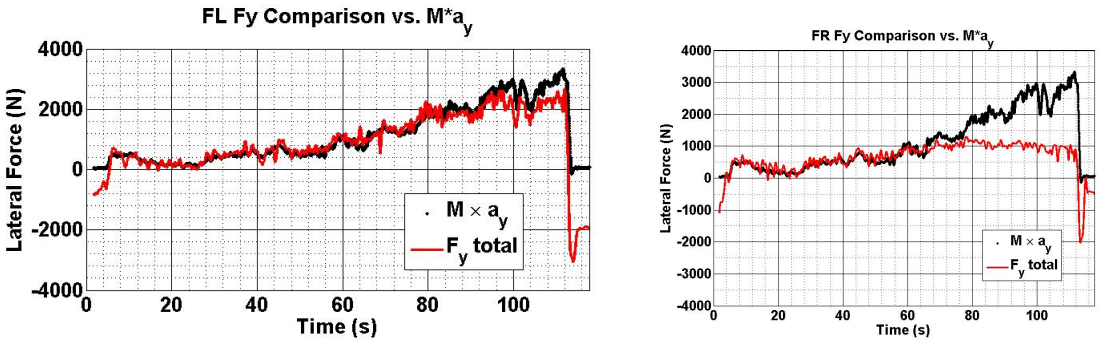

Figure 4.16: Front Wheel Strain Gauge Lateral Force Measurement vs. Total Vehicle Force for 50 ft. radius turn

increases in speed and experiences more roll. The wheel has not ceased to make contact with the ground, as there is still lateral force in the right wheel. However, recall from the tire curves that a lower Fz dictates a lower available lateral force. So as the Fz changes, the lateral force reflects that dynamic and the strain gauge is able to capture this effect. Many researchers have show the ability to detect two-wheel liftoff to be a critical part of preventing vehicle rollover, as two-wheel liftoff is the initial step in vehicle rollovers[12, 30]. The ability to detect this effect with strain gauges could be used in a stability control system or autonomous vehicle even without the aid of GPS. Additionally, the strain gauges can detect this effect before the wheel actually lifts off.

4.2.4 Surface Variations - Transition between asphalt and gravel

Another application of this work is the potential for terrain characterization by looking at the differences in force measurements on various types of terrains. Initially, data runs were only performed on the asphalt surface of the NCAT skid pad. However, one of the data runs looked at trying to detect a sudden change in the driving surface. A sinusoidal steering input was applied as a constant velocity on the asphalt. Then at 24 seconds, the vehicle transitioned from asphalt to a gravel/sand surface. As seen in Figure 4.17, the model only has the steer angle inputs and does not account for the change in $\mu$of the road surface, so the

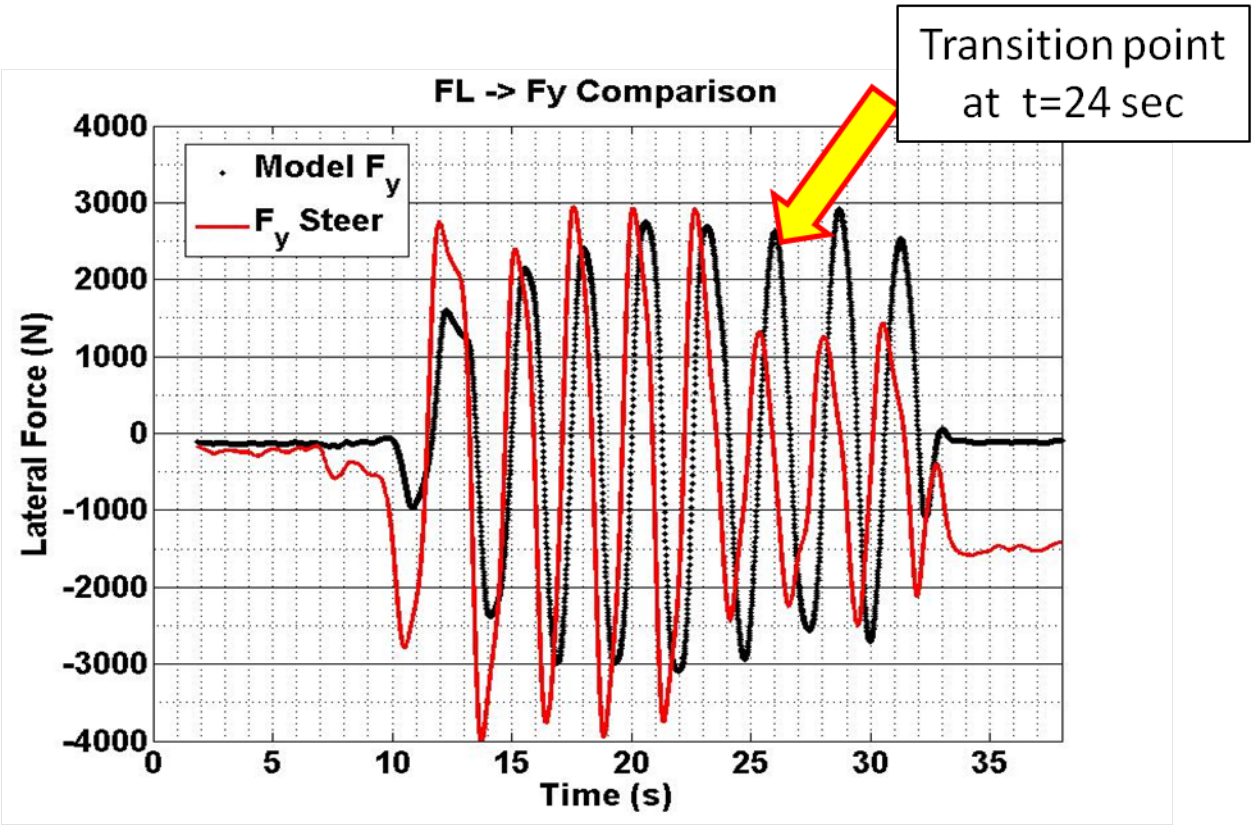

Figure 4.17: Strain gauge lateral force measurement of surface transition between asphalt and gravel

forces remain of a larger magnitude. However, the gravel surface limits the available lateral force of the tire, which in turn is captured by the strain gauges.

Only one data run was explored to consider the possible application of this work, but a tremendous amount of potential can be seen by the initial results. Future work and testing on various surfaces may produce empirical models that can be used to assist or replace other terrain classification techniques. The knowledge of the terrain can dramatically affect the performance of a UGV or off-road vehicle, and knowledge of this information would be tremendously beneficial to any stability control system. For example, using the aforementioned method of detecting lateral force, a UGV may be able to tell if it has veered off of an asphalt road and driving on the gravel/dirt shoulder.

This chapter introduced an experimental setup of a system that measures the lateral and vertical forces in the suspension linkages using strain gauges mounted to the linkages

and a linear potentiometer to measure deflection. Data acquisition methods are presented, and a test platform is detailed including all of the sensors used for data collection. Data is presented from two different dynamic driving maneuvers on the test platform: a 50 ft. radius turn at an increasing velocity and a sinusoidal steering input at a constant velocity. This data shows that the strain gauges and deflection measurements are in fact valid methods to capture the forces of the vehicle in the vertical and lateral directions. While discrepancies exist in the magnitudes of the measured values when compared to the expected values, the trends match very well. These errors can likely be attributed to unmodeled effects.

Chapter 5

Conclusions and Future Work

5.1 Conclusions

In this thesis, a method has been presented to capture the lateral and vertical tire forces of a ground vehicle using suspension deflection potentiometers and strain gauges. An accurate off-road vehicle model was developed to establish the expected values of tire forces during various maneuvers. Various vehicle parameters were explored and identified in an attempt to improve the accuracy of the model. A thorough analysis of the selection, mounting, and data acquisition of a system using strain gauges and linear potentiometers was presented in Chapter 3, and the experimental setup of the test platform was shown in Chapter 4.

The results of this work indicate that this method would be a good starting point for future development as an subsystem of an unmanned ground vehicle system. While the scope of this thesis is limited to one test platform and two relatively benign maneuvers, the system is scalable to a range of various vehicles and situations that would benefit from the vehicle dynamic information this system can capture. Overall, the system performed well and showed good results when comparing the measured values to the expected values from the models. There is an absolute need for improving the knowledge of the tire forces for ground vehicles, and this work presents a step in a new direction towards that end. This system is relatively low in cost when compared to GPS and inertial sensors. It also has the added benefit of not requiring GPS, which would be immensely beneficial in areas such as heavy foliage, canyons, and other types of terrain frequently encountered by off-road vehicles where GPS is not readily available. Furthermore, this system can be ruggedized to create a robust system capable of operating in many different environments. All things considered,

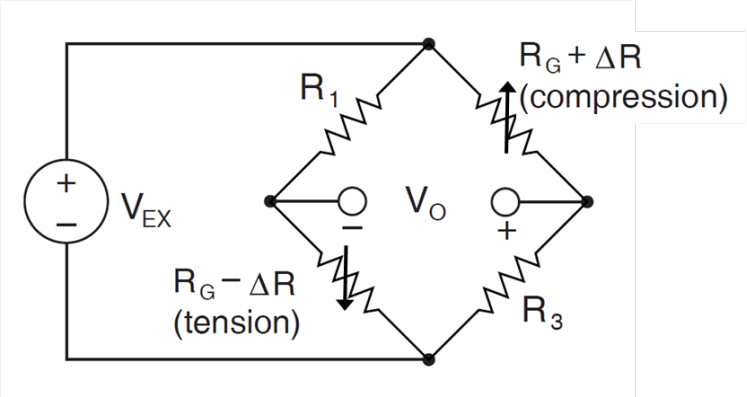

Figure 5.1: Strain Gauge Bridge Circuit for measurement of Axial Strain Only (rejects bending strain)

this is a very viable option to a very real problem in the scope of unmanned ground vehicle operation.

While the total system did work well, as with any real world application, there are numerous areas for improvement and alteration of the presented methodology. It was noted in many instances that error sources were present that could not be accounted for in the analysis of tire forces. Many of these potential sources of error are discussed in the following section.

5.2 Comments on Possible Error Sources

5.2.1 Strain Gauge Bridge Circuit Installation

It was discovered during the analysis done in this thesis that a majority of the strain gauges were incorrectly connected to their respective bridge completion circuits. The problem was resolved by the simple switching of four wires in the gauge circuits.

In an effort to eliminate bending strain and only capture axial strain, the half-bridge circuit was selected and implemented. By correctly placing the gauges, it is possible to completely remove the effects of bending strain, which was desirable for capturing the lateral force of these members, as shown in Figure 5.1.

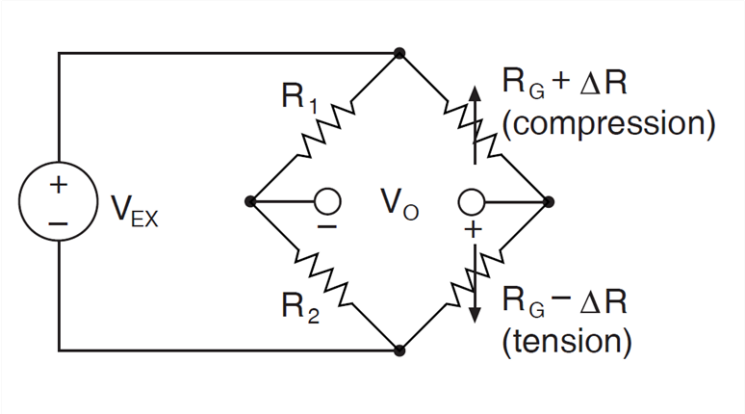

Figure 5.2: Strain Gauge Bridge Circuit for measurement of Bending Strain Only (rejects axial strain)

However, data sheets provided by the manufacturer were misleading as to the correct location of these gauges in the bridge. For this reason, the gauges, or more specifically the Wheatstone bridge circuits, were initially implemented incorrectly. While the goal was actually to eliminate bending strain and capture axial strain, the converse of that was achieved by mounting the gauges in a configuration that rejects axial and only captures bending strain, as seen in Figure 5.2.

Essentially, this mistake caused the half bridge circuits on 12 out of the 16 strain gauges measure the vertical loading which was due to the bending strain. Consequently, these gauges were not able to be verified in the lateral direction. The only gauges that measured lateral force were the steering tie rod strain gauges because they were implemented as $\frac{1}{4}$ bridge circuits and the location of the gauge does not matter. The analysis presented in this thesis was still valid using only the two steering strain gauges, as these sensors responded very well and were able to capture many of the lateral dynamics tested in Chapter 4.

This problem was corrected and the new data provided much better results for lateral force analysis. Regardless of the wiring method of the strain gauge circuits, there was enough evidence in both methods to conclude that the strain gauges do in fact capture the forces in the suspension linkages and are a valid method for directly measuring the forces generated at the tire. Surprisingly, the gauges that measured the bending stress actually trended correctly

with the vertical force measurements, thus indicating that not only would the lateral strain gauges work but also there is potential for using a "strain-gauge-only" setup to capture both vertical and lateral forces.

The only gauges to never accurately capture dynamics of the vehicle were the two gauges mounted to the upper A-arm in the front of the vehicle. This a-arm is unique in the geometry. It has a highly irregular cross sectional area and consists of multiple pieces of metal welded together instead of a singular piece. Also, mounting difficulties in this sensor and inability to correctly identify the expected strain in this member to adjust the amplifier gain rendered this measurement ineffective. It cannot be concluded whether the ineffectiveness on this member was due to the complications of the member geometry, incorrect mounting, or inadequate amplification of the output signal. However, it was observed that the gauges performed better on the suspension linkages with simpler geometry and easier gauge mounting conditions.

5.2.2 GPS Lever Arm Effects and IMU misalignment

A critical assumption of this work is that the measurements of the data and the forces from the model all originate at the center of gravity of the vehicle. This poses a slight problem as the GPS is mounted on the top of the vehicle and the IMU is mounted behind the seat of the vehicle some distance away from the CG. Methods are implemented in this work to rotate and translate the measurements into the vehicle body frame from the GPS frame, as well as translate the IMU from its mounted location to the CG of the vehicle. However, the location of the CG is not known precisely, and is only estimated using imprecise methods. Improving the knowledge of the exact CG location would likely eliminate many of the sources of error in the data collection as well as help explain some of the discrepancies between the data and the model.

Also, it is hypothesized that the IMU coordinate frame is not exactly identical to the vehicle coordinate frame due to misalignment. When the Prowler ATV was sitting on level jacks, (completely static), the IMU had a static bias of $+0.39\ m/s^2$in the y-axis and a bias

of $+0.18\ m/s^2$ in the x-axis. These values could potentially be due to the IMU not being mounted in the same coordinate frame as the vehicle. It is worth noting that these values are relatively small relative to the measurements presented in this thesis. When considering the fact that the goal of the thesis is not improving the accuracy of the method but rather proving the validation of the measurement concept, it was determined that this misalignment of the measurement method was not a significant source of the error. However, improvements to the results are expected if this issue is addressed.

5.2.3 GPS Latency

Because of the derivative nature of certain GPS measurements, the signal can actually be delayed [8, 25]. This is due to the way the velocity measurements are calculated between two data points. The actual timing of the measurement exists between the two data points, and is then reported at some Δt later. The delay has been shown to be 1/2 of the sample time of the GPS system. The Novatel GPS installed on the Prowler is known to have this issue. However, it was unclear whether the Septentrio had was not clear whether or not the problem existed. It is important however, to determine which measurements, if any, have this delay as it can affect sideslip, attitude, and velocity measurement accuracy when compared to other sensors. When comparing the data from the Septentrio and Novatel course measurements, the two align nearly perfectly with almost no delay. Therefore it is concluded that it does in fact measure the velocities in the same manner, and suffers from the same half-sample time delay as the Novatel. Note, this Δt is not the same as the Novatel since the two are sampled at two different frequencies. The Novatel is sampled at $20Hz$, and has a delay time of $T_{delay} = 0.025s$. The Septentrio is sampled at $10Hz$, and has a delay time of $T_{delay} = 0.05s$. The data has been corrected for this and using the GPS time stamp information in the GPS message, the two sensors were able to be synchronized.

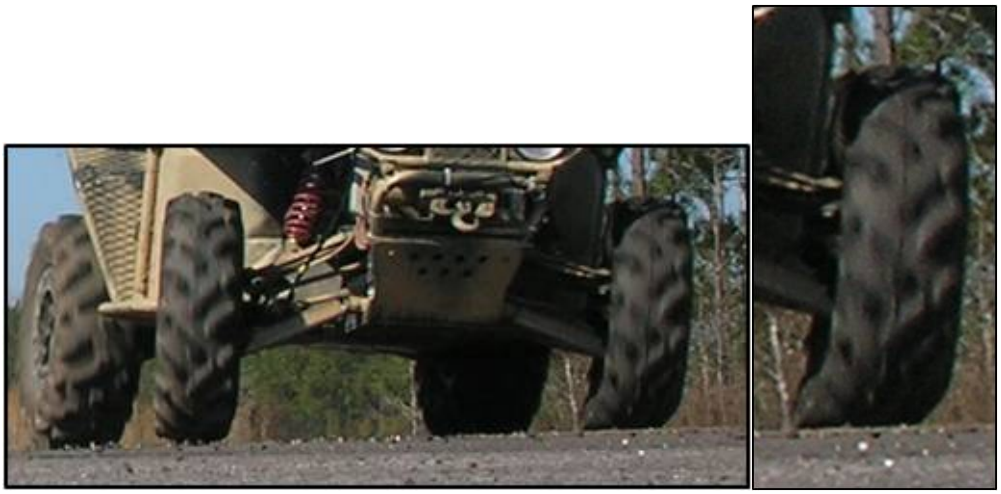

Figure 5.3: Lateral deformation of an ATV tire during cornering

5.2.4 Tire Model Inaccuracy

Many various tire models were considered in this work. However, the tire models were only compared at a higher level as to their application to this work. There is the possibility for exploration of more thorough analysis of tire models, specifically for ATV tires and integration of those models into the analysis. There are many effects that are highly, highly nonlinear and difficult to model and capture. This is amplified by the unique nature of ATV tires with their low inflation pressures and tremendous amounts of deformation in both the lateral and axial directions. Also, the aggressive tread patterns create irregular contact patches that may or may not be accurately captured by the tire models in this thesis. Figure 5.3 shows an example of the lateral deformation experienced by a typical ATV tire.

5.2.5 Nonlinearity in steer angle at hand wheel (and at tires)

Because steer angle is measured at a point before the rack / pinion, it is modeled as linearly related between the handwheel and at the contact patch. However, Ryu showed this to be nonlinear in nature[25]. There is combined with the effect of trapezoidal steer, due to the way in which the steering tie rod is mounted which is not accounted for. Furthermore, slop in the steer angle is seen in the data. When "centering" the steering wheel from the left

or from the right, the same steer angle at the handwheel does not yield the same steering angle at the wheel.

Additionally, all these factors are compounded by possible error in the lack of precision of the mechanical turnplates used to calibrate the potentiometer. These turnplates, while good for rough estimates of steer angle, do not provide the necessary precision needed to accurately calibrate the steering potentiometer. Improved calibration methods would almost certainly improve the results of the model.

A solution for future consideration would be implementation of alternative methods of measuring steer angle. The string potentiometer method was cheaper and had a much simpler implementation. However, it also had the added drawback of only providing a singular steer angle measurement as opposed to individual right and left steering measurements. Many models simplify the steer angle using the assumption that the angle is the same for both front tires. However, when calibrating the steering potentiometer, it was discovered that the steering angle at each wheel vary from left to right by as much as 5 deg. at the limits. As previously stated, this is compounded by the large amount of mechanical play in the steering linkages, including the universal joints and the rack and pinion. It is proposed that if linear potentiometers were mounted linearly along the tie rod, these problems would be eliminated or minimized and the steer angle measurement accuracy would greatly improve.

5.2.6 Camber Thrust / Roll Steer compensation

The effects of lateral force are not only from slip angle generation, but also from camber thrust when the independent suspensions can jounce and rebound during roll [14] . This effect is not accounted for in the model. However, in the presence of large amounts of vehicle roll and weight transfer, this effect is more pronounced. As seen in Figure 5.4, the Prowler experiences significant amounts of suspension jounce and rebound. Note the variations in the highlighted (yellow) lines showing the variations in geometry and camber from the left side to the right side of the vehicle.

Figure 5.4: Effects of camber thrust and roll steer from suspension jounce and rebound

Furthermore, the pronounced roll seen in Figure 5.4 can have an effect on the steer angle through a phenomena called roll steer, where the steer angle for each wheel is actually affect by the suspension geometry in jounce and rebound. As with the camber thrust, this is not accounted for in the model and data. Improvements would be expected in the model matching the physical data if these effects were included.

5.3 Future Work

In considering future potential for the work presented in this thesis, there are many potential improvements that could be made to the presented work as well as tests and experiments to extend the research into new and interesting directions. This section details some of the ideas and areas for future potential work related to this thesis.

5.3.1 Intermediate Testing

One of the first and most obvious directions for *any* research is the improvement of the methodologies presented. One aspect of this research that could be improved upon is what would be called "intermediate" testing. What that means is that the system was conceived and developed on paper and in simulation. Then, the system was transferred directly onto a complex vehicle platform on a relatively large scale (all 4 wheels, all suspension linkages). The research would benefit from a step in between where perhaps the individual linkages were studied and forces, both bending and axial, were better understood within the linkages. Whether constructing enhanced FEA models and algorithms or mounting the assembly onto a test rig to induce known loads, there are a number of possibilities for improving the results of this work. Figure 5.5 summarizes and highlights this intermediate testing step.

Testing in this manner would allow for the isolation of loading individual suspension components with known loads in a controlled environment. Better empirical models could be developed and a better understanding of the behavior of the individual linkages and the assembly as a whole would be gained. Conditions such as road surface, vibrational noise, and

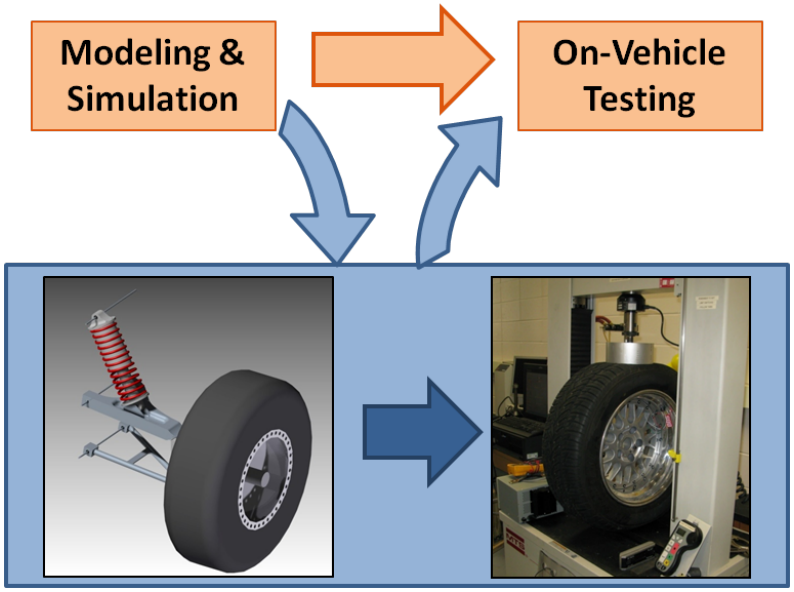

Figure 5.5: Future Work: Intermediate testing of the Prowler suspension components

temperature effects would also be mitigated in this testing environment and would likely add great value to the results of this thesis. Furthermore, additional analysis could be conducted as to parameters such as camber stiffness, aligning moments, and other tire / suspension interactions.

5.3.2 Implementing longitudinal force measurement methods

As discussed in Section 2.3, there are 3 components to capturing the tire force at the tire contact patch completely: F_x, F_y, and F_z. However, only two of those forces were discussed and analyzed in this thesis. The inclusion of longitudinal force into the algorithms is a logical future step towards better knowledge of tire forces. Much like the lateral force models, longitudinal force is based on slip generation. The slip in the longitudinal direction is typically measured as the difference between the vehicle velocity at the wheel and the angular rate at the wheel. Accurately measuring the wheel speed with a sensor and comparing that to the GPS sensors already involved would be an initial step towards capturing the longitudinal force and integrating that method into the methods presented in this thesis.

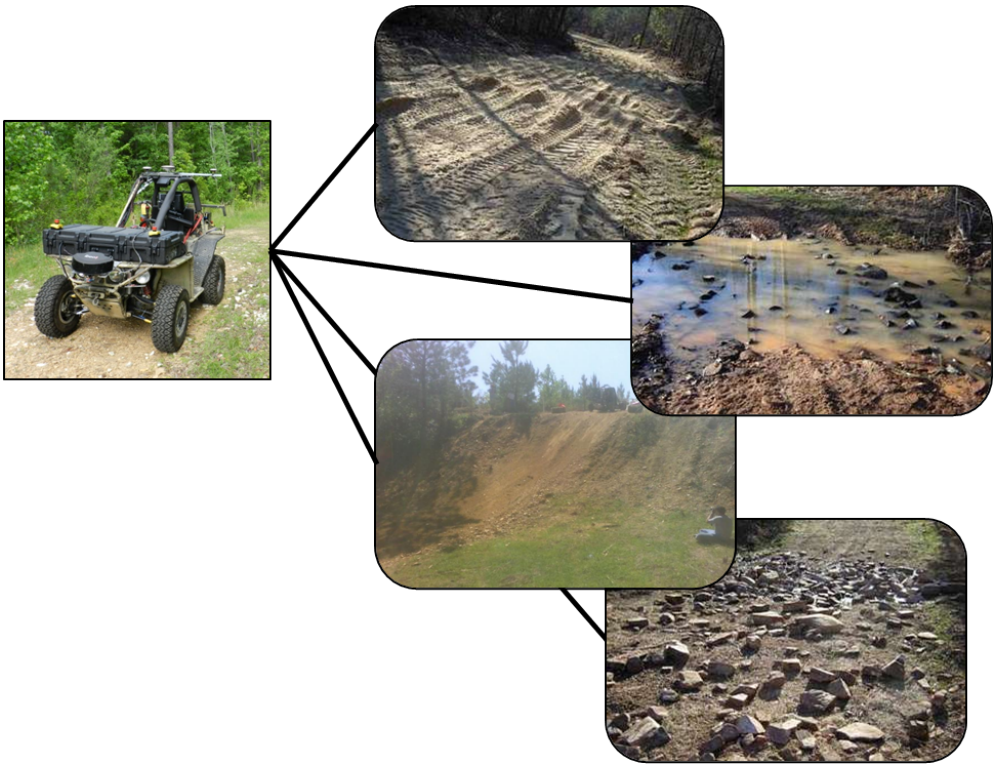

Figure 5.6: Future Work: Testing the Prowler ATV on various types of terrain and surfaces

5.3.3 Measurements on Varied Terrain and Surfaces

Ultimately, as the title says, the work in this thesis is geared towards off-road vehicles. The work presented sought to develop a method of measurement for improvement of off-road vehicles, ATVs, and UGVs. However, the methods and results presented were decidedly "on-road" as they were proven on flat, level asphalt. In order to truly gauge the value of a system such as this, it is critical to test the system off-road on various terrains and in different situations that would resemble day to day operation of an ATV or UGV. The National Center for Asphalt Testing at Auburn University has a 3.7 mile mini-baja test track that would provide ample situations to test many different types of terrains and surfaces, as well as the robustness and ruggedness of the system. It is recommended that after improvement and corrections listed in the previous bullets, the direction of the research be taken to the off-road environment for further development and analysis.

Bibliography

[1] *Vehicle Sideslip and Roll Parameter Estimation using GPS*, 2002.

[2] Federal motor vehicle safety standards, electronic stability control systems, controls and displays, 2007.

[3] R. Anderson and D.M. Bevly. Estimation of tire cornering stiffness using gps to improve model based estimation of vehicle states. In *Intelligent Vehicles Symposium, 2005. Proceedings. IEEE*, pages 801 – 806, June 2005.

[4] J. M. Badalamenti and Jr. G. R. Doyle. Radial-interradial spring tire models. *Journal of Vibration Acoustics Stress and Reliability in Design*, 110(1):70–75, 1988.

[5] S.C. Baslamisli, I. Polat, and I.E. Kose. Gain scheduled active steering control based on a parametric bicycle model. In *Intelligent Vehicles Symposium, 2007 IEEE*, pages 1168 –1173, june 2007.

[6] D. Bevly. *High speed, dead reckoning, and towed implement control for automatically steered farm tractors using GPS*. PhD thesis, Stanford University, August 2001.

[7] D.M. Bevly, J. Ryu, and J.C. Gerdes. Integrating ins sensors with gps measurements for continuous estimation of vehicle sideslip, roll, and tire cornering stiffness. *Intelligent Transportation Systems, IEEE Transactions on*, 7(4):pages 483 –493, Dec. 2006.

[8] D.M. Bevly, R. Sheridan, and J.C. Gerdes. Integrating ins sensors with gps velocity measurements for continuous estimation of vehicle sideslip and tire cornering stiffness. In *Proceedings of the 2001 American Control Conference*, volume 1, pages 25 –30 vol.1, 2001.

[9] Yen-Chi Chang and Tseng-Ti Fu. A useful tire model for atv ride performance on rough roads, 10 2010.

[10] Wanki Cho, Jangyeol Yoon, Seongjin Yim, Bongyeong Koo, and Kyongsu Yi. Estimation of tire forces for application to vehicle stability control. *Vehicular Technology, IEEE Transactions on*, 59(2):638 –649, feb. 2010.

[11] R. Daily, W. Travis, and D. Bevly. Cascaded observers to improve lateral vehicle state and tyre parameter estimates. *International Journal of Vehicle Autonomous Systems*, 5(3-4):230–255, 2007.

[12] D. Edwards. Parameter estimation techniques for determining safe vehicle speeds in ugvs. Master's thesis, Auburn University, May 2008.

[13] P.S. Els. The applicability of ride comfort standards to off-road vehicles. *Journal of Terramechanics*, 42(1):47 – 64, 2005.

[14] T. D. Gillespie. *Fundamentals of Vehicle Dynamics*. Society of Automotive Engineers, 1992.

[15] R. Green. A non-contact method for sensing tire contact patch deformation using a monocular vision system and speckled image tracking. Master's thesis, Auburn University, August 2011.

[16] Xu Guan, Su Jian, Zhang Libin, Gong Haibin, and Xu Xiangguo. Research on automobile suspension performance evaluation system with adjusting-frequency method. In *Research Challenges in Computer Science, 2009. ICRCCS '09. International Conference on*, pages 202 –205, dec. 2009.

[17] Jin-Oh Hahn, R. Rajamani, and L. Alexander. Gps-based real-time identification of tire-road friction coefficient. *Control Systems Technology, IEEE Transactions on*, 10(3):331 –343, May 2002.

[18] Fei Han, Zheng Gui, and Haosu Zhang. Fea of tire-soil model for off-road vehicle. In *Mechanic Automation and Control Engineering (MACE), 2010 International Conference on*, pages 5930 –5933, June 2010.

[19] G. Koch, T. Kloiber, and B. Lohmann. Nonlinear and filter based estimation for vehicle suspension control. In *Decision and Control (CDC), 2010 49th IEEE Conference on*, pages 5592 –5597, dec. 2010.

[20] Shiang-Lung Koo, Han-Shue Tan, and M. Tomizuka. Nonlinear tire lateral force versus slip angle curve identification. In *American Control Conference, 2004. Proceedings of the 2004*, volume 3, pages 2128 –2133 vol.3, 30 2004-july 2 2004.

[21] D. Krueger. Investigation of lateral performance of an atv tire on natural, deformable surfaces. Master's thesis, Auburn University, 2007.

[22] Jilai Li, Wen Gao, and Huawei Liang. Researches on the method of the hardware in loop simulation for vehicle stability control system based on scilab/scicos. In *Proc. IEEE Intelligent Vehicles Symp*, pages 820–823, 2009.

[23] M. Ohori, T. Ishizuka, T. Fujita, N. Masaki, and Y. Suizu. Fundamental study of smart tire system. In *Intelligent Transportation Systems Conference, 2006. ITSC '06. IEEE*, pages 1519 –1524, sept. 2006.

[24] M. Richier, R. Lenain, B. Thuilot, and C. Debain. On-line estimation of a stability metric including grip conditions and slope: application to rollover prevention for all-terrain vehicles. In *Proceedings of IEEE/RSJ International Conference on Intelligent Robots and Systems*, pages 25–30, San Francisco, Sept 2011. IEEE.

[25] J. Ryu. *State and Parameter Estimation for Vehicle Dynamics Control Using GPS*. PhD thesis, Stanford University, December 2004.

[26] M. Sergio, N. Manaresi, M. Tartagni, R. Guerrieri, and R. Canegallo. On road tire deformation measurement system using a capacitive-resistive sensor. In *Sensors, 2003. Proceedings of IEEE*, volume 2, pages 1059 – 1063 Vol.2, oct. 2003.

[27] D.E. Smith and J.M. Starkey. Effects of model complexity on the performance of automated vehicle steering controllers: Model development, validation and comparison. *Vehicle System Dynamics: International Journal of Vehicle Mechanics and Mobility*, 24(2):163–181, 1995.

[28] J. Stephant, A. Charara, and D. Meizel. Force model comparison on the wheel-ground contact for vehicle dynamics. In *Intelligent Vehicle Symposium, 2002. IEEE*, volume 2, pages 589 – 593 vol.2, june 2002.

[29] Mark H. Warner. Atv rollover resistance: Testing of side-by-side atv rollover initiations, 04 2010.

[30] R. Whitehead, W. Travis, D. Bevly, and G. Flowers. A study of the effect of various vehicle properties on rollover propensity. Automotive Dynamics, Stability, and Controls Conference and Exhibition, May 2004.

[31] C. Yue, T. Butsuen, and J. K. Hedrick. Alternative control laws for automotive active suspensions. In *American Control Conference, 1988*, pages 2373 –2378, june 1988.

Appendices

Appendix A

Prowler ATV Platform & Hardware

A.1 Vehicle Properties

The Prowler ATV was used as the platform for data collection and model validation. It is manufactured by ATV Corp., in Orange, CA. ATV Corp. is a subsidiary of Phoenix International, Inc.

Prowler II (Internally Transportable / Light Tactical All Terrain Vehicle) Specifications

- Power Plant : 660 cc 4-Stroke Single, Liquid Cooled, Electric Start with Auxiliary Auto - Decompression Recoil Pull
- Power Train : Fully Automatic Transmission with HI/Lo Range, Reverse and Park (Limited Slip 4WD, 4WD Diff Lock, 2WD)
- Construction : Sealed Tubular Structure with Chromoly Roll Cage and Cargo Racks
- Operation : Standard Automotive Driver Controls with Sealed Rack and Pinion Steering, Console Mounted Dual Range Shifter and Parking Brake Lever
- Top Speed : 63 mph (4WD, Hi Range)
- Suspension :
  - Front - Independent Double Wishbone, Adjustable Preload Reservoir Shock Absorbers, 8" Travel
  - Rear - Independent Double Wishbone, Adjustable Preload Reservoir Shock Absorbers, 9" Travel, Sway Bar

Figure A.1: Prowler ATV

- Braking :
  - Front - Dual Hydraulic Disc
  - Rear - Shaft Mounted Hydraulic Disc with 4 piston opposed Calipers,
  - Full Engine Braking on each of all 4 Drive wheels
- Payload : 1000 lb (1+ : 1 payload to weight ratio exclusive of crew)
- Towing Capacity : 2250 lb (terrain dependent) Winch : 3000 lb, with Wireless Remote Control
- Tires / Wheels : EMT Run Flat / Double Reinforced Rims
- Fuel Capacity : 16 gal. (with optional in line spare tank)
- Ground Clearance : 12.5" (13.5" @ Approach and Departure)
- Wheel Base : 75.25" Track Width : 46" front, 43" rear (center to center)
- Overall Width : 54" Overall Length : 113"

Figure A.2: Crossbow IMU440

- Height : 69.5”
- Weight : (dry) 1100 lb
- Ford Depth : 36”

A.2 Sensor Specifications

The Prowler was modified and fitted with a number of sensors and actuators to allow for data collection and vehicle automation. Below is a list of the vehicle sensors and actuators installed.

- Steering Control – Integrated incremental Encoder to output steering position (4000 ppr) via RS232 connection
- Throttle Control – DC Stepmotor with encoder feedback via RS232 connection
- Braking Control – Integrated incremental Encoder to output steering position (2000 ppr) via RS232 connection
- Crossbow IMU 440 CC (Accelerations, Angular Rates)
  - Update Rate 2-100 Hz

  - Angular Rates (yaw, pitch, roll)
    * Range: Roll, Pitch, Yaw Rates ± 200 °
    * Bias: Roll, Pitch, Yaw Rates <± 0.75 °/sec
    * Scale Factor Accuracy < 1 %
    * Non-Linearity < 0.5 % FS
    * Resolution < 0.06 °/sec
    * Bandwidth > 25 Hz
    * Random Walk < 4.5 °/hr1/2
  - Acceleration (x,y,z)
    * Range X/Y/Z ± 4 g
    * Bias: X/Y/Z <± 15 mg
    * Scale Factor Accuracy < 1 %
    * Non-Linearity < 1 %FS
    * Resolution < 0.6 mg
    * Bandwidth > 25 Hz
    * Random Walk < 1.0 m/s/hr1/2
  - Output RS-232

- Race Technology Hall Effect Sensors (Wheel speed, vehicle velocity)
  - Switching time – Rise (10 to 90%) 15 μsec. Max.
  - Switching time – Fall (90 to 10%) 1.0 μsec. Max.
  - Capable of measuring zero velocity.
  - Connected through microcontroller circuit

- Novatel GPS System (Position, Velocity)

Figure A.3: Septentrio Three-Antennae PolaRx2e GPS System

  - Input Voltage: 9-18 VDC
  - Com Ports 1x RS-232, 2x RS-232/422, 1x USB 1.1
  - Data Sampling at 20 Hz
  - Velocity Accuracy 0.03 m/s RMS
  - Horizontal Position Accuracy (RMS) Typically between 1-3 m
  - Elevation Position Accuracy Typically 2x horizontal position accuracy, or 2-6 m

- Septentrio GPS System (Position, Velocity, Attitude)
  -
  - Data Sampling at 10 Hz
  - Outputs Position, Velocity, Heading, Pitch, and Roll

A.3 Computer System

The computers and hardware were mounted in a case on the front of the vehicle.

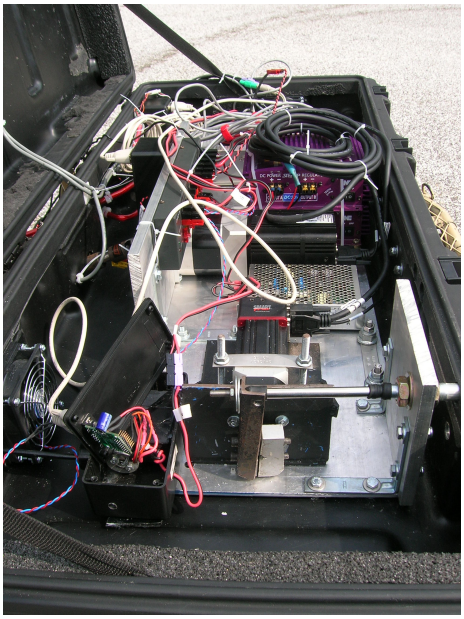

Figure A.4: Prowler Hardware and Component Case

Figure A.5: Advantech Ruggedized Computer for Data Logging

- Advantech Compact Embedded Computer
  - Linux operating system (Ubuntu)
  - 2 x RS-232 ports and 5 x RS-232/422/485 ports
  - Vehicle Command Codes / interfacing written in C++ using MOOS (Mission Oriented Operating System)

Appendix B

Circuit Diagrams

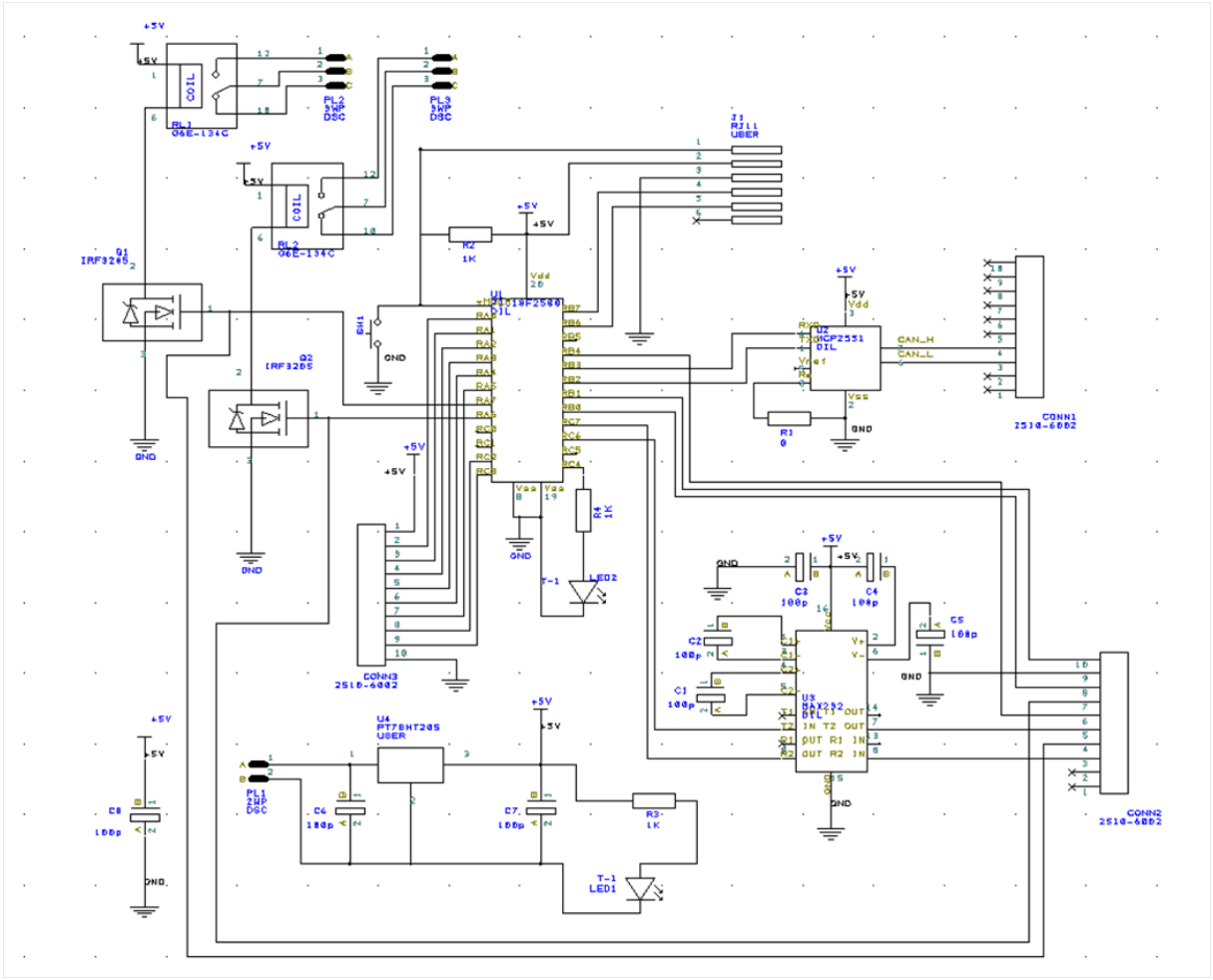

Figure B.1: Data Acquisition Circuit Schematic

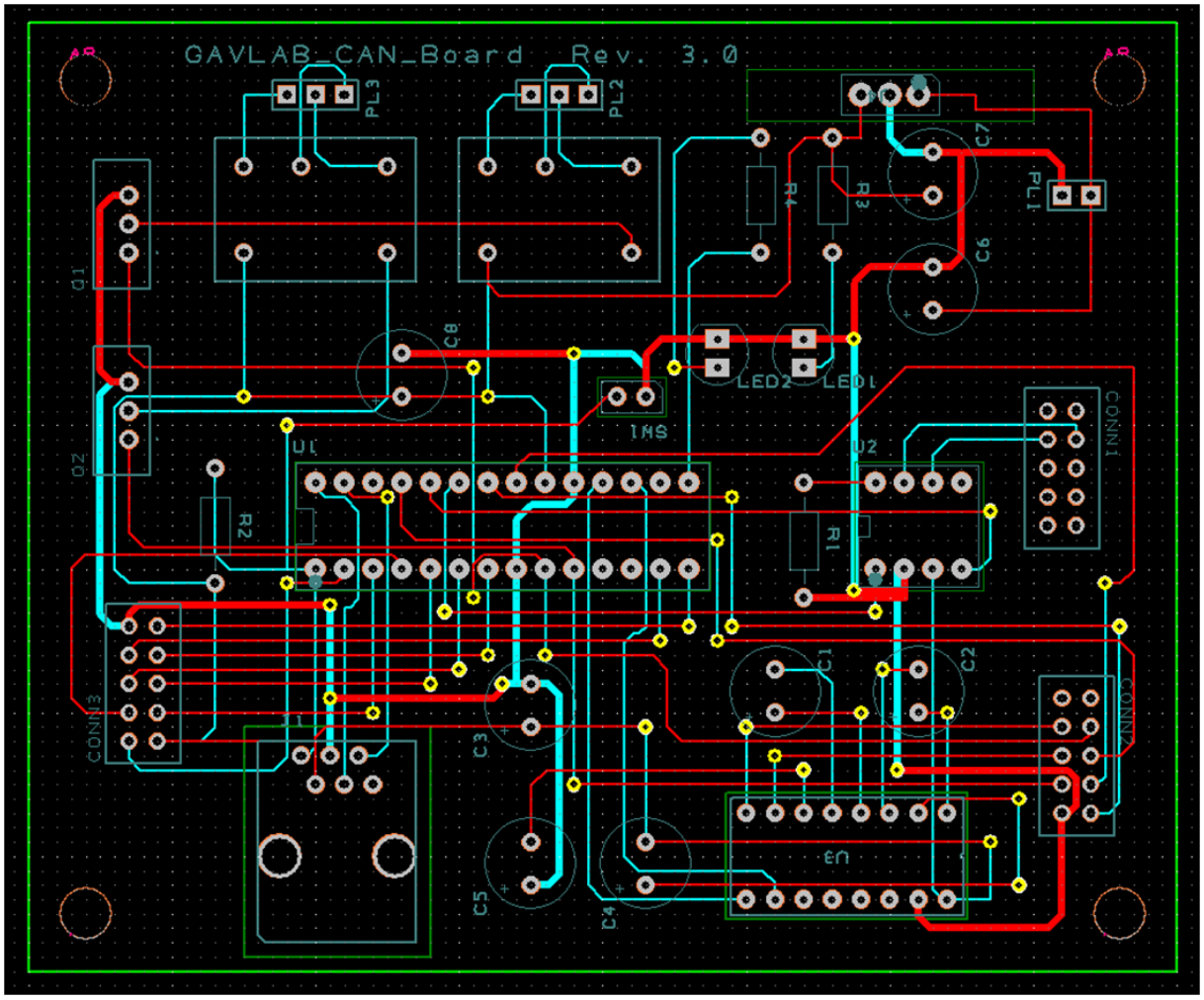

Figure B.2: Data Acquisition Circuit PCB layout